ระเบียบวิธีสมการปริพันธ์ขอบเขตเชิงเอกฐานต่ำสำหรับการวิเคราะห์หน่วยแรงทีทั่วไปของรอยร้าวในตัวกลางสนามร่วมสามมิติ

นายนฤเทพ สุกุลธนาศร

วิทยานิพนธ์นี้เป็นส่วนหนึ่งของการศึกษาตามหลักสูตรปริญญาวิศวกรรมศาสตรมหาบัณฑิต
สาขาวิชาวิศวกรรมโยธา ภาควิชาวิศวกรรมโยธา
คณะวิศวกรรมศาสตร์ จุฬาลงกรณ์มหาวิทยาลัย
ปีการศึกษา 2560

WEAKLY SINGULAR BOUNDARY INTEGRAL EQUATION METHOD FOR A NALYSIS OF GENERALIZED T-STRESSES OF CRACKS IN 3D COUPLED-FIELD MEDIA

Mr. Naruethep Sukulthanasorn

A Thesis Submitted in Partial Fulfillment of the Requirements
for the Degree of Master of Engineering Program in Civil Engineering
Department of Civil Engineering
Faculty of Engineering
Chulalongkorn University
Academic Year 2017

Thesis Title	WEAKLY SINGULAR BOUNDARY INTEGRAL EQUATION METHOD FOR ANALYSIS OF GENERALIZED T-STRESSES OF CRACKS IN 3D COUPLED-FIELD MEDIA
By	Mr. Naruethep Sukulthanasorn
Field of Study	Civil Engineering
Thesis Advisor	Associate Professor Jaroon Rungamornrat, Ph.D.
Thesis Co-Advisor	Assistant Professor Akira Furukawa, D.Eng.

Accepted by the Faculty of Engineering, Chulalongkorn University in Partial Fulfillment of the Requirements for the Master's Degree

.....Dean of the Faculty of Engineering
(Associate Professor Supot Teachavorasinskun, D.Eng.)

THESIS COMMITTEE

.....Chairman
(Professor Teerapong Senjuntichai, Ph.D.)

.....Thesis Advisor
(Associate Professor Jaroon Rungamornrat, Ph.D.)

.....Thesis Co-Advisor
(Assistant Professor Akira Furukawa, D.Eng.)

.....Examiner
(Associate Professor Akhrawat Lenwari, Ph.D.)

.....External Examiner
(Assistant Professor Chinapat Buachart, Ph.D.)

นฤเทพ สุกุลธนาศร : ระเบียบวิธีสมการปริพันธ์ขอบเขตเชิงเอกฐานต่ำสำหรับการวิเคราะห์หน่วยแรงทีทั่วไปของรอยร้าวในตัวกลางสนามร่วมสามมิติ (WEAKLY SINGULAR BOUNDARY INTEGRAL EQUATION METHOD FOR ANALYSIS OF GENERALIZED T-STRESSES OF CRACKS IN 3D COUPLED-FIELD MEDIA) อ.ที่ปรึกษาวิทยานิพนธ์หลัก: รศ. ดร. จรูญ รุ่งอมรรัตน์, อ.ที่ปรึกษาวิทยานิพนธ์ร่วม: ผศ. ดร. อากิระ ฟุรุคาวะ, 86 หน้า.

วิทยานิพนธ์ฉบับบนี้นำเสนอการพัฒนาระเบียบวิธีสมการเชิงปริพันธ์พื้นผิวสำหรับวิเคราะห์หน่วยแรงทีทั่วไปของรอยร้าวในปริภูมิสามมิติหลากสนาม คู่ของสมการเชิงปริพันธ์รูปแบบอ่อนสำหรับแรงทั่วไปบนผิวรอยร้าวและสำหรับอนุพันธ์ของการขจัดทั่วไปบนผิวรอยร้าวถูกสร้างขึ้นภายใต้กรอบทั่วไปทำให้สามารถจำลองวัสดุประเภทต่างๆได้หลากหลายรวมถึงวัสดุยืดหยุ่น วัสดุไพอิโซอิเลกทริก วัสดุไพอิโซแมกเนติก และวัสดุไพอิโซอิเลกโตรแมกเนติก รอยร้าวที่มีเรขาคณิตทั่วไป และแรงกระทำแบบต่างๆในรูปแบบเดียวกัน นอกจากนี้ สมการกำกับเชิงปริพันธ์สุดท้ายเกี่ยวข้องเฉพาะเคอร์เนลที่มีความเป็นเอกฐานต่ำ ซึ่งทำให้สามารถตีความค่าปริพันธ์ที่เกี่ยวข้องแบบปกติตามหลักการผลรวมของรีมานน์ และสามารถใช้ฟังก์ชันฐานแบบต่อเนื่องในการประมาณผลเฉลยได้ ระเบียบวิธีบาวดารีเอลิเมนต์แบบสมมาตรของกาเลอร์คินและระเบียบวิธีกาเลอร์คินถูกนำมาประยุกต์ใช้เพื่อแก้สมการเชิงปริพันธ์ทั้งสองสมการ นอกจากนี้มีการใช้การประมาณแบบพิเศษบริเวณขอบรอยร้าวเพื่อยกระดับคุณภาพของผลเฉลยโดยใช้เพียงแค่โครงตาข่ายแบบหยาบเท่านั้น ค่าหน่วยแรงทีทั่วไปบริเวณขอบรอยร้าวหาได้โดยใช้สูตรที่พัฒนาขึ้นในรูปของค่าอนุพันธ์ของผลรวมของการขจัดทั่วไปบนผิวรอยร้าว ผลในหลายกรณีถูกนำเสนอไม่เพียงเพื่อยืนยันความถูกต้องของระเบียบวิธีที่พัฒนาขึ้นเท่านั้นแต่แสดงให้เห็นถึงความสามารถและสมรรถนะในเชิงการคำนวณด้วย

ภาควิชา	วิศวกรรมโยธา	ลายมือชื่อนิสิต	.....
สาขาวิชา	วิศวกรรมโยธา	ลายมือชื่อ อ.ที่ปรึกษาหลัก	.....
ปีการศึกษา	2560	ลายมือชื่อ อ.ที่ปรึกษาร่วม	.....

5970217621 : MAJOR CIVIL ENGINEERING
KEYWORDS: SGBEM / CRACK / COUPLED-FIELD / T-STRESS

NARUETHEP SUKULTHANASORN: WEAKLY SINGULAR BOUNDARY INTEGRAL EQUATION METHOD FOR ANALYSIS OF GENERALIZED T-STRESSES OF CRACKS IN 3D COUPLED-FIELD MEDIA. ADVISOR: ASSOC. PROF. JAROON RUNGAMORNRAT, Ph.D., CO-ADVISOR: ASST. PROF. AKIRA FURUKAWA, D.Eng., 86 pp.

This thesis presents the development of a weakly singular boundary integral equation method for the analysis of the generalized T-stress of isolated cracks embedded in a coupled-field whole space. A pair of weak-form integral equations, one for crack-face generalized traction and the other for the gradient of the crack-face generalized displacement, is established in a general framework allowing various types of materials including elastic, piezoelectric, piezomagnetic and piezoelectromagnetic solids, general crack geometry and loading conditions to be handled in a unified fashion. In addition, the final governing integral equations contain only weakly singular kernels and this, as a result, renders the integral interpretation in terms of Riemann sum and the use of continuous basis functions in the approximation possible. Both symmetric Galerkin boundary element method and the Galerkin technique are employed to solve the pair of weak-form integral equations. Special near-front approximation is also employed to enhance the quality of solution near the crack front with the use of relatively coarse meshes. Explicit formula in terms of the gradient of the sum of the crack-face generalized displacement along the crack front is proposed to extract the generalized T-stress. Extensive results are reported not only to validate the present technique but also to demonstrate its capability and computational robustness

Department:	Civil Engineering	Student's Signature	.....
Field of Study:	Civil Engineering	Advisor's Signature	.....
Academic Year:	2017	Co-Advisor's Signature	.....

ACKNOWLEDGEMENTS

First of all, I would like to express my gratitude and appreciation to my advisor, Associate Professor Dr. Jaroon Rungamornrat, for useful and valuable suggestion to overcome the problems along the path until my thesis was successful, and I am very thankful for his support that making me becomes a good researcher in the future. I am also grateful to my co-advisor, Assistant Professor Dr. Akira Furukawa for giving opportunity to me for short-term visiting at Tokyo Institute of Technology, his warm welcome and support help me to gain a lot of valuable experience during my stay in Japan. I am grateful to my seniors and colleagues that give useful knowledge and insightful discussion for me; in addition, when I am stressful form research, they will help and encourage that give me strength to carry on; and I am very appreciate to all previous works that allow me to use it for being reference. I am thankful for my family and partner, for their understanding, supporting, and being by my side. Finally, I wish to express my appreciate for Department of Civil Engineering, Chulalongkorn University and Junior Science Talent Project, NSTDA that provided the scholarship for me to proceed my thesis and master's degree; and Graduate School, Chulalongkorn University that awarded the financial support when I visited at Japan.

CONTENTS

Page

LIST OF TABLES

Tables **Page**

LIST OF FIGURES

Figures **Page**

CHAPTER 1
INTRODUCTION

This chapter consists of four main parts. The first part provides the motivation and significance underlying the present study. Then, results from an extensive review of historical background and advances in the modeling and analysis of fracture problems are reported. Next, the statement of a research problem, specific objectives, scope of work, and methodology and research procedure are briefly summarized. Finally, resulting outcomes and contribution of the present study are addressed.

1.1 MOTIVATION AND SIGNIFICANCE

The classical theory of linear fracture mechanics has been successfully employed, for the past several decades, in the modeling, analysis, and assessment of fracture-induced failure mechanisms of components and parts made of various types of materials such as elastic solids (e.g., William, 1957; Paris and Erdogan, 1960; Irwin, 1961; Foreman *et al.*, 1967; Nakamura and Park,1990) and fully coupled-field media (e.g., Pak, 1992; Park and Sun, 1995; Zhang *et al.*, 2002; Gao *et al.*, 2003; Ma *et al.*, 2007; Ma *et al.*, 2015). The majority of those existing works is based primarily on the well-known assumptions that the inelastic deformation and nonlinear processes induced due to the presence of discontinuity are only pertained in a sufficiently small region surrounding the fracture front and are negligible (e.g., small scale yielding concept) and the fracture-related responses (e.g., crack growth criteria and the direction of crack advances) are governed or dictated only by a dominant, singular part of the near-front stress and generalized stress fields. It is evident from the primitive work of William (1957) for linear elastic media and its analogous extension for coupled-field materials that such the singular term contained in the near-front field expansion can be completely described by a single set of parameters known as the intensity factors. The knowledge of this fracture data is, therefore, essential and, at the same time, sufficient for establishing single-parameter-based fracture models relying only upon the singular field. However, various past evidences have indicated that integrating the nonsingular part of the near-front field into those models can further enhance or improve their

capability to simulate fracture phenomena (e.g., Ayatollahi *et al*., 2002; Sedinghiani *et al*., 2011; Cheng et al., 2012; Cheng et al., 2012). Within the context of linear elasticity, a nonsingular part of stress existing along the crack front, commonly known as the T-stress, has been found to significantly affect the hydrostatic tri-axiality ahead of the crack front, crack growth resistance curve, direction and stability of crack advances, and size and shape of the inelastic region surrounding the crack front (e.g., Cotterell, 1966; Williams and Ewing, 1972; Rice, 1974; Du and Hancock, 1991; Ayatollahi *et al.*, 1998; Smith *et al.*, 2001; Tvergaard, 2008). In addition, Larsson and Carlsson (1973) found that the conventional boundary layer technique integrating only the stress intensity factors was not a suitable approach for modeling real crack problems. However, once enhanced by adding the information of the T-stress, the modified boundary layer approach can provide more accurate prediction of the stress intensity factor at the first plastic yielding stage for various types of specimens. Similar to the elastic case, the important role of nonsingular terms in simulations of cracks in coupled-field media such as piezoelectric materials has also been investigated and confirmed (e.g., Zhu and Yang, 1999; Hao and Biao, 2004; Li and Lee, 2004; Viola *et al.*, 2008; Liu *et al.*, 2012). Two-parameter-based fracture models, integrating both the singular and nonsingular data along the crack front, have been found promising and increasingly employed by many investigators, in the past three decades, to study cracks in various aspects.

To facilitate the use of two-parameter-based fracture models in fracture simulations, the analysis technique capable of extracting the information of both intensity factors and the nonsingular terms along the crack front must be supplied. For instance, in the simulation of crack advances in an elastic medium, both the stress intensity factors and T-stress must be accurately calculated at any analysis step and then used as the basic information in the growth law to propagate the crack. To achieve such a crucial task, a powerful and robust solution procedure must be employed to handle not only the inherent complexity associated with the problem at the initial stage but also the general crack geometry resulting from the crack evolution. On the basis of an extensive literature survey, the computational technology for determining the intensity factors of cracks in both single and coupled-field media has been well established and

various existing techniques have been found to have the vast capabilities to treat problems in a general context (e.g., Xu and Ortiz, 1993; Li *et al*., 1998; Xu, 2000; Haas and Kuhn, 2002; Frangi *et al*., 2002; Sanz *et al*., 2005; Qin *et al*., 2007; Rungamornrat and Mear, 2008b,c; Phongtinnaboot *et al*., 2011; Rungamornrat *at al*., 2015). Unlike the intensity factors, existing solution procedures for calculating the nonsingular terms such as the T-stress and generalized T-stress are relatively few and most of them are of limited capabilities. While several analytical schemes were proposed to establish explicit solutions of the T-stress and generalized T-stress along the crack front (e.g., Wang, 2004; Hao and Biao, 2004; Li and Lee, 2004; Kirilyuk and Levchuk, 2007; Zhong and Li, 2008; Viola *et al*., 2008; Liu *et al*., 2012; Rungamornrat and Pinitpanich, 2016; Rungamornrat *et al*., 2018), such derived solutions are of limited uses due mainly to relatively simple settings and assumptions considered when the problems were formulated (e.g., geometries of cracks and bodies, material properties, loading conditions, crack-face conditions, etc.). To circumvent the limitation of analytical procedures, computational packages have been continuously proposed for determining the nonsingular fracture data (e.g., Nakamura and Parks, 1992; Henry and Luxmoore, 1995; Sladek *et al*., 1997; Zhu and Yang, 1999; Fett *et al*., 2006; Tran, 2010; Subsathapol *et al*., 2014; Limwibul *et al*., 2016). Those offered analysis packages commonly consist of two main routines, one associated with the analysis of field equations to obtain primary unknowns and the other corresponding to the post-process of solved data to attain the nonsingular terms along the crack front. The accuracy and computational efficiency of each technique depends primarily on those two routines.

A group of techniques based upon boundary integral equations has been proved efficient for fracture modeling and analysis since the first routine involves field equations of reduced spatial dimensions and primary unknowns are associated with quantities on the boundary of a body and crack surfaces (e.g., Cruse, 1988; Xu and Ortiz, 1993; Li *et al*., 1998; Xu, 2000; Rungamornrat and Mear, 2008b). Such positive feature renders the boundary integral equation methods (BIEMs) computationally attractive when employed to handle evolving cracks. It is important to remark, however, that due to the suppression of primary unknowns to those on the boundary and cracks, field quantities within the domain must be obtained later via the post-process algorithm.

In addition, the extraction of the fracture data such as the intensity factors and nonsingular terms directly from the interior near-front field is non-trivial in terms of computational efficiency and accuracy. For instance, the post-process for the T-stress using the path independent integrals (e.g., Sladek et al., 1997; Shah *et al*., 2005) requires the nontrivial evaluation of interior fields along the computational path. To maintain the benefit of BIEMs, alternative but efficient post-process schemes requiring only information on the crack surface have been sought. Recently, a technique based upon applying the additional displacement integral equation for cracks to determine the sum of the crack-face displacement and using such information to directly post-process for the T-stress was proposed by Tran (2010) and Rungamornrat *et al*. (preparation for publication) for cracks in two- and three-dimensional media, respectively. Such technique was also extended to treat cracks in an elastic half-space (Pham *et al.*, 2015) and cracks in couple-field media (Subsathapol *et al*., 2014; Limwibul *et al*., 2016). While this proposed technique already resolved the post-process issue regarding to the use of interior near-front field, the explicit formula used to extract the information of the T-stress and generalized T-stress still involves derivatives of the sum of the crack-face displacement. It is commonly known from the finite element approximation theory that the post-process for derivatives of approximate solutions can further degrade their accuracy. No evidence, to the best knowledge of the investigator, has been shown in the literature to support further enhancement of such technique. This gap of knowledge is considered significant and it, as a result, provides the underlying motivation of the present study.

1.2 REVIEW OF RELEVANT LITERATURE

In this section, the summary of relevant literatures involving the calculation of nonsingular terms of cracks (e.g., T-stress and generalized T-stress) in both single and couple-field media (e.g., elastic, piezoelectric, and piezoelectromagnetic solids) is reported. In addition to that indicated in the previous section, technical details of each previous work are elaborated as necessary in order to adequately provide the historical background and the current state of the art of this specific discipline. Results from the extensive review are organized into two parts, one associated with analytical techniques

and the development of explicit solutions and the other corresponding to the implementation of computational procedures and post-process algorithms.

Various analytical techniques were proposed in the literature and successfully utilized to derive explicit solutions of the T-stress for cracks in elastic media (e.g., Wang, 2004; Kirilyuk and Levchuk, 2007; Schutte and Molla-Abbasi, 2007; Wang and Chen, 2014; Hua *et al.*, 2015; Rungamornrat and Pinitpanich, 2016) and the generalized T-stress for cracks in piezoelectric media (e.g., Hao and Biao, 2004; Li and Lee, 2004; Zhong and Li, 2008; Viola *et al*., 2008; Liu *et al*., 2012; Rungamornrat *et al*., 2018). In those studies, Stroh formalism, solution representations (e.g., real and complex potential theories) and methods based upon integral transforms (e.g., Hankel integral transform and Fourier integral transform) were mainly employed to obtain basic field quantities and such information in the vicinity of the crack front is then used to obtain the nonsingular fracture data via the post-process algorithm such as the stress difference method (e.g., Wang, 2004) and the formula resulting from the asymptotic near-front expansion (e.g., Rungamornrat and Pinitpanich, 2016; Rungamornrat *et al*., 2018). Derived explicit solutions for simple cracks under certain fundamental loading conditions (e.g., concentrated forces and charges) were further utilized as Green's function to establish post-process formula for computing the T-stress and generalized T-stress of the same crack under general loading conditions (e.g., Fett, 1997; Schutte and Molla-Abbasi, 2007; Rungamornrat and Pinitpanich, 2016; Rungamornrat *et al*., 2018). Other explicit expressions were also proposed based upon the known solutions for certain fundamental cases together with the weight-function technique (e.g., Hua *et al.*, 2015). While a set of explicit solutions/expressions/formula for nonsingular terms was derived, they are clearly of limited uses in the fracture modeling due primarily to the relatively simple and very specific settings considered in the problem formulation. The capability to handling general crack geometry, loading conditions and material properties is an essential issue especially when simulations of crack advances are of interest.

Advance in the development of numerical procedures for the analysis of nonsingular terms of cracks in various types of materials has been continuously grown in the past three decades. The key objective of most of existing studies was to seek a

technique that yields sufficiently accurate results and, at the same time, is computationally robust and user friendly. Methods based upon the finite element approximation have been widely utilized as the basic tool for performing the analysis of basic fields (e.g., displacements and stresses) within the cracked media. Such finite element solutions were then post-processed for the T-stress data along the crack front by various investigators via Eshelby's method, interaction integrals and path independent contour integrals based on Betti-Rayleigh reciprocal theorem (e.g., Cardew *et al.*, 1985; Kfouri, 1986; Nakamura and Parks, 1992; Sladek *et al*., 1997; Zhao *et al.*, 2001; Chen *et al.*, 2001; Kim and Paulino, 2003; Wang, 2003; Wang and Bell, 2004). Other approaches such as the method of Green's function, reciprocal integrals and the weight function scheme (e.g., Sham, 1991; Wang, 2002a; Wang, 2002b; Fett and Rizzi, 2006; Lewis and Wang, 2008) and the method of superposition (e.g. Wang and Bell, 2004; Molla-Abbasi and Schutte, 2008; Meshii *et al.*, 2010) were also utilized along with the finite element results to extract the T-stress solutions for various cases. While the FE-based techniques have circumvented the limited capability of analytical and semi-analytical schemes, the analysis of field problems still requires the discretization of solution over the whole domain and this poses serious issue on computational efficiency and simplicity when used to handle crack evolution. In addition, standard finite element procedure generally requires relatively very fine mesh in the region surrounding the cracks in order to achieve the high accuracy of approximate solutions especially when the fracture data along the crack front is of primary interest (e.g., Ayhan et al., 2006). It is remarked also that the post-process algorithm mentioned above does not directly involve the information of near-front fields and still requires nontrivial evaluation of involved path integrals. The techniques, which directly exercise the near-front solutions such as a boundary-layer method based on the subtraction of tangential stress components (e.g., Lasson and Carlsson, 1973; Leevers and Radon, 1982) and a method using the near-front crack-face displacement (e.g. Al-Ani and Hancock, 1991 ; Ayatollahi *et al.*, 1998) were also recognized. The performance of such two methods when applied to three-dimensional crack problems was investigated by Henry and Luxmoore (1995). Recently, a group of techniques based upon scaled boundary finite element methods which combine both analytical

feature and the finite element approximation was proposed for the analysis of T-stress of cracks in two-dimensional elastic media (e.g., Saputra *et al.,* 2015; Chowdhury *et al.,* 2015). While such numerical procedures reduce one spatial dimension in the discretization and provide a direct mean to calculate the fracture data at the crack tip, their computational efficiency is still questionable when dealing with non-planar and multiple cracks and large scale problems.

Alternative numerical techniques based upon boundary integral equations have been extensively established for solving linear boundary value problems in mechanics (e.g., Liggett and Liu, 1983; Cruse, 1988; Brebbia and Dominguez, 1989) and they have been proved computationally efficient for linear fracture analysis (e.g., Gu and Yew, 1988; Xu and Ortiz, 1993; Li *et al*., 1998; Pan and Yuan, 2000; Xu, 2000; Frangi *et al*., 2002; Ariza and Dominguez, 2004; Rungamornrat and Mear, 2008b,c; Phongtinnaboot *et al*., 2011; Rungamornrat et al., 2015). One of the positive features of those methods is that the key governing equations can be formulated in terms of unknowns on the boundary and the crack surface, thus rendering the reduction of one spatial dimension in the solution discretization procedure. The less number of degrees of freedom is generally required, in comparison with the domain-based schemes such as the finite element method, especially when an unbounded medium is to be treated. In addition, such low dimension of discretization also renders the techniques in this group suitable for simulating crack evolutions. Within the context of linear fracture analysis, studies related to the development and use of boundary integral equation methods in the analysis of nonsingular fracture data along the crack front are significantly less in comparison with those for determining the intensity factors (e.g., Li *et al*., 1998; Xu, 2000; Frangi *et al*., 2002; Rungamornrat and Mear, 2008b,c; Phongtinnaboot *et al*., 2011; Rungamornrat et al., 2015). Results from a careful review of relevant research articles are summarized as follows. Sladek *et al*. (1997) proposed a conventional boundary element method together with the nonsingular integral formula for computing the T-stress of cracks in a two-dimensional, isotropic elastic finite media. In their work, the post-process algorithm still requires the knowledge of the field along a selected path and such data at any point must be obtained before applying the contour integral. Sutradhar and Paulino (2004) developed a hypersingular symmetric Galerkin boundary

element method (SGBEM) to solve cracks in two-dimensional, isotropic, linear elastic infinite and finite bodies. Similar to the work of Sladek *et al*. (1997), the same type of path independent integral was employed to post-process for the T-stress. Later, Yu *et al.* (2006) investigated crack emanating from a circular hole in a two-dimensional, rectangular elastic plate subjected to uniform tension and bending loads. In the analysis, the boundary element method was employed to solve for the key unknowns on the boundary and crack and the M-contour integral scheme was adopted to obtain the T-stress at the crack-tip. Again, in their technique, the additional post-process for stresses within the body must be carried out before applying the contour integral. To enhance the efficiency of the post-process algorithm, Tran (2010) employed the weak-form displacement integral equation for cracks in addition to the weak-form traction integral equation used in the weakly singular symmetric Galerkin boundary element method (SGBEM) to compute the sum of the crack-face displacement. Such additional crack-face data was then employed to compute the T-stress at the crack tip. The explicit formula of the T-stress proposed by Tran (2010) does not require the information of interior fields and the evaluation of any integral but still involves the calculation of derivatives of the sum of the crack-face displacement. Another approach was introduced by Phan (2011) in the analysis of cracks in two-dimensional, elastic infinite and finite bodies. In his work, a hypersingular SGBEM was used to solve the boundary value problem for the boundary data and the relative crack-face displacement, and a novel non-singular boundary integral formula containing only the crack-face displacement data was established and used in the post-process for the T-stress. While such proposed formula does not require the information of elastic fields within the body, the evaluation of all involved integrals over the entire crack can be computationally demanding.

Due to attractive features of the technique proposed by Tran (2010), it was further extended by Rungamornrat et al. (preparation for publication) for cracks in three-dimensional, anisotropic linear elastic infinite media, by Subsathaphol (2013) and Subsathaphol *et al*. (2015) for impermeable cracks in three-dimensional, linear piezoelectric infinite media, and later by Limwibul (2015) and Limwibul *et al*. (2016) to take the influence of different crack-face electrical/mechanical conditions into

account. The generalization to handle cracks in linear elastic half-space under several types of boundary conditions was also recognized in the work of Pham *et al*. (2015). While this particular technique was successfully implemented for various scenarios, the post-process for extracting the T-stress or generalized T-stress data still requires the calculation of derivatives of the sum of the crack-face displacement or generalized displacement along the crack front and this can lead to the degradation of the solution accuracy (e.g., Pham *et al*., 2015). To overcome such difficulty, Tran and Mear (2018) recently proposed an alternative by replacing the weak-form displacement integral equation for cracks by that involving the surface gradient of the sum of the crack-face displacement. Such the novel integral equation can provide the direct crack-face data to be employed in the post-process formula without the requirement for differentiations. While the technique developed by Tran and Mear (2018) is computationally promising for the analysis of nonsingular fracture data, the formulation and implementation are still restricted to cracks in two-dimensional media. The generalization to handle three-dimensional cracks problems for both single and couple-field media has not been recognized in the literature.

1.3 OBJECTIVE

The key objective of the present study is to develop a numerical procedure, based upon a weakly singular boundary integral equation method fully equipped with a direct post-process algorithm, for determining the generalized T-stress of cracks in three-dimensional, linear coupled-field media. The accuracy and efficiency of the developed technique are also investigated.

1.4 SCOPE OF WORK

The present study is conducted within the following framework: (i) a domain containing cracks is infinite and made of a homogeneous, linear couple-field material obeying a linear constitutive law which is expressible in a form similar to Hooke's law of elastic solids, (ii) the law of conservation governing the body flux and the measure of change in the state variable are linear and expressible in a form similar to equilibrium equations and kinematics of linear elasticity, (iii) a volumetric distributed source is absent, (iv)

crack surface is piecewise smooth and subjected to prescribed surface flux, and (v) only the generalized T-stress along the crack front is of interest.

1.5 METHODOLOGY AND PROCEDURE

The proposed research consists of five main tasks including the setup of linear coupled-field boundary value problems, the formulation of governing integral equations for cracked bodies, the implementation of a solution procedure for determining primary unknowns, the post-process for fracture data of interest, and the verification and investigation of the developed technique. The key methodology and procedure to achieve each main task is outlined below.

1.5.1 Setup of linear coupled-field boundary value problems

Basic field equations for linear elasticity (i.e., equilibrium equations, constitutive laws, and strain-displacement relations) are generalized, by simply modifying the definition and dimensions of involving field quantities, to be capable of handling various types of governing physics including both single-field and coupled-field media. A final set of generalized field equations is still of the same form as those for linear elasticity and it equally applies to problems of steady-state heat conduction, steady-state flow in porous media, Laplace's equations, linear elasticity, and linear coupled-field media (e.g., piezoelectric, piezomagnetic, and piezoelectromagnetic materials).

1.5.2 Formulation of governing integral equations for crack body

(1) An integral relation for the state variable within an infinite cracked medium is established first from the basic field equations using Gauss-divergence theorem and Green's functions of the state variable and the body flux. Such integral relation is then used along with the generalized constitutive law to establish the integral relation for the body flux.

(2) A systematic regularization technique, based upon the exchange of derivatives between the kernels and crack-face data using the integration by parts via Stokes' theorem, similar to that proposed by Rungamornrat and Senjuntichai (2009) is

employed to establish singularity-reduced integral representations for both state variable and body flux.

(3) A weakly singular, weak-form integral equation for the crack-face surface flux is established from the integral relation for the body flux using the weight residual technique and the integration by parts via Stokes' theorem. The resulting weak-form integral equation contains only weakly singular kernels and the jump in the crack-face state variable serves as the primary unknowns of this equation.

(4) A weakly singular, weak-form integral equation for the surface gradient of the crack-face state variable is established by first taking limit of the singularity-reduced integral relation for the state variable to point on the crack surface, then forming the surface gradient of the resulting integral equation, and finally employing the weight residual technique along with the integration by parts via Stokes' theorem. The final weak-form integral equation contains only weakly singular kernels and involves both the unknown jump in crack-face state variable and the unknown surface gradient of the sum of the crack-face state variable.

(5) A pair of weakly singular, weak-form integral equations for the crack-face surface flux and the surface gradient of the crack-face state variable constitutes the complete set of integral equations governing the unknown crack-face data.

1.5.3 Implementation of solution procedure

(1) A weakly singular SGBEM (e.g., Rungamornrat and Mear, 2008a,b; Rungamornrat and Senjuntichai, 2009; Phongtinnaboot *et al*., 2011; Rungamornrat et al., 2015) is adopted to solve the weakly singular, weak-form integral equation for the crack-face surface flux for the unknown jump in the crack-face state variable. Special crack-tip elements with the same structure of element shape functions as those proposed by Li et al. (1998) and Rungamornrat and Mear (2008b) are employed to enhance the approximation of the near-front jump in the crack-face state variable. Special quadrature rules are employed to handle both weakly singular and nearly singular double surface integrals resulting from the discretization and the interpolation technique is utilized to avoid the direct evaluation of the contour integral in the calculation of kernels for general coupled-field media.

(2) A standard Galerkin technique and finite element approximation is employed to solve the weakly singular, weak-form integral equation for the surface gradient of the sum of the crack-face state variable. The solved jump in the crack-face state variable serves as the known data in this analysis step. The treatment of all involved nearly singular and weakly singular double surface integrals and the calculation of kernels follow the same procedure as that utilized in the SGBEM.

1.5.4 Post-process for generalized T-stress

(1) A structure of an asymptotic near-front expansion of the body flux is obtained following the same analogy as that employed by William (1957) for cracks in elastic media.

(2) An explicit post-process formula for the generalized T-stress is developed, in terms of the surface gradient of the sum of the state variable along the crack front, using the constitutive relation and the continuity of the finite part of body flux and gradient of the state variable along crack boundary.

1.5.5 Verification and investigation of developed technique

(1) An implemented numerical procedure in terms of an in-house computer code is verified by comparing results with reliable benchmark solutions such as those associated with a penny-shaped crack in elastic and piezoelectric infinite media (e.g., Wang, 2004; Zhao *et al*., 2006; Rungamornrat and Pinitpanich, 2016; Rungamornrat *et al*., 2018).

(2) The convergence behavior of numerical solutions is also investigated via the comparison of results from a series of mesh refinement.

1.6 OUTPUT AND CONTRIBUTION

The merit of the present research relied mainly upon the development and implementation of a novel weakly singular integral equation for the surface gradient of the sum of the crack-face state variable to treat cracks in a relatively broad, three-dimensional setting. The direct post-process algorithm proposed in the present study

for extracting nonsingular fracture data also underpin the capability of the developed technique. The underlying integral formulation which is established in a general framework to handle various types of single-field and coupled-field problems together with a simple post-process algorithm should highlight the novelty and significant contribution of the present work to further enhance the computational technology. In particular, the availability of such the powerful analysis tool should enable the fracture modeling and simulations to be performed in a larger setting. While the development is carried out strictly to cracks in an infinite whole space, results gained from the present study provide a fundamental and sufficient basis for the extension to treat cracks in finite or other types of bodies.

CHAPTER 2
PROBLEM FORMULATION

This chapter mainly presents the formulation of a general boundary value problem and the development of boundary integral equations governing cracks in a general, linear coupled-field infinite medium. A set of basic field equations is established first in a sufficiently general form allowing a variety of problems to be treated and boundary integral relations of Somigliana-type are then developed for the surface of discontinuity embedded in a whole space. A systematic regularization technique is then applied to derive a pair of weakly singular weak-form boundary integral equations governing the unknown crack-face data.

2.1 PROBLEM DESCRIPTION

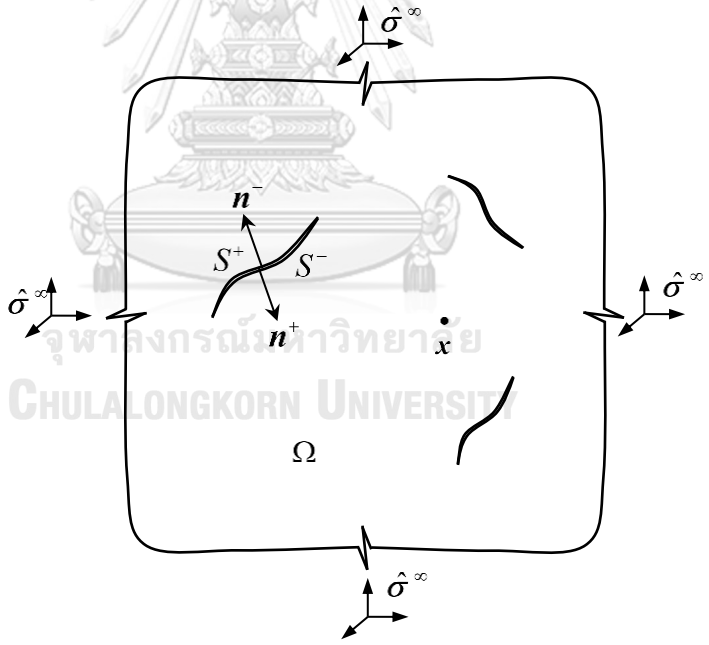

Figure 2.1 Schematic of isolated cracks in linear whole space under crack-face and remote loading

Consider a three-dimensional body Ω occupying a whole Euclidean space $\mathbb{R}^3$ (i.e., $\Omega = \mathbb{R}^3$) as illustrated in Figure 2.1. Let $\{O; x_1, x_2, x_3\}$ be a Cartesian coordinate system with *O* denoting the origin and x_i denoting the coordinate along the direction of a unit

base vector $\boldsymbol{e}_i$. A state of the body is described by a collection of α vector fields $\boldsymbol{u}^{(1)}$, $\boldsymbol{u}^{(2)}$, …, $\boldsymbol{u}^{(\alpha)}$ and β scalar fields $\phi^{[1]}$, $\phi^{[2]}$, …, $\phi^{[\beta]}$ and this collection is termed the state variables. It is remarked that α and β are nonnegative integers and $\alpha+\beta>0$. Components of the state variables referring to the coordinate system $\{O;x_1,x_2,x_3\}$ can be stored, for convenience in further development, in a single $3\alpha+\beta$-component vector $\hat{\boldsymbol{u}}$ such that $u_i^{(k)}=\hat{u}_{3(k)+i-3}$ and $\phi^{[k]}=\hat{u}_{3\alpha+[k]}$. Here and in what follows, lower case indices with the parenthesis range from 1 to α; lower case indices with the bracket range from 1 to β; and lower case indices without the parenthesis and bracket range from 1 to 3. The measure of change of all state variables across the entire body is denoted by a collection of α symmetric second-order tensor fields $\boldsymbol{\varepsilon}^{(1)}$, $\boldsymbol{\varepsilon}^{(2)}$, …, $\boldsymbol{\varepsilon}^{(\alpha)}$ and β vector fields $\boldsymbol{g}^{[1]}$, $\boldsymbol{g}^{[2]}$, …, $\boldsymbol{g}^{[\beta]}$ and these quantities are termed the state-variable variations. In the present study, the state-variable variations are assumed to be linearly related to the state variables by

$$\boldsymbol{\varepsilon}^{(k)}=\frac{1}{2}\left[\nabla\boldsymbol{u}^{(k)}+\nabla^T\boldsymbol{u}^{(k)}\right]\Leftrightarrow\varepsilon_{ij}^{(k)}=\frac{1}{2}\left[\frac{\partial u_i^{(k)}}{\partial x_j}+\frac{\partial u_j^{(k)}}{\partial x_i}\right] \tag{2.1}$$

$$\boldsymbol{g}^{[k]}=\nabla\phi^{[k]}\Leftrightarrow g_i^{[k]}=\frac{\partial\phi^{[k]}}{\partial x_i} \tag{2.2}$$

where ∇ denotes a standard gradient operator and ∇^T denotes its transpose. Consistent with the case of state variables, components of all state-variable variations referring to the coordinate system $\{O;x_1,x_2,x_3\}$ are stored in a single 3x($3\alpha+\beta$)-matrix $\hat{\boldsymbol{\varepsilon}}$ such that $\varepsilon_{ij}^{(k)}=\hat{\varepsilon}_{i:3(k)+j-3}$ and $g_i^{[k]}=\hat{\varepsilon}_{i:3\alpha+k}$ where the semicolon ":" is used here with the only purpose to separate the indices of rows and columns of the matrix. With the definition of $\hat{\boldsymbol{u}}$ and $\hat{\boldsymbol{\varepsilon}}$, the relations (2.1) and (2.3) can be now rewritten in a more concise indicial form as

$$\hat{\varepsilon}_{iJ} = \begin{cases} \dfrac{1}{2}\left[\dfrac{\partial \hat{u}_J}{\partial x_i} + \dfrac{\partial \hat{u}_{3(k)+i-3}}{\partial x_j} \right], & J = 3(k) + j - 3 \le 3\alpha,\ j \in \{1,2,3\} \\ \dfrac{\partial \hat{u}_J}{\partial x_i}, & J > 3\alpha \end{cases} \tag{2.3}$$

where the upper case indices, used here and in what follows, range from 1 to $3\alpha + \beta$. The internal flux induced within the body due to the non-zero state-variable variations (or, equivalently, the nonhomogeneous state variables), termed the body flux, is measured by a collection of α symmetric second-order tensor fields $\boldsymbol{\sigma}^{(1)}$, $\boldsymbol{\sigma}^{(2)}$, …, $\boldsymbol{\sigma}^{(\alpha)}$ and β vector fields $\boldsymbol{s}^{[1]}$, $\boldsymbol{s}^{[2]}$, …, $\boldsymbol{s}^{[\beta]}$. The intensity of the body flux depends primarily on the behavior of a material constituting the body and, in the present study, the following linear constitutive laws are considered:

$$\boldsymbol{\sigma}^{(k)} = \boldsymbol{E}^{(k)(r)}\boldsymbol{\varepsilon}^{(r)} + \boldsymbol{D}^{(k)[r]}\boldsymbol{g}^{(r)} \Leftrightarrow \sigma_{ij}^{(k)} = E_{ijpq}^{(k)(r)}\varepsilon_{pq}^{(r)} + D_{ijp}^{(k)[r]}g_p^{[r]} \tag{2.4}$$

$$\boldsymbol{s}^{[k]} = \boldsymbol{D}^{[k](r)}\boldsymbol{\varepsilon}^{(r)} + \boldsymbol{C}^{[k][r]}\boldsymbol{g}^{(r)} \Leftrightarrow s_i^{[k]} = D_{pqi}^{[k](r)}\varepsilon_{pq}^{(r)} + C_{ip}^{[k][r]}g_p^{[r]} \tag{2.5}$$

where $\boldsymbol{E}^{(k)(r)}$, $\boldsymbol{D}^{(k)[r]}$, and $\boldsymbol{C}^{(k)[r]}$ are fourth-order, third-order, and second-order tensors of material constants, respectively, and repeated indices imply the summation over their range. In addition, the material is postulated to possess following symmetries: $E_{ijpq}^{(k)(r)} = E_{jipq}^{(k)(r)} = E_{ijqp}^{(k)(r)} = E_{pqij}^{(k)(r)}$, $E_{ijpq}^{(k)(r)} = E_{ijpq}^{(r)(k)}$, $D_{ijp}^{(k)[r]} = D_{jip}^{(k)[r]}$, $D_{ijp}^{[k](r)} = D_{jip}^{[k](r)}$, $D_{ijp}^{(k)[r]} = D_{ijp}^{[r][k]}$, $C_{ip}^{[k][r]} = C_{pi}^{[k][r]}$, and $C_{ip}^{[k][r]} = C_{ip}^{[r][k]}$. Components of the body flux can then be stored, in a similar fashion, in a single 3x(3α+β)-matrix $\hat{\boldsymbol{\sigma}}$ such that $\sigma_{ij}^{(k)} = \hat{\sigma}_{i:3(k)+j-3}$ and $s_i^{[k]} = \hat{\sigma}_{i:3\alpha+k}$. By combining the relations (2.1)-(2.2) and the constitutive relations (2.4) and (2.5) and then using the introduced concise notations, it leads to the relation between the body flux and the state variables of the form

$$\hat{\sigma}_{iJ} = \hat{E}_{iJKm}\hat{u}_{K,m} \tag{2.6}$$

where $\hat{E}_{iJKm}$ is termed a generalized moduli and defined in terms of $\boldsymbol{E}^{(k)(r)}$, $\boldsymbol{D}^{(k)[r]}$, and $\boldsymbol{C}^{(k)[r]}$ in a manner consistent with the body flux $\hat{\sigma}_{iJ}$ and the state variable $\hat{u}_K$. It is important to note that due to the symmetric properties of $\boldsymbol{E}^{(k)(r)}$, $\boldsymbol{D}^{(k)[r]}$, and $\boldsymbol{C}^{(k)[r]}$, it

can readily be verified that $\hat{E}_{iJKm} = \hat{E}_{mKJi}$. Finally, the body flux must satisfy the following laws of conservations:

$$\nabla \cdot (\boldsymbol{\sigma}^{(k)})^T + \boldsymbol{b}^{(k)} = \mathbf{0} \Leftrightarrow \sigma_{ij,i}^{(k)} + b_j^{(k)} = 0 \tag{2.7}$$

$$\nabla \cdot \boldsymbol{s}^{[k]} + a^{[k]} = 0 \Leftrightarrow s_{i,i}^{[k]} + a^{[k]} = 0 \tag{2.8}$$

where $\nabla \cdot$ denotes the divergence operator and a collection of α prescribed vector fields $\boldsymbol{b}^{(1)}$, $\boldsymbol{b}^{(2)}$, …, $\boldsymbol{b}^{(\alpha)}$ and β prescribed scalar fields $a^{[1]}$, $a^{[2]}$, …, $a^{[\beta]}$ is termed the distributed body source. By storing components of the distributed body source in a single $3\alpha+\beta$-component vector $\hat{\boldsymbol{b}}$ such that $b_i^{(k)} = \hat{b}_{3(k)+i-3}$ and $a^{[k]} = \hat{b}_{3\alpha+[k]}$, the laws of conservation (2.7) and (2.8) simply reduces in form to

$$\hat{\sigma}_{iJ,i} + \hat{b}_J = 0 \tag{2.9}$$

The field equations (2.3), (2.6) and (2.9) constitute a complete set of equations governing the state variables $\hat{\boldsymbol{u}}$, the state-variable variations $\hat{\boldsymbol{\varepsilon}}$, and the body flux $\hat{\boldsymbol{\sigma}}$.

At any point on a smooth surface, the surface flux described by a collection of α vector fields $\boldsymbol{t}^{(1)}$, $\boldsymbol{t}^{(2)}$, …, $\boldsymbol{t}^{(\alpha)}$ and β scalar fields $d^{[1]}$, $d^{[2]}$, …, $d^{[\beta]}$ can be related to the body flux and the outward unit normal vector to the surface $\boldsymbol{n}$ via the laws of conservation by

$$\boldsymbol{t}^{(k)} = (\boldsymbol{\sigma}^{(k)})^T \boldsymbol{n} \Leftrightarrow t_i^{(k)} = \sigma_{ji}^{(k)} n_j \tag{2.10}$$

$$d^{[k]} = \boldsymbol{s}^{[k]} \boldsymbol{n} \Leftrightarrow d^{[k]} = s_j^{[k]} n_j \tag{2.11}$$

Again, the relations (2.10) and (2.11) can also be expressed in a concise form as

$$\hat{t}_J = \hat{\sigma}_{iJ} n_i \tag{2.12}$$

It is worth noting that the field equations (2.3), (2.6) and (2.9) along with the relation (2.12) and the involved field quantities, via the notation introduced above, are of the same form as that for problems in linear elasticity. In addition, this form of general field equations can be applied to various classes of linear problems via the proper change of the two integers α and β. For instance, field problems governed by Laplace's or generalized Laplace's equation can be handled by setting $\alpha = 0, \beta = 1$; linear elasticity

problems are obtained by taking $\alpha = 1, \beta = 0$; linear piezoelectric and linear piezomagnetic problems are handled by setting $\alpha = 1, \beta = 1$; and linear piezoelectromagnetic are obtained by taking $\alpha = 1, \beta = 2$.

Now, it is ready to further provide the clear description of a problem to be investigated in the present study. The body Ω shown in Figure 2.1 is made of a material obeying the constitutive law (2.6) with the generalized moduli $\hat{E}_{iJKm}$ constant throughout and is free of the distributed body source (i.e., $\hat{b}_J = 0$). The medium contains isolated surfaces across which the state variables experience the jump. The surface of discontinuity is represented by two geometrically identical surfaces S^+ and S^- whose outward unit normal vectors at the coincident points, denoted respectively by $\boldsymbol{n}^+$ and $\boldsymbol{n}^-$, satisfy $\boldsymbol{n}^+ = -\boldsymbol{n}^-$. In the present study, the attention is restricted only to the case that the surface of discontinuity is piecewise smooth, free of the jump in the state variables along its boundary, and subjected to fully prescribed surface flux. From now on, a term "crack" is used, for convenience and establishing the connection to problems in linear elasticity, to designate this type of discontinuity. In addition to the surface flux applied to the crack surface, the body is subjected to the constant remote body flux $\hat{\boldsymbol{\sigma}}^{\infty}$

2.2 STANDARD INTEGRAL RELATIONS

As an essential component in the development of standard integral relations for cracks in an infinite medium, fundamental solutions of an uncracked whole space subjected to a particular distributed body source $\hat{b}_J^P(\boldsymbol{\xi} - \boldsymbol{x}) = \delta_{JP}\delta(\boldsymbol{\xi} - \boldsymbol{x})$ where δ_{JP} denotes the generalized Kronecker symbol and $\delta(\boldsymbol{\xi} - \boldsymbol{x})$ is the Dirac-delta distribution center at $\boldsymbol{x}$ is established first. A system of partial differential equation governing the state-variable fundamental solution $U_J^P(\boldsymbol{\xi} - \boldsymbol{x})$ and the associated body flux $\Lambda_{iJ}^P(\boldsymbol{\xi} - \boldsymbol{x})$ is given by

$$\Lambda_{iJ,i}^P(\boldsymbol{\xi} - \boldsymbol{x}) + \delta_{JP}\delta(\boldsymbol{\xi} - \boldsymbol{x}) = 0 \tag{2.13}$$

$$\Lambda_{iJ}^P(\boldsymbol{\xi} - \boldsymbol{x}) = \hat{E}_{iJKm}U_{K,m}^P(\boldsymbol{\xi} - \boldsymbol{x}) \tag{2.14}$$

By applying the same solution technique via the Radon integral transform suggested by Rungamornrat and Mear (2008a), the state-variable fundamental solution $U_J^P(\boldsymbol{\xi}-\boldsymbol{x})$ can be obtained explicitly as

$$U_J^P(\boldsymbol{\xi}-\boldsymbol{x}) = \frac{1}{8\pi^2 r}\oint_{\boldsymbol{z}\cdot\boldsymbol{r}=0} (\boldsymbol{z},\boldsymbol{z})^{-1}_{JP} ds(\boldsymbol{z}) \tag{2.15}$$

where $\boldsymbol{r}=\boldsymbol{\xi}-\boldsymbol{x}$, $r=\|\boldsymbol{r}\|$, $\boldsymbol{z}$ is a unit vector along the plane $\boldsymbol{z}\cdot\boldsymbol{r}=0$, $(\boldsymbol{z},\boldsymbol{z})$ is a symmetric matrix defined by $(\boldsymbol{z},\boldsymbol{z})_{JP}=z_i E_{iJPj} z_j$, and $(\boldsymbol{z},\boldsymbol{z})^{-1}$ stands for the inverse of $(\boldsymbol{z},\boldsymbol{z})$. The body-flux fundamental solution $\Lambda_{iJ}^P(\boldsymbol{\xi}-\boldsymbol{x})$ can readily be obtained by substituting (2.15) into the constitutive relation (2.14). It is obviously seen that $U_J^P(\boldsymbol{\xi}-\boldsymbol{x})$ and $\Lambda_{iJ}^P(\boldsymbol{\xi}-\boldsymbol{x})$ are singular only at $\boldsymbol{\xi}=\boldsymbol{x}$ of order $1/r$ and $1/r^2$, respectively, and, in addition, $U_J^P(\boldsymbol{\xi}-\boldsymbol{x})=U_P^J(\boldsymbol{\xi}-\boldsymbol{x})$.

By combing (2.6) and (2.9) and setting $\hat{b}_J=0$, it yields a system of partial differential equations governing the state variables of a cracked medium shown in Figure 2.1:

$$\hat{E}_{iJKm}\hat{u}_{K,mi}=0 \tag{2.16}$$

Taking the inner product between (2.16) and $U_J^P(\boldsymbol{\xi}-\boldsymbol{x})$ and then integrating the result over the entire body Ω lead to

$$\int_\Omega U_J^P(\boldsymbol{\xi}-\boldsymbol{x})\hat{E}_{iJKm}\hat{u}_{K,mi}(\boldsymbol{\xi})dV(\boldsymbol{\xi})=0 \tag{2.17}$$

By performing the integration by parts via Gauss-divergence theorem and then using the constitutive law (2.6), it gives rise to

$$\begin{aligned}\int_\Omega \hat{E}_{iJKm}U^P_{J,i}(\boldsymbol{\xi}-\boldsymbol{x})\hat{u}_{K,m}(\boldsymbol{\xi})dV(\boldsymbol{\xi}) &= \int_{S^+} U_J^P(\boldsymbol{\xi}-\boldsymbol{x})\hat{t}_J^+(\boldsymbol{\xi})dS(\boldsymbol{\xi}) + \int_{S^-} U_J^P(\boldsymbol{\xi}-\boldsymbol{x})\hat{t}_J^-(\boldsymbol{\xi})dS(\boldsymbol{\xi}) \\ &\quad + \int_{\partial\Omega} U_J^P(\boldsymbol{\xi}-\boldsymbol{x})\hat{\sigma}_{iJ}(\boldsymbol{\xi})n_i(\boldsymbol{\xi})dS(\boldsymbol{\xi})\end{aligned} \tag{2.18}$$

where $\hat{t}_J^+(\boldsymbol{\xi}) = \hat{\sigma}_{iJ}(\boldsymbol{\xi}) n_i^+(\boldsymbol{\xi})$ and $\hat{t}_J^-(\boldsymbol{\xi}) = \hat{\sigma}_{iJ}(\boldsymbol{\xi}) n_i^-(\boldsymbol{\xi})$ denote the prescribed surface fluxes on the crack surfaces S^+ and S^-, respectively. By recalling the symmetry $\hat{E}_{iJKm} = \hat{E}_{mKJi}$ and (2.14), the relation (2.18) reduces to

$$\begin{aligned}\int_\Omega \Lambda_{mK}^P(\boldsymbol{\xi}-\boldsymbol{x})\hat{u}_{K,m}(\boldsymbol{\xi})dV(\boldsymbol{\xi}) = &\int_{S^+} U_J^P(\boldsymbol{\xi}-\boldsymbol{x})\hat{t}_J^+(\boldsymbol{\xi})dS(\boldsymbol{\xi}) + \int_{S^-} U_J^P(\boldsymbol{\xi}-\boldsymbol{x})\hat{t}_J^-(\boldsymbol{\xi})dS(\boldsymbol{\xi}) \\ &+ \int_{\partial\Omega} U_J^P(\boldsymbol{\xi}-\boldsymbol{x})\hat{\sigma}_{iJ}(\boldsymbol{\xi}) n_i(\boldsymbol{\xi})dS(\boldsymbol{\xi})\end{aligned} \tag{2.19}$$

By performing the integration by parts of the integral on the left hand side via Gauss-divergence theorem, it yields

$$\begin{aligned}\int_\Omega \Lambda_{mK,m}^P(\boldsymbol{\xi}-\boldsymbol{x})\hat{u}_K(\boldsymbol{\xi})dV(\boldsymbol{\xi}) = &-\int_{S^+} U_J^P(\boldsymbol{\xi}-\boldsymbol{x})\hat{t}_J^+(\boldsymbol{\xi})dS(\boldsymbol{\xi}) - \int_{S^-} U_J^P(\boldsymbol{\xi}-\boldsymbol{x})\hat{t}_J^-(\boldsymbol{\xi})dS(\boldsymbol{\xi}) \\ &+ \int_{S^+} \Lambda_{mK}^P(\boldsymbol{\xi}-\boldsymbol{x}) n_m^+(\boldsymbol{\xi})\hat{u}_K^+(\boldsymbol{\xi})dS(\boldsymbol{\xi}) + \int_{S^-} \Lambda_{mK}^P(\boldsymbol{\xi}-\boldsymbol{x}) n_m^-(\boldsymbol{\xi})\hat{u}_K^-(\boldsymbol{\xi})dS(\boldsymbol{\xi}) \\ &- \int_{\partial\Omega} U_J^P(\boldsymbol{\xi}-\boldsymbol{x})\hat{\sigma}_{iJ}(\boldsymbol{\xi}) n_i(\boldsymbol{\xi})dS(\boldsymbol{\xi}) + \int_{\partial\Omega} \Lambda_{mK}^P(\boldsymbol{\xi}-\boldsymbol{x}) n_m(\boldsymbol{\xi})\hat{u}_K(\boldsymbol{\xi})dS(\boldsymbol{\xi})\end{aligned} \tag{2.20}$$

where $\hat{u}_K^+$ and $\hat{u}_K^-$ denote the values of state variables on the crack surfaces S^+ and S^-, respectively. From the definition of the body-flux fundamental solution and properties of δ_{JP} and $\delta(\boldsymbol{\xi}-\boldsymbol{x})$, the integral relation (2.20) becomes

$$\begin{aligned}\hat{u}_P(\boldsymbol{x}) = &\int_{S^+} U_J^P(\boldsymbol{\xi}-\boldsymbol{x})\hat{t}_J^+(\boldsymbol{\xi})dS(\boldsymbol{\xi}) + \int_{S^-} U_J^P(\boldsymbol{\xi}-\boldsymbol{x})\hat{t}_J^-(\boldsymbol{\xi})dS(\boldsymbol{\xi}) \\ &- \int_{S^+} \Lambda_{mK}^P(\boldsymbol{\xi}-\boldsymbol{x}) n_m^+(\boldsymbol{\xi})\hat{u}_K^+(\boldsymbol{\xi})dS(\boldsymbol{\xi}) - \int_{S^-} \Lambda_{mK}^P(\boldsymbol{\xi}-\boldsymbol{x}) n_m^-(\boldsymbol{\xi})\hat{u}_K^-(\boldsymbol{\xi})dS(\boldsymbol{\xi}) \\ &+ \int_{\partial\Omega} U_J^P(\boldsymbol{\xi}-\boldsymbol{x})\hat{\sigma}_{iJ}(\boldsymbol{\xi}) n_i(\boldsymbol{\xi})dS(\boldsymbol{\xi}) - \int_{\partial\Omega} \Lambda_{mK}^P(\boldsymbol{\xi}-\boldsymbol{x}) n_m(\boldsymbol{\xi})\hat{u}_K(\boldsymbol{\xi})dS(\boldsymbol{\xi})\end{aligned} \tag{2.21}$$

By using the remote condition, the identical geometry of S^+ and S^-, $\boldsymbol{n}^+ = -\boldsymbol{n}^-$, and the continuity of $U_J^P(\boldsymbol{\xi}-\boldsymbol{x})$ and $\Lambda_{iJ}^P(\boldsymbol{\xi}-\boldsymbol{x})$ across the cracks, it leads to the integral relation for the state variables

$$\hat{u}_P(\boldsymbol{x}) = \hat{u}_P^\infty(\boldsymbol{x}) + \int_{S^+} U_J^P(\boldsymbol{\xi}-\boldsymbol{x})\Sigma\hat{t}_J(\boldsymbol{\xi})dS(\boldsymbol{\xi}) - \int_{S^+} \Lambda_{mK}^P(\boldsymbol{\xi}-\boldsymbol{x}) n_m^+(\boldsymbol{\xi})\Delta\hat{u}_K(\boldsymbol{\xi})dS(\boldsymbol{\xi}) \tag{2.22}$$

where $\Sigma\hat{t}_J = \hat{t}_J^+ + \hat{t}_J^-$ and $\Delta\hat{u}_K = \hat{u}_K^+ - \hat{u}_K^-$ are the sum of the crack-face surface flux and the jump in the crack-face state variables, respectively. The integral relation (2.22) is of the same form as that of Somigliana's identity. To establish the integral relation for the body flux, the integral relation (2.22) is first substituted into (2.6) and then using the constitutive law, the reciprocity $U_J^P(\boldsymbol{\xi}-\boldsymbol{x}) = U_P^J(\boldsymbol{\xi}-\boldsymbol{x})$, the translational properties $\partial U_J^P/\partial\xi_i = -\partial U_J^P/\partial x_i$ and $\partial\Lambda_{mK}^P/\partial\xi_i = -\partial\Lambda_{mK}^P/\partial x_i$, it finally yields

$$\hat{\sigma}_{iJ}(\boldsymbol{x}) = \hat{\sigma}_{iJ}^{\infty}(\boldsymbol{x}) - \int_{S^+} \Lambda_{iJ}^P(\boldsymbol{\xi}-\boldsymbol{x})\Sigma\hat{t}_P(\boldsymbol{\xi})dS(\boldsymbol{\xi}) + \int_{S^+} \Sigma_{iJ}^{lK}(\boldsymbol{\xi}-\boldsymbol{x})n_l^+(\boldsymbol{\xi})\Delta\hat{u}_K(\boldsymbol{\xi})dS(\boldsymbol{\xi}) \tag{2.23}$$

where the function $\Sigma_{iJ}^{lK}(\boldsymbol{\xi}-\boldsymbol{x})$ is defined by

$$\Sigma_{iJ}^{lK}(\boldsymbol{\xi}-\boldsymbol{x}) = \hat{E}_{iJPm}\frac{\partial\Lambda_{lK}^P(\boldsymbol{\xi}-\boldsymbol{x})}{\partial\xi_m} \tag{2.24}$$

From the singularity behavior of $\Lambda_{iJ}^P(\boldsymbol{\xi}-\boldsymbol{x})$, the function $\Sigma_{iJ}^{lK}(\boldsymbol{\xi}-\boldsymbol{x})$ is singular at $\boldsymbol{\xi}=\boldsymbol{x}$ of order $1/r^3$. It is noted that the integral relation for the state variable (2.22) involves the weakly singular kernel $U_J^P(\boldsymbol{\xi}-\boldsymbol{x})$ and the strongly kernel $\Lambda_{iJ}^P(\boldsymbol{\xi}-\boldsymbol{x})$ whereas the integral relation for the body flux (2.23) contains the strongly singular kernel $\Lambda_{iJ}^P(\boldsymbol{\xi}-\boldsymbol{x})$ and the hypersingular kernel $\Sigma_{iJ}^{lK}(\boldsymbol{\xi}-\boldsymbol{x})$.

2.3 SINGULARITY-REDUCED INTEGRAL RELATIONS

By following the same strategy proposed by Rungamornrat and Mear (2008a), the strongly singular kernel $\Lambda_{iJ}^P(\boldsymbol{\xi}-\boldsymbol{x})$ and the hypersingular kernel $\Sigma_{iJ}^{lK}(\boldsymbol{\xi}-\boldsymbol{x})$ can be decomposed into

$$\Lambda_{iJ}^P(\boldsymbol{\xi}-\boldsymbol{x}) = H_{iJ}^P(\boldsymbol{\xi}-\boldsymbol{x}) + \varepsilon_{ism}\frac{\partial G_{mJ}^P(\boldsymbol{\xi}-\boldsymbol{x})}{\partial\xi_s} \tag{2.25}$$

$$\Sigma_{lK}^{iJ}(\boldsymbol{\xi}-\boldsymbol{x}) = -\hat{E}_{sKJi}\delta(\boldsymbol{\xi}-\boldsymbol{x}) + \varepsilon_{lqm}\frac{\partial}{\partial\xi_q}\varepsilon_{irt}\frac{\partial}{\partial\xi_r}C_{mK}^{tJ}(\boldsymbol{\xi}-\boldsymbol{x}) \tag{2.26}$$

where $G^P_{mJ}(\boldsymbol{\xi}-\boldsymbol{x})$ and $C^{tJ}_{mK}(\boldsymbol{\xi}-\boldsymbol{x})$ are unknown weakly singular functions and $H^P_{iJ}(\boldsymbol{\xi}-\boldsymbol{x})$ is a prescribed function defined by

$$H^P_{iJ}(\boldsymbol{\xi}-\boldsymbol{x}) = -\frac{\delta_{JP}}{4\pi r^3}(\xi_i - x_i) \tag{2.27}$$

The existence of the functions $G^P_{mJ}(\boldsymbol{\xi}-\boldsymbol{x})$ and $C^{tJ}_{mK}(\boldsymbol{\xi}-\boldsymbol{x})$ in the decompositions (2.25) and (2.26) and the corresponding solution procedure follow directly the work of Rungamornrat and Mear (2008a). The explicit expression of $G^P_{mJ}(\boldsymbol{\xi}-\boldsymbol{x})$ and $C^{tJ}_{mK}(\boldsymbol{\xi}-\boldsymbol{x})$ is given by

$$G^P_{mJ}(\boldsymbol{\xi}-\boldsymbol{x}) = \frac{\varepsilon_{mqa}E_{qJKl}}{8\pi^2 r}\oint_{\mathbf{z}\cdot\mathbf{r}=0} z_a z_l (\mathbf{z},\mathbf{z})^{-1}_{KP} ds(\mathbf{z}) \tag{2.28}$$

$$C^{tJ}_{mK}(\boldsymbol{\xi}-\boldsymbol{x}) = \frac{A^{tJPl}_{mKQs}}{8\pi^2 r}\oint_{\mathbf{z}\cdot\mathbf{r}=0} z_s z_l (\mathbf{z},\mathbf{z})^{-1}_{PQ} ds(\mathbf{z}) \tag{2.29}$$

where ε_{mqa} is a standard permutation symbol and the constants A^{tJPl}_{mKQs} are defined in terms of the generalized moduli by

$$A^{tJPl}_{mKQs} = \varepsilon_{ptd}\varepsilon_{pmq}\left\{\hat{E}_{dJPl}\hat{E}_{qKQs} - \frac{1}{3\alpha+\beta}\hat{E}_{lQPs}\hat{E}_{dJKq}\right\} \tag{2.30}$$

It is evident from (2.27), (2.28) and (2.29) that $H^P_{iJ}(\boldsymbol{\xi}-\boldsymbol{x})$, $G^P_{mJ}(\boldsymbol{\xi}-\boldsymbol{x})$ and $C^{tJ}_{mK}(\boldsymbol{\xi}-\boldsymbol{x})$ are singular at $\boldsymbol{\xi}=\boldsymbol{x}$ of order $1/r^2$, $1/r$ and $1/r$, respectively.

By employing the decomposition (2.25) in the integral relation for the state variables (2.22) and then performing the integration by parts of an integral involving the kernel $G^P_{mJ}(\boldsymbol{\xi}-\boldsymbol{x})$ via Stokes' theorem, it leads to an alternative, singularity-reduced integral representation for the state variables:

$$\begin{aligned}\hat{u}_P(\boldsymbol{x}) = \hat{u}^{\infty}_P(\boldsymbol{x}) &+ \int_{S^+} U^P_J(\boldsymbol{\xi}-\boldsymbol{x})\Sigma\hat{t}_J(\boldsymbol{\xi})dS(\boldsymbol{\xi}) - \int_{S^+} H^P_{mJ}(\boldsymbol{\xi}-\boldsymbol{x})n^+_m(\boldsymbol{\xi})\Delta\hat{u}_J(\boldsymbol{\xi})dS(\boldsymbol{\xi}) \\ &+ \int_{S^+} G^P_{mJ}(\boldsymbol{\xi}-\boldsymbol{x})D_m\Delta\hat{u}_J(\boldsymbol{\xi})dS(\boldsymbol{\xi})\end{aligned} \tag{2.31}$$

where $D_m = n_l \varepsilon_{ism} \partial / \partial \xi_s$ is the surface differential operator and the contribution of the line integral along the boundary of the crack vanishes due to the closure condition (i.e., $\Delta \hat{u}_J = 0$ on ∂S^+). Since $H^P_{mJ} n^+_m$ is singular at $\boldsymbol{\xi} = \boldsymbol{x}$ of order $1/r$ (see the work of Xiao, 1998), the integral relation (2.31) involves only weakly singular kernels.

Similarly, the singularity-reduced body-flux integral relation can be derived as follow: first, the decompositions of $\Lambda^P_{iJ}(\boldsymbol{\xi} - \boldsymbol{x})$ and $\Sigma^{lK}_{iJ}(\boldsymbol{\xi} - \boldsymbol{x})$ given by (2.25) and (2.26) are substituted into the body-flux integral relation (2.23); next, an integral containing the kernel $C^{tJ}_{mK}(\boldsymbol{\xi} - \boldsymbol{x})$ is integrated by parts via Stokes' theorem; and, finally, the translational properties of both $G^P_{mJ}(\boldsymbol{\xi} - \boldsymbol{x})$ and $C^{tJ}_{mK}(\boldsymbol{\xi} - \boldsymbol{x})$ are utilized. The resulting integral relation is given by

$$\begin{aligned} \hat{\sigma}_{lK}(\boldsymbol{x}) = \hat{\sigma}^{\infty}_{lK} + \varepsilon_{lrt} \frac{\partial}{\partial x_r} \left\{ \int_{S^+} G^K_{tJ}(\boldsymbol{\xi} - \boldsymbol{x}) \Sigma t_J(\boldsymbol{\xi}) dS(\boldsymbol{\xi}) + \int_{S^+} C^{tK}_{mJ}(\boldsymbol{\xi} - \boldsymbol{x}) D_m \Delta \hat{u}_J(\boldsymbol{\xi}) dS(\boldsymbol{\xi}) \right\} \\ - \int_{S^+} H^J_{lK}(\boldsymbol{\xi} - \boldsymbol{x}) \Sigma t_J(\boldsymbol{\xi}) dS(\boldsymbol{\xi}) \end{aligned} \tag{2.32}$$

It is seen that the alternative, body-flux integral relation (2.32) contains only strongly singular kernels of order $1/r^2$.

A pair of singularity-reduced integral relations (2.31) and (2.32) can be used in the post-process for the state variables and body flux at any interior point and, at the same time, constitutes an essential component in the development of integral equations governing the unknown crack-face data as described in the following chapter.

2.4 WEAKLY SINGULAR WEAK-FORM INTEGRAL EQUATIONS

By taking limit, as point $\boldsymbol{x}$ approaches a smooth point $\boldsymbol{y} \in S^+$, of the state-variable integral relation (2.31) and noting the contribution of a source embedded in the strongly singular kernel $H^P_{iJ}(\boldsymbol{\xi} - \boldsymbol{x})$, it leads to a state-variable integral equation

$$\begin{aligned} \frac{1}{2} \Sigma \hat{u}_P(\boldsymbol{y}) - \hat{u}^{\infty}_P(\boldsymbol{y}) = \int_{S^+} U^P_J(\boldsymbol{\xi} - \boldsymbol{y}) \Sigma \hat{t}_J(\boldsymbol{\xi}) dS(\boldsymbol{\xi}) - \int_{S^+} H^P_{mJ}(\boldsymbol{\xi} - \boldsymbol{y}) n^+_m(\boldsymbol{\xi}) \Delta \hat{u}_J(\boldsymbol{\xi}) dS(\boldsymbol{\xi}) \\ + \int_{S^+} G^P_{mJ}(\boldsymbol{\xi} - \boldsymbol{y}) D_m \Delta \hat{u}_J(\boldsymbol{\xi}) dS(\boldsymbol{\xi}) \end{aligned} \tag{2.33}$$

where $\Sigma\hat{u}_P = \hat{u}_P^+ + \hat{u}_P^-$ denotes the sum of crack-face state variables. The integral equation for the surface gradient of the sum of the crack-face state variable can now be obtained by directly applying the surface differential operator D_s to (2.33) and the final result is given by

$$\frac{1}{2} D_s \Sigma\hat{u}_P(\boldsymbol{y}) - D_s \hat{u}_P^{\infty}(\boldsymbol{y}) = D_s \Psi_P(\boldsymbol{y}) \tag{2.34}$$

where the function $\Psi_P(\boldsymbol{y})$ is defined by

$$\begin{aligned}\Psi_P(\boldsymbol{y}) = &\int_{S^+} U_J^P(\boldsymbol{\xi}-\boldsymbol{y})\Sigma\hat{t}_J(\boldsymbol{\xi})dS(\boldsymbol{\xi}) - \int_{S^+} H_{mJ}^P(\boldsymbol{\xi}-\boldsymbol{y})n_m^+(\boldsymbol{\xi})\Delta\hat{u}_J(\boldsymbol{\xi})dS(\boldsymbol{\xi}) \\ &+ \int_{S^+} G_{mJ}^P(\boldsymbol{\xi}-\boldsymbol{y})D_m\Delta\hat{u}_J(\boldsymbol{\xi})dS(\boldsymbol{\xi})\end{aligned} \tag{2.35}$$

The weak-form statement of (2.33), established by applying a standard weight residual technique, takes the form

$$\begin{aligned}\int_{S^+} \tilde{t}_P(\boldsymbol{y})\left\{\frac{1}{2}\Sigma\hat{u}_P(\boldsymbol{y}) - \hat{u}_P^{\infty}(\boldsymbol{y})\right\}dS(\boldsymbol{y}) = &\int_{S^+} \tilde{t}_P(\boldsymbol{y})\int_{S^+} U_J^P(\boldsymbol{\xi}-\boldsymbol{y})\Sigma\hat{t}_J(\boldsymbol{\xi})dS(\boldsymbol{\xi})dS(\boldsymbol{y}) \\ &- \int_{S^+} \tilde{t}_P(\boldsymbol{y})\int_{S^+} H_{mJ}^P(\boldsymbol{\xi}-\boldsymbol{y})n_m^+(\boldsymbol{\xi})\Delta\hat{u}_J(\boldsymbol{\xi})dS(\boldsymbol{\xi})dS(\boldsymbol{y}) \\ &+ \int_{S^+} \tilde{t}_P(\boldsymbol{y})\int_{S^+} G_{mJ}^P(\boldsymbol{\xi}-\boldsymbol{y})D_m\Delta\hat{u}_J(\boldsymbol{\xi})dS(\boldsymbol{\xi})dS(\boldsymbol{y})\end{aligned} \tag{2.36}$$

where $\tilde{t}_P(\boldsymbol{y})$ is a vector containing sufficiently smooth test functions. The weak-form integral equation (2.35) contains only weakly singular kernels of order $1/r$ and involves two sets of unknown crack-face data, one associated with the sum of the crack-face state variables $\Sigma\hat{u}_P$ and the other corresponding to the jump in the crack-face surface flux $\Delta\hat{u}_J$. An alternative weak-form integral equation for the crack-face data $\Sigma\hat{u}_P$, expressed in terms of its surface gradients $D_s\Sigma\hat{u}_P$, can be established from the integral equation (2.34). Applying the weight residual technique to (2.34) yields

$$\int_{S^+} \tilde{\tau}_{sP}(\boldsymbol{y})\left\{\frac{1}{2} D_s\Sigma\hat{u}_P(\boldsymbol{y}) - D_s\hat{u}_P^{\infty}(\boldsymbol{y})\right\}dS(\boldsymbol{y}) = \int_{S^+} \tilde{\tau}_{sP}(\boldsymbol{y}) D_s\Psi_P(\boldsymbol{y})dS(\boldsymbol{y}) \tag{2.37}$$

where $\tilde{\tau}_{sP}(\boldsymbol{y})$ denotes a collection of sufficiently smooth test functions. Note that the resulting integral equation (2.34) still involves strongly singular kernels due to the surface differential operator D_s. To further regularize such strong singularity, the integral on the right hand side of (2.37) is integrated by parts via Stokes' theorem and the final weak-form equation becomes

$$\int_{S^+} \tilde{\tau}_{sP}(\boldsymbol{y}) \left\{ \frac{1}{2} D_s \Sigma \hat{u}_P(\boldsymbol{y}) - D_s \hat{u}_P^{\infty}(\boldsymbol{y}) \right\} dS(\boldsymbol{y}) = -\int_{S^+} D_s \tilde{\tau}_{sP}(\boldsymbol{y}) \Psi_P(\boldsymbol{y}) dS(\boldsymbol{y}) + \int_{\partial S^+} \tilde{\tau}_{sP}(\boldsymbol{y}) \Psi_P(\boldsymbol{y}) dy_s \quad (2.38)$$

From the structure of $\Psi_P(\boldsymbol{y})$ defined in (2.35), the weak-form integral equation (2.38) is apparently weakly singular in the sense that all involved kernels are singular of order $1/r$. Similar to the integral equation (2.36), the weak-form equation (2.38) contains two sets of unknown crack-face data, the surface gradient of the sum of the crack-face state variables $D_s \Sigma \hat{u}_P$ and the jump in the crack-face surface flux $\Delta \hat{u}_J$.

In the derivation of the weak-form integral equation for the surface flux on the crack, the body-flux integral relation is employed by first forming the product $\hat{\sigma}_{lK}(\boldsymbol{x}) n_l^+(\boldsymbol{y})$ for any smooth point $\boldsymbol{y} \in S^+$ and then taking the limit an interior point $\boldsymbol{x} \to \boldsymbol{y} \in S^+$ to obtain

$$\begin{aligned} \frac{1}{2} \Delta \hat{t}_K(\boldsymbol{y}) - \hat{\sigma}_{lK}^{\infty} n_l^+(\boldsymbol{y}) = D_t \left\{ \int_{S^+} G_{tJ}^K(\boldsymbol{\xi} - \boldsymbol{x}) \Sigma t_J(\boldsymbol{\xi}) dS(\boldsymbol{\xi}) + \int_{S^+} C_{mJ}^{tK}(\boldsymbol{\xi} - \boldsymbol{x}) D_m \Delta \hat{u}_J(\boldsymbol{\xi}) dS(\boldsymbol{\xi}) \right\} \\ - n_l^+(\boldsymbol{y}) \int_{S^+} H_{lK}^J(\boldsymbol{\xi} - \boldsymbol{x}) \Sigma t_J(\boldsymbol{\xi}) dS(\boldsymbol{\xi}) \end{aligned} \quad (2.39)$$

where $\Delta \hat{t}_K = \hat{t}_K^+ - \hat{t}_K^-$ denotes the jump in the crack-face surface flux and the contribution of the source contained in the kernel $H_{lK}^J(\boldsymbol{\xi} - \boldsymbol{x})$ is already taken into account. Taking the inner product between (2.39) and a vector of sufficiently well-behaved test functions $\tilde{v}_K$, then integrating the result over the crack, and finally performing the integration by parts of terms involving the surface differential operator D_t yield

$$\int_{S^+} \tilde{v}_K(\boldsymbol{y}) \left\{ \frac{1}{2} \Delta \hat{t}_K(\boldsymbol{y}) - \hat{\sigma}^{\infty}_{lK} n_l^+(\boldsymbol{y}) \right\} dS(\boldsymbol{y}) = -\int_{S^+} D_t \tilde{v}_K(\boldsymbol{y}) \int_{S^+} G^K_{tJ}(\boldsymbol{\xi} - \boldsymbol{y}) \Sigma t_J(\boldsymbol{\xi}) dS(\boldsymbol{\xi}) dS(\boldsymbol{y})$$
$$- \int_{S^+} D_t \tilde{v}_K(\boldsymbol{y}) \int_{S^+} C^{tK}_{mJ}(\boldsymbol{\xi} - y) D_m \Delta \hat{u}_J(\boldsymbol{\xi}) dS(\boldsymbol{\xi}) dS(\boldsymbol{y}) \quad (2.40)$$
$$- \int_{S^+} \tilde{v}_K(\boldsymbol{y}) \int_{S^+} H^J_{lK}(\boldsymbol{\xi} - \boldsymbol{y}) n_l^+(\boldsymbol{y}) \Sigma t_J(\boldsymbol{\xi}) dS(\boldsymbol{\xi}) dS(\boldsymbol{y})$$

In the development of (2.40), the test functions $\tilde{v}_K$ are chosen specifically to satisfy the same closure condition along the crack boundary as that of $\Delta \hat{u}_J$ and this, as a result, eliminates the contribution of all line integrals resulting from Stokes' theorem. Clearly, the weak-form equation (2.40) contains only weakly singular kernels of order $1/r$ and clearly involves a single set of unknown crack-face data, i.e., the jump in the crack-face state variables.

A pair of weakly singular, weak-form integral equations (2.36) and (2.40) or (2.38) and (2.40) is adequate for formulating a boundary value problem of isolated cracks in a whole space made of general coupled-field materials. Note in particular that those weak-form integral equations involve the unknown sum of and jump in the state variable across the crack surface while containing the prescribed crack-face surface flux, in terms of the sum of and jump in the crack-face surface flux, and the prescribed remote body flux.

CHAPTER 3
SOLUTION IMPLEMENTATIONS

In this chapter, a numerical technique for solving a system of integral equations governing cracks in a general coupled-field whole space is proposed. Components essential for the development of such solution procedure including the solution discretization, evaluation of involved kernels and double surface integrals, and the post-process algorithm for generalized T-stress, are briefly addressed.

3.1 KEY GOVERNING INTEGRAL EQUATIONS

A pair of weakly singular, weak-form integral equations (2.38) and (2.40) derived in Chapter 2 is utilized as the key governing equations of a boundary value problem of cracks in linear coupled-field media. Those integral equations can be re-expressed, in a more concise form suiting further reference and discussion, as

$$\mathcal{D}(\tilde{\boldsymbol{\tau}}, \Sigma\hat{\boldsymbol{u}}) + \mathcal{H}(\tilde{\boldsymbol{\tau}}, \Delta\hat{\boldsymbol{u}}) + \mathcal{G}(\tilde{\boldsymbol{\tau}}, \Delta\hat{\boldsymbol{u}}) = 2\mathcal{D}(\tilde{\boldsymbol{\tau}}, \hat{\boldsymbol{u}}^{\infty}) + \mathcal{U}(\tilde{\boldsymbol{\tau}}, \Sigma\hat{\boldsymbol{t}}) \tag{3.1}$$

$$\mathcal{C}(\tilde{\boldsymbol{v}}, \Delta\hat{\boldsymbol{u}}) = -\bar{\mathcal{D}}(\tilde{\boldsymbol{v}}, \Delta\hat{\boldsymbol{t}}) + 2\bar{\mathcal{D}}(\tilde{\boldsymbol{v}}, \hat{\boldsymbol{\sigma}}^{\infty}\boldsymbol{n}^{+}) - \bar{\mathcal{H}}(\tilde{\boldsymbol{v}}, \Sigma\hat{\boldsymbol{t}}) - \bar{\mathcal{G}}(\tilde{\boldsymbol{v}}, \Sigma\hat{\boldsymbol{t}}) \tag{3.2}$$

where all involved linear and bilinear integral operators are defined, for any $3\alpha+\beta$-component vectors $\boldsymbol{U}$, $\boldsymbol{V}$ and any 3x($3\alpha+\beta$)-matrix $\boldsymbol{T}$, by

$$\mathcal{D}(\boldsymbol{T}, \boldsymbol{V}) = \frac{1}{2}\int_{S^+} T_{sP}(\boldsymbol{y}) D_s V_P(\boldsymbol{y}) dS(\boldsymbol{y}) \tag{3.3}$$

$$\bar{\mathcal{D}}(\boldsymbol{U}, \boldsymbol{V}) = \frac{1}{2}\int_{S^+} U_K(\boldsymbol{y}) V_K(\boldsymbol{y}) dS(\boldsymbol{y}) \tag{3.4}$$

$$\begin{aligned}\mathcal{U}(\boldsymbol{T}, \boldsymbol{V}) = &\int_{\partial S^+} T_{sP}(\boldsymbol{y}) \int_{S^+} U_J^P(\boldsymbol{\xi} - \boldsymbol{y}) V_J(\boldsymbol{\xi}) dS(\boldsymbol{\xi}) dy_s \\ &- \int_{S^+} D_s T_{sP}(\boldsymbol{y}) \int_{S^+} U_J^P(\boldsymbol{\xi} - \boldsymbol{y}) V_J(\boldsymbol{\xi}) dS(\boldsymbol{\xi}) dS(\boldsymbol{y})\end{aligned} \tag{3.5}$$

$$\mathcal{C}(\boldsymbol{U}, \boldsymbol{V}) = \int_{S^+} D_t U_K(\boldsymbol{y}) \int_{S^+} C_{mJ}^{tK}(\boldsymbol{\xi} - \boldsymbol{x}) D_m V_J(\boldsymbol{\xi}) dS(\boldsymbol{\xi}) dS(\boldsymbol{y}) \tag{3.6}$$

$$\mathcal{H}(\boldsymbol{T},\boldsymbol{V}) = \int_{\partial S^+} T_{sP}(\boldsymbol{y}) \int_{S^+} H^P_{mJ}(\boldsymbol{\xi}-\boldsymbol{y}) n^+_m(\boldsymbol{\xi}) V_J(\boldsymbol{\xi}) dS(\boldsymbol{\xi}) dy_s - \int_{S^+} D_s T_{sP}(\boldsymbol{y}) \int_{S^+} H^P_{mJ}(\boldsymbol{\xi}-\boldsymbol{y}) n^+_m(\boldsymbol{\xi}) V_J(\boldsymbol{\xi}) dS(\boldsymbol{\xi}) dS(\boldsymbol{y}) \tag{3.7}$$

$$\bar{\mathcal{H}}(\boldsymbol{U},\boldsymbol{V}) = \int_{S^+} U_K(\boldsymbol{y}) \int_{S^+} H^J_{lK}(\boldsymbol{\xi}-\boldsymbol{y}) n^+_l(\boldsymbol{y}) V_J(\boldsymbol{\xi}) dS(\boldsymbol{\xi}) dS(\boldsymbol{y}) \tag{3.8}$$

$$\mathcal{G}(\boldsymbol{T},\boldsymbol{V}) = \int_{S^+} D_s T_{sP}(\boldsymbol{y}) \int_{S^+} G^P_{mJ}(\boldsymbol{\xi}-\boldsymbol{y}) D_m V_J(\boldsymbol{\xi}) dS(\boldsymbol{\xi}) dS(\boldsymbol{y}) - \int_{\partial S^+} T_{sP}(\boldsymbol{y}) \int_{S^+} G^P_{mJ}(\boldsymbol{\xi}-\boldsymbol{y}) D_m V_J(\boldsymbol{\xi}) dS(\boldsymbol{\xi}) dy_s \tag{3.9}$$

$$\bar{\mathcal{G}}(\boldsymbol{U},\boldsymbol{V}) = \int_{S^+} D_t U_K(\boldsymbol{y}) \int_{S^+} G^K_{tJ}(\boldsymbol{\xi}-\boldsymbol{y}) V_J(\boldsymbol{\xi}) dS(\boldsymbol{\xi}) dS(\boldsymbol{y}) \tag{3.10}$$

It is evident that the weak-form integral equation (3.1) involve two sets of unknown crack-face data (i.e., the sum of the crack-face state variables $\Sigma\hat{\boldsymbol{u}}$ which appear in terms of its surface gradients and the jump in the crack-face state variables $\Delta\hat{\boldsymbol{u}}$) and two sets of prescribed data (i.e., the state variables $\hat{\boldsymbol{u}}^\infty$ associated with the prescribed remote body flux $\hat{\boldsymbol{\sigma}}^\infty$ and the sum of the crack-face surface flux $\Sigma\hat{\boldsymbol{t}}$). Unlike (3.1), the weak-form integral equation (3.2) contains only the unknown jump in the crack-face state variables $\Delta\hat{\boldsymbol{u}}$ and the prescribed data associated with the crack-face surface flux $\Sigma\hat{\boldsymbol{t}}$, $\Delta\hat{\boldsymbol{t}}$ and the remote body flux $\hat{\boldsymbol{\sigma}}^\infty$. Due to the one-way coupling feature of (3.1) and (3.2), it is clearly inefficient to solve this system of equations simultaneously. In the present study, the weak-form equation (3.2) will be solved first to obtain the unknown crack-face data $\Delta\hat{\boldsymbol{u}}$ and such solution will serves as the known information in the weak-form equation (3.1). The other set of unknown crack-face data, the surface gradients of $\Sigma\hat{\boldsymbol{u}}$, can subsequently be obtained by solving (3.1). It should be clear from (2.31) and (2.32) that once the jump in the crack-face state variables $\Delta\hat{\boldsymbol{u}}$ is solved, the state variables and the body flux at any interior point of the medium can be calculated from those integral formulae. In addition, by following the same strategy proposed by Rungamornrat and Mear (2008b,c) and Rungamornrat and Senjuntichai (2009), the solved data $\Delta\hat{\boldsymbol{u}}$ can be further employed to extract the information of the intensity factors along the edge of the crack. In the post-process of those quantities, the

information of $\Sigma\hat{\boldsymbol{u}}$ and its surface gradients is clearly not required and, as a result, the weak-form integral equation (3.1) is not necessary to be solved. In the present study, the crack-face data $\Sigma\hat{\boldsymbol{u}}$ is of primary interest since such information can be further exploited to directly extract the information of the generalized T-stress along the boundary of the crack.

3.2 SOLUTION PROCEDURE FOR $\Delta\hat{\boldsymbol{u}}_J$

The weakly singular, symmetric Galerkin boundary element method (SGBEM) similar to that reported by Li et al. (1998), Rungamornrat and Mear (2008b,c), and Rungamornrat and Senjuntichai (2009) is extended to solve the weak-form integral equation (3.2) for the unknown jump in the crack-face state variables $\Delta\hat{u}_J$. The solution discretization follows directly the Galerkin strategy and standard finite element approximation; more specifically, the test function $\tilde{v}_K$ and the trial function $\Delta\hat{u}_J$ are discretized as

$$\Delta\hat{u}_J(\xi)=\sum_{h=1}^{N}\Delta u_J^{*(h)}\phi^{(h)}(\xi);\qquad \tilde{v}_K(\mathbf{y})=\sum_{h=1}^{N}v_K^{*(h)}\phi^{(h)}(\mathbf{y}) \tag{3.11}$$

where $\Delta u_J^{*(h)}$ are nodal degrees of freedom associated with the h^{th} node; $v_K^{*(h)}$ are arbitrary nodal constants associated with the h^{th} node; $\phi^{(h)}$ denotes the nodal basis functions associated with the h^{th} node; and N is the number of nodes resulting from the discretization. By substituting (3.11) into (3.2) and then employing the arbitrariness of $v_K^{*(h)}$, it yields a system of linear algebraic equations

$$\mathbf{C}\Delta\mathbf{U}=\mathbf{D}^{\infty}-\mathbf{D}^{\mathbf{0}}-\mathbf{H}^{\mathbf{0}}-\mathbf{G}^{\mathbf{0}} \tag{3.12}$$

where $\Delta\mathbf{U}$ is a vector consisting of unknown nodal degrees of freedom defined by $[\Delta\mathbf{U}]_{\rho(h-1)+J}=\Delta u_J^{*(h)}$ with $\rho=3\alpha+\beta$ and the coefficient matrix $\mathbf{C}$ and the known vectors $\mathbf{D}^{\infty},\mathbf{D}^{0},\mathbf{H}^{0},\mathbf{G}^{0}$ are given by

$$[\mathbf{C}]_{\rho(h-1)+K,\rho(r-1)+J}=\int_{S^+}D_t\phi^{(h)}(\boldsymbol{y})\int_{S^+}C_{mJ}^{tK}(\boldsymbol{\xi}-\boldsymbol{x})D_m\phi^{(r)}(\boldsymbol{\xi})dS(\boldsymbol{\xi})dS(\boldsymbol{y}) \tag{3.13}$$

$$[\mathbf{D}^{\infty}]_{\rho(h-1)+K} = \int_{S^+} \phi^{(h)}(\boldsymbol{y})\hat{\sigma}^{\infty}_{lK} n^+_l(\boldsymbol{y}) dS(\boldsymbol{y}) \tag{3.14}$$

$$[\mathbf{D}^{0}]_{\rho(h-1)+K} = \frac{1}{2}\int_{S^+} \phi^{(\mathrm{h})}(\boldsymbol{y})\Delta\hat{t}_K(\boldsymbol{y}) dS(\boldsymbol{y}) \tag{3.15}$$

$$[\mathbf{H}^{0}]_{\rho(h-1)+K} = \int_{S^+} \phi^{(h)}(\boldsymbol{y}) \int_{S^+} H^J_{lK}(\boldsymbol{\xi}-\boldsymbol{y}) n^+_l(\boldsymbol{y}) \Sigma\hat{t}_J(\boldsymbol{\xi}) dS(\boldsymbol{\xi}) dS(\boldsymbol{y}) \tag{3.16}$$

$$[\mathbf{G}^{0}]_{\rho(h-1)+K} = \int_{S^+} D_t\phi^{(h)}(\boldsymbol{y}) \int_{S^+} G^K_{tJ}(\boldsymbol{\xi}-\boldsymbol{y}) \Sigma\hat{\boldsymbol{t}}_J(\boldsymbol{\xi}) dS(\boldsymbol{\xi}) dS(\boldsymbol{y}) \tag{3.17}$$

In particular, nodal basis functions generated systematically by a finite element mesh are employed and a near-front approximation of $\Delta\hat{u}_J$ is enhanced by using special crack-tip elements proposed by Li *et al*. (1998) and Rungamornrat and Mear (2008b) for cracks in elastic media and by Rungamornrat and Mear (2008c) for cracks in piezoelectric media. To construct a system of linear algebraic equations resulting from the solution discretization, the evaluation of all involved kernels and all types of double surface integrals are properly treated using the strategy described in Rungamornrat and Mear (2008b) and Xiao (1998), respectively. The linear solution of such the system is then obtained via a preconditioning conjugate gradient algorithm.

3.3 SOLUTION PROCEDURE FOR $\Sigma\hat{\boldsymbol{u}}_J$

Once the jump in the crack-face state variables $\Delta\hat{u}_J$ is solved, it is then substituted into (3.1) and the resulting weak-form equation contains the only unknown in terms of the surface gradients of $\Sigma\hat{\boldsymbol{u}}$, i.e., $D_s\Sigma\hat{u}_P$. Note, in addition, that the bilinear operator $\boldsymbol{\mathcal{D}}$ is not only kernel free but also defined in terms of a single surface integral. To solve this weak-form integral equation, a standard procedure based on Galerkin technique and finite element approximation is adopted. In particular, the test function $\tilde{\tau}_{sP}$ and trial function $D_s\Sigma\hat{u}_P$ are approximated by

$$D_s\Sigma\hat{u}_P(\mathbf{y}) - 2D_s\hat{u}^{\infty}_P(\mathbf{y}) = \tilde{D}_s\Sigma\tilde{u}_P(\mathbf{y}) \approx \sum_{h=1}^{N} (D\Sigma\hat{u})^{*(h)}_{sP}\phi^{(h)}(\mathbf{y}); \quad \tilde{\tau}_{sP}(\mathbf{y}) = \sum_{h=1}^{N} \tau^{*(h)}_{sP}\phi^{(h)}(\mathbf{y}) \tag{3.18}$$

where $D_s\Sigma\tilde{u}_P$ denotes the surface gradient of the sum of the crack-face state variable less that inducing by the remote loading in the un-cracked case; $\phi^{(h)}$ denotes the nodal basis shape function associated with the h^{th} node; $(D\Sigma\tilde{u})_{sP}^{*(h)}$ are unknown nodal quantities associated with the h^{th} node; and $\tau_{sP}^{*(h)}$ are arbitrary constants corresponding to the h^{th} node. Due to the regular behavior of $D_s\Sigma\tilde{u}_P$ on the entire crack surface, continuous basis functions constructed on a mesh of standard isoparametric elements are utilized in the approximation of both solution and test functions. By substituting (3.18) into (3.1), it results in

$$\mathbf{K}[\mathbf{D\Sigma U}] = \mathbf{T}^o - \mathbf{B\Delta U} \tag{3.19}$$

where $\mathbf{D\Sigma U}$ isa vector of nodal unknowns defined by $[\mathbf{D\Sigma U}]_{3\rho(r-1)+\rho(J-1)+k} = (D\Sigma\hat{u})_{kJ}^{*(r)}$ and the coefficient matrices $\mathbf{K}$, $\mathbf{B}$ and the known vector $\mathbf{T}^0$ are defined by

$$[\mathbf{K}]_{3\rho(h-1)+\rho(P-1)+s,3\rho(r-1)+\rho(J-1)+k} = \frac{1}{2}\int_{S^+} \psi^{(h)}(\boldsymbol{y})\psi^{(r)}(\boldsymbol{y})\delta_{sk}\delta_{PJ}\,dS(\boldsymbol{y}) \tag{3.20}$$

$$\begin{aligned}[\boldsymbol{T}^0]_{3\rho(h-1)+\rho(P-1)+s} = {} & \frac{1}{2}\int_{\partial S^+} \psi^{(h)}(\boldsymbol{y})\int_{S^+} U_J^P(\boldsymbol{\xi}-\boldsymbol{y})\Sigma\hat{\boldsymbol{t}}_J(\boldsymbol{\xi})\,dS(\boldsymbol{\xi})\,dy_s \\ & - \int_{S^+} D_s\psi^{(h)}(\boldsymbol{y})\int_{S^+} U_J^P(\boldsymbol{\xi}-\boldsymbol{y})\Sigma\hat{\boldsymbol{t}}_J(\boldsymbol{\xi})\,dS(\boldsymbol{\xi})\,dS(\boldsymbol{y})\end{aligned} \tag{3.21}$$

$$\begin{aligned}[\boldsymbol{B}]_{3\rho(h-1)+\rho(P-1)+s,\rho(r-1)+J} = {} & \int_{\partial S^+} \psi^{(h)}(\boldsymbol{y})\int_{S^+} H_{mJ}^P(\boldsymbol{\xi}-\boldsymbol{y})n_m^+(\boldsymbol{\xi})\psi^{(r)}(\boldsymbol{\xi})\,dS(\boldsymbol{\xi})\,dy_s \\ & - \int_{S^+} D_s\psi^{(h)}(\boldsymbol{y})\int_{S^+} H_{mJ}^P(\boldsymbol{\xi}-\boldsymbol{y})n_m^+(\boldsymbol{\xi})\psi^{(r)}(\boldsymbol{\xi})\,dS(\boldsymbol{\xi})\,dS(\boldsymbol{y}) \\ & + \int_{S^+} D_s\psi^{(h)}(\boldsymbol{y})\int_{S^+} G_{mJ}^P(\boldsymbol{\xi}-\boldsymbol{y})D_m\psi^{(r)}\,dS(\boldsymbol{\xi})\,dS(\boldsymbol{y}) \\ & - \int_{\partial S^+} \psi^{(h)}(\boldsymbol{y})\int_{S^+} G_{mJ}^P(\boldsymbol{\xi}-\boldsymbol{y})D_m\psi^{(r)}\,dS(\boldsymbol{\xi})\,dy_s\end{aligned} \tag{3.22}$$

According to (3.20), it is clear that the coefficient matrix $\mathbf{K}$ is symmetric. The numerical integration of both path and surface integrals follows the same strategy as that reported by Rungamornrat and Mear (2008b) and Limwibul *et al*. (2016). Certain components used in the development of SGBEM are also adopted, here, to treat the

double surface integrals containing the prescribed or solved data. The resulting system of linear algebraic equations (3.19) is then solved by the preconditioning conjugate gradient.

3.4 POST-PROCESS FOR GENERALIZED T-STRESS

Once the surface gradient of the sum of the crack-face state variables ($D_s\Sigma\hat{u}_P$) is solved, a generalized T-stress, defined as the finite part of the body flux along the boundary of the crack, can be determined from this set of data as described below.

Let $\boldsymbol{x}_c$ denote a nodal point located at the crack boundary and $\{\boldsymbol{x}_c;\bar{x}_1,\bar{x}_2,\bar{x}_3\}$ be a local Cartesian coordinate system with the origin at $\boldsymbol{x}_c$ and the unit base vectors $\{\bar{\boldsymbol{e}}_1,\bar{\boldsymbol{e}}_2,\bar{\boldsymbol{e}}_3\}$ as shown in Figure 3.1. In particular, $\bar{\boldsymbol{e}}_2=-\boldsymbol{n}^+$ whereas $\bar{\boldsymbol{e}}_3$ and $\bar{\boldsymbol{e}}_1$ are chosen tangent and normal to the crack-front at $\boldsymbol{x}_c$, respectively. By extending the work of Subsathaphol *et al*. (2015) and Limwibul *et al*. (2016), the nonsingular part of the body flux along the boundary of the crack, represented by a collection of α symmetric second-order tensors $T_{ij}^{(1)}$, $T_{ij}^{(2)}$, …, $T_{ij}^{(\alpha)}$ and β vectors $Q_i^{[1]}$, $Q_i^{[2]}$, …, $Q_i^{[\beta]}$ can be related to the finite part of the state-variable variation at the same point, denoted by a collection of α symmetric second-order tensors $\bar{\varepsilon}_{ij}^{0(1)}$, $\bar{\varepsilon}_{ij}^{0(2)}$, …, $\bar{\varepsilon}_{ij}^{0(\alpha)}$ and β vectors $\bar{g}_i^{0[1]}$, $\bar{g}_i^{0[2]}$, …, $\bar{g}_i^{0[\beta]}$, via the constitutive relations (2.4) and (2.5), i.e.,

$$T_{ij}^{(k)}=\bar{E}_{ijpq}^{(k)(r)}\bar{\varepsilon}_{pq}^{0(r)}+\bar{D}_{ijp}^{(k)[r]}\bar{g}_p^{0[r]} \tag{3.23}$$

$$Q_i^{[k]}=\bar{D}_{pqi}^{[k](r)}\bar{\varepsilon}_{pq}^{0(r)}+\bar{C}_{ip}^{[k][r]}\bar{g}_p^{0[r]} \tag{3.24}$$

where the “bar” superscript is used to designate components in the local coordinate system $\{\boldsymbol{x}_c;\bar{x}_1,\bar{x}_2,\bar{x}_3\}$. From the continuity of the finite part of the body flux at the point $\boldsymbol{x}_c$, it can be verified that the following out-of-plane components $\{T_{12}^{(1)},T_{22}^{(1)},T_{23}^{(1)}\}$, $\{T_{12}^{(2)},T_{22}^{(2)},T_{23}^{(2)}\}$, …, $\{T_{12}^{(\alpha)},T_{22}^{(\alpha)},T_{23}^{(\alpha)}\}$ and $Q_2^{[1]}$, $Q_2^{[2]}$, …, $Q_2^{[\beta]}$ are known and can be obtained in terms of the prescribed surface flux on the crack at $\boldsymbol{x}_c$. The remaining

components, i.e., $\{T_{11}^{(1)}, T_{33}^{(1)}, T_{13}^{(1)}\}$, $\{T_{11}^{(2)}, T_{33}^{(2)}, T_{13}^{(2)}\}$, …, $\{T_{11}^{(\alpha)}, T_{33}^{(\alpha)}, T_{13}^{(\alpha)}\}$ and $\{Q_1^{[1]}, Q_3^{[1]}\}$, $\{Q_1^{[2]}, Q_3^{[2]}\}$, …, $\{Q_1^{[\beta]}, Q_3^{[\beta]}\}$ are unknown a priori and termed, here, the generalized T-stress components. From the relations (2.1) and (2.2), the finite part of the state-variable variations are related to the sum of the crack-face state variables at the point x_c by

$$\bar{\varepsilon}_{ij}^{0(k)} = \frac{1}{4}\left[\frac{\partial \Sigma \bar{u}_i^{(k)}}{\partial \bar{x}_j} + \frac{\partial \Sigma \bar{u}_j^{(k)}}{\partial \bar{x}_i}\right] \tag{3.25}$$

$$\bar{g}_i^{0[k]} = \frac{1}{2}\frac{\partial \Sigma \bar{\phi}^{[k]}}{\partial \bar{x}_i} \tag{3.26}$$

By first applying the coordinate transformation to the solved data $D_s \Sigma \hat{u}_P$ in the global coordinate system, it leads to the surface gradients $\bar{D}_s \Sigma \bar{\hat{u}}_P$ defined in the local coordinate system $\{x_c; \bar{x}_1, \bar{x}_2, \bar{x}_3\}$. The in-plane components of $\bar{\varepsilon}_{ij}^{0(k)}$ and $\bar{g}_i^{0[k]}$ (i.e., $\{\bar{\varepsilon}_{11}^{0(k)}, \bar{\varepsilon}_{33}^{0(k)}, \bar{\varepsilon}_{13}^{0(k)}\}$ and $\{\bar{g}_1^{0[k]}, \bar{g}_3^{0[k]}\}$) can then be obtained directly from the information $\bar{D}_s \Sigma \bar{\hat{u}}_P$; by following relations below:

$$\bar{\varepsilon}_{11}^{0(k)} = \frac{1}{2}\bar{a}_{3s}\bar{a}_{1P} D_s \Sigma \hat{u}_{3(k)+P-3} \tag{3.27}$$

$$\bar{\varepsilon}_{33}^{0(k)} = -\frac{1}{2}\bar{a}_{1s}\bar{a}_{3P} D_s \Sigma \hat{u}_{3(k)+P-3} \tag{3.28}$$

$$\bar{\varepsilon}_{13}^{0(k)} = \frac{1}{4}(\bar{a}_{3s}\bar{a}_{3P} D_s \Sigma \hat{u}_{3(k)+P-3} - \bar{a}_{1s}\bar{a}_{1P} D_s \Sigma \hat{u}_{3(k)+P-3}) \tag{3.29}$$

$$\bar{g}_1^{0[k]} = \frac{1}{2}\bar{a}_{3s} D_s \Sigma \hat{u}_{3\alpha+[k]} \tag{3.30}$$

$$\bar{g}_3^{0[k]} = -\frac{1}{2}\bar{a}_{1s} D_s \Sigma \hat{u}_{3\alpha+[k]} \tag{3.31}$$

where $\bar{a}_{ij}$ denotes the cosine of the angle between i^{th} and j^{th} coordinate axis. By combing the known information of the in-plane components of the finite part of the state-variable variation and the out-of-plane components of the finite part of the body

flux, (3.23) and (3.24) yield a system of linear algebraic equations sufficient for determining the generalized T-stress components. According to (3.27)-(3.21), It clearly seen that the surface gradient of sum of crack-face state variable can be directly used for obtaining the generalized T-stresses by using generalized constitutive relations that without additional approximation in the post-process procedure.

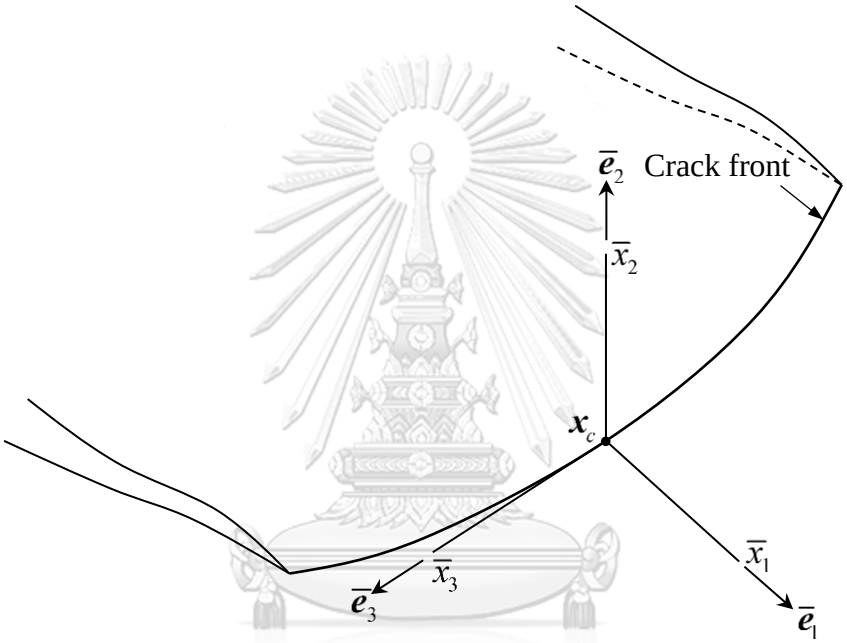

Figure 3.1 Schematic of crack boundary and local coordinate system used for calculating generalized T-stress

CHAPTER 4
NUMERICAL RESULTS AND DISCUSSIONS

This chapter presents numerical results of the generalized T-stresses obtained from the proposed technique. Computational performance including the accuracy and convergence is carefully investigated through various examples involving both linear single and couple-field media. Various type of loading conditions (e.g., uniformly distributed crack-face loading, linearly distributed crack-face loading, and uniform remote loading) and planar, non-planar and multiple cracks are considered in the numerical study to demonstrate the capability and versatility of the technique. As the essential step in the verification of the integral formulation and the implementation of solution procedure and post-process algorithm for determining the generalized T-stress, results for a penny-shaped crack in both single and couple-field media are obtained and then compared with reliable benchmark solutions. Then, results for more complicated fracture problems involving non-planar and multiple cracks are reported.

In the numerical study, standard 6-node and 8-node isoparametric C^0-elements are employed to discretize both the sum of and jump in the crack-face generalized displacement on the majority of the crack surface whereas standard 9-node isoparametric C^0-elements and special 9-node crack-tip elements are utilized to discretize, respectively, the sum of and jump in the crack-face generalized displacement in a region adjacent to the crack front. A series of meshes, with significant difference of element size, is adopted to investigate the convergence of numerical solutions. Three representative material models including a transversely isotropic linear elastic material (Mat-1), a transversely isotropic linear piezoelectric material (Mat-2), and a transversely isotropic linear piezoelectromagnetic material (Mat-3) with all material parameters given in Tables 4.1-4.3 are utilized in the numerical simulations.

Table 4.1 Material parameters of a representative transversely isotropic linear elastic material (Mat-1) used in numerical study (Watanavit and Rungamornrat, 2017)

Elastic constants (x 10^9 Pa)	E_{1111}	126.00
	E_{1122}	55.00
	E_{1133}	53.00
	E_{3333}	117.00
	E_{1313}	35.30

Table 4.2 Material parameters of a representative transversely isotropic linear piezoelectric material (Mat-2) used in numerical study (Phongtinnaboot *et al*., 2011)

Elastic constants (x 10^9 Pa)	E_{1111}	126.00
	E_{1122}	55.00
	E_{1133}	53.00
	E_{3333}	117.00
	E_{1313}	35.30
Piezoelectric constants (C/m^2)	E_{1134}	-6.50
	E_{3334}	23.30
	E_{1314}	17.00
Dielectric permittivities (x 10^{-9} C/(Vm))	$-E_{1414}$	15.10
	$-E_{3434}$	13.00

Table 4.3 Material parameters of a representative transversely isotropic linear piezoelectromagnetic material $BaTiO_3$-$CoFe_2O_4$ (Mat-3) used in numerical study (Sladek *et al*., 2008)

Elastic constants (x 10^9 Pa)	E_{1111}	226.00
	E_{1122}	125.00
	E_{1133}	124.00
	E_{3333}	216.00
	E_{2323}	44.00
Piezoelectric constants (C/m^2)	E_{1134}	-2.20
	E_{3334}	9.30
	E_{1314}	5.80
Piezomagnetic constants (N/Am)	E_{1135}	290.00
	E_{3335}	350.00
	E_{1315}	275.00
Magneto-electric coefficients (x 10^{-12} Ns/(Am))	$-E_{1415}$	5.37
	$-E_{3435}$	2737.50
Dielectric permittivities (x 10^{-10} C/(Vm))	$-E_{1414}$	56.40
	$-E_{3434}$	63.50
Magnetic permittivities (x 10^{-6} $Ns^2/(C^2)$)	$-E_{1515}$	297.00
	$-E_{3535}$	83.50

4.1 VERIFICATION

In order to verify the proposed technique, simple crack problems with available analytical solution are considered. From an extensive literature survey, it has been found that the closed form solutions of the generalized T-stresses of an isolated penny-shaped crack were reported by Rungamornrat and Pinitpanich (2016) for a transversely isotropic linear elastic infinite medium and by Rungamornrat *et al.* (2018) for a transversely isotropic linear piezoelectric medium. For the case of a penny-shaped crack embedded in a transversely isotropic linear piezoelectromagnetic medium, the

complete field was obtained by Zhao *et al*. (2006) and such results can then be used to directly post-process for the generalized T-stress via the technique proposed by Rungamornrat and Pinitpanich (2016) and Rungamornrat *et al*. (2018). Solutions for those three cases constitute the sufficient basis for the verification of the present technique.

Consider a penny shaped crack of radius a embedded in a whole space with the axis of material symmetry directing perpendicular to the plane of the crack as shown in Figure 4.1. The crack front is parameterized by

$$x_1 = a\cos\theta,\ x_2 = a\sin\theta,\ x_3 = 0 \tag{4.1}$$

where $\theta \in [0, 2\pi]$ denotes the angular position. The whole space is made of Mat-1, Mat-2 or Mat-3 with material parameters given in Tables 4.1-4.3.

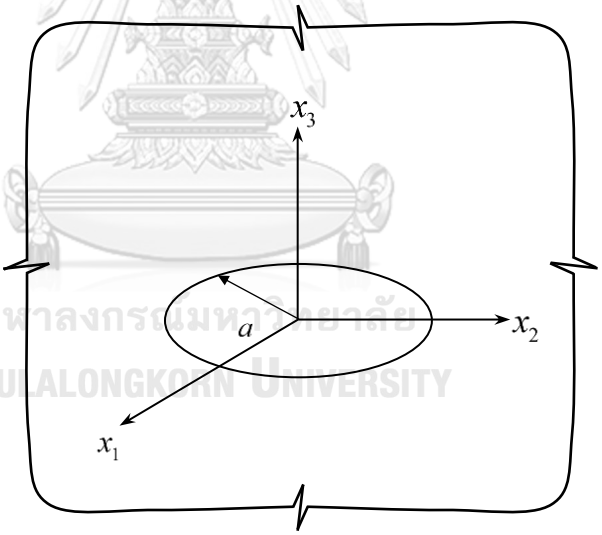

Figure 4.1 Schematic of a penny-shaped crack of radius a embedded in a couple-field whole space

Following six loading conditions are considered: (i) uniformly distributed normal mechanical crack-face traction $t_3^+ = -t_3^- = \sigma_0$ (see Figure 4.2(a)), (ii) linearly distributed normal mechanical crack-face traction $t_3^+ = -t_3^- = \sigma_0(1+x_1/a)/2$ (see Figure

4.2(b)), (iii) nonlinearly distributed normal mechanics crack-face traction $t_3^+ = -t_3^- = \sigma_0(1+x_1/a)^2/4$ (see Figure 4.2(c)), (iv) uniform remote mechanical loading $\sigma_{33}^\infty = 2\sigma_{11}^\infty = 2\sigma_0$ (see Figure 4.2(d)), (v) uniform remote electrical loading $\sigma_{34}^\infty = 2\sigma_{14}^\infty = 2d_0$ (see Figure 4.2(e)), and (vi) combined uniform remote mechanical-electro-magnetic loading in x_3-direction $\sigma_{33}^\infty = \sigma_0$, $\sigma_{34}^\infty = d_0$, $\sigma_{35}^\infty = b_0$ (see Figure 4.2(f)) where $\sigma_0 = 1\times10^6\ \mathrm{N}/m^2$, $d_0 = 1\times10^{-3} C/m^2$ and $b_0 = 1\times10^{-3} N/Am$ are taken in the numerical study. The loading conditions (i)-(iv) are applied for the whole space made of Mat-1, the loading conditions (i)-(v) are applied for the whole space made of Mat-2, and the loading conditions (i), (iv) and (vi) are applied for the whole space made of Mat-3.

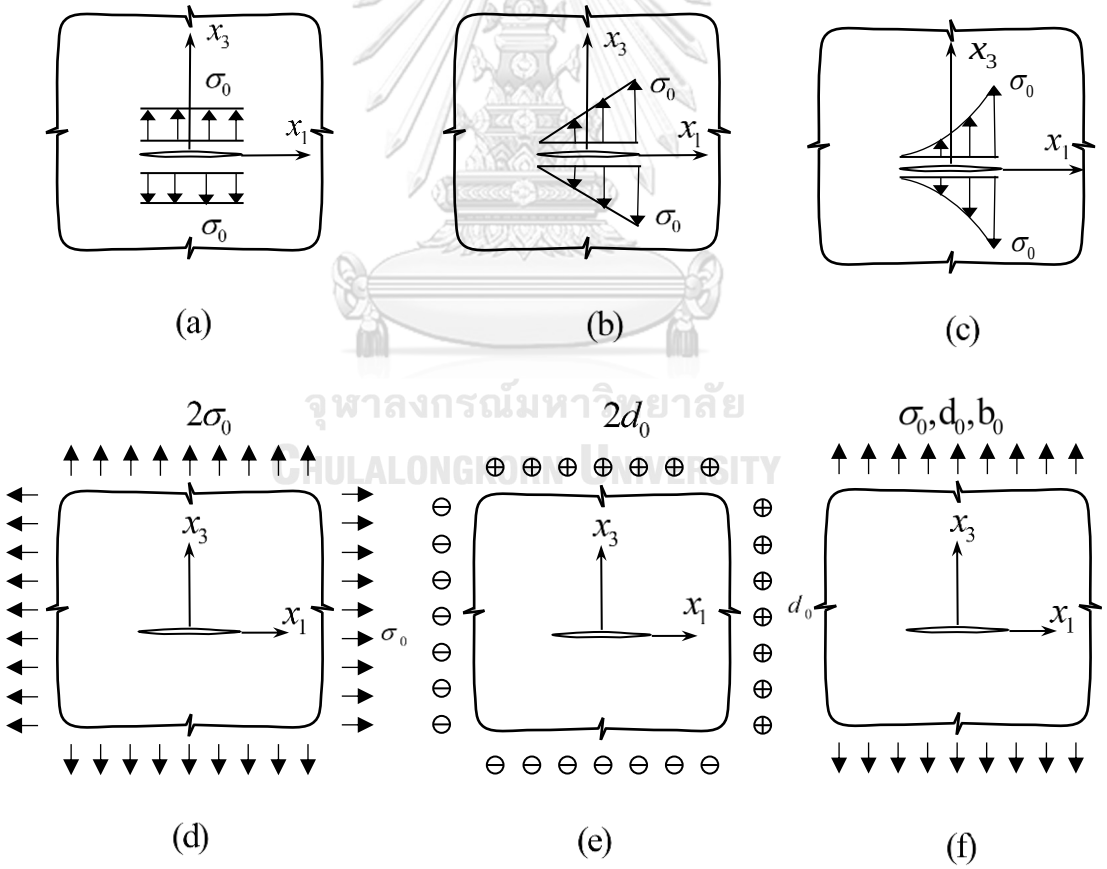

Figure 4.2 Schematic of six loading conditions considered in the analysis of a penny-shaped crack in a couple-field whole space.

In the analysis, three meshes of a penny-shaped crack shown in Figure 4.3 are adopted; in particular, Mesh-1 contains 8 elements with 4 crack-tip elements, Mesh-2 contains 36 elements with 12 crack-tip elements and Mesh-3 contains 144 elements with 24 elements.

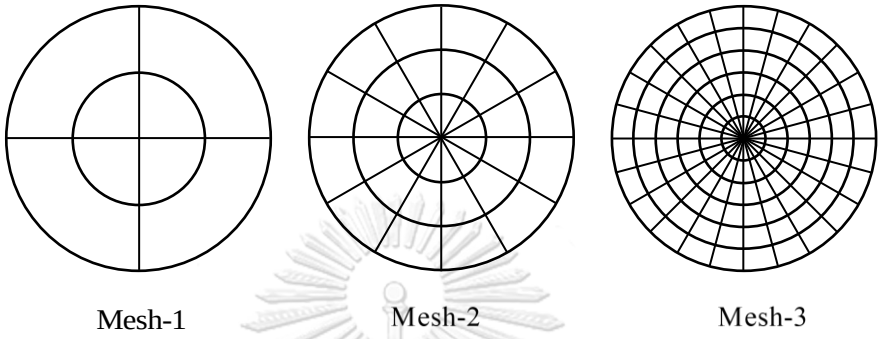

Figure 4.3 Schematic of three meshes of a penny-shaped crack in this present study.

4.1.1 Uniformly distributed normal mechanical crack-face traction

For this particular loading condition, the whole space made of elastic, piezoelectric and piezoelectromagnetic materials (i.e., Mat-1, Mat-2 and Mat-3) are considered. Numerical results for the generalized T-stresses are normalized by the existing exact solution (e.g., Rungamornrat and Pinitpanich, 2016; Rungamornrat *et al.*, 2018; and constructed based on the work of Zhao et al., 2006) and then reported in Table 4.4 for all three meshes. Obtained results indicate that for all three types of materials considered, only T_{11} and T_{33} are non-zero and they constant along the crack front due to the axisymmetry. In addition, numerical results generated by the proposed technique exhibit excellent agreement with the exact solutions and are slightly dependent on the level of mesh refinement. Clearly, the difference, in comparison with the exact solution, does not exceed 0.25% for results obtained from the Mesh-1 and 0.05% for those obtained from the Mesh-2 and Mesh-3.

Table 4.4 Normalized generalized T-stress components T_{11} and T_{33} for a penny shaped crack subjected to uniformly distributed normal mechanical crack-face traction

Mesh	Mat-1		Mat-2		Mat-3	
	$\frac{T_{11}}{T_{11}^{exact}}$	$\frac{T_{33}}{T_{33}^{exact}}$	$\frac{T_{11}}{T_{11}^{exact}}$	$\frac{T_{33}}{T_{33}^{exact}}$	$\frac{T_{11}}{T_{11}^{exact}}$	$\frac{T_{33}}{T_{33}^{exact}}$
1	0.9980	1.0008	0.9975	1.0009	0.9983	1.0004
2	0.9996	0.9997	0.9995	0.9997	0.9996	0.9997
3	0.9996	0.9999	0.9995	0.9999	0.9995	0.9998

4.1.2 Linearly distributed normal mechanical crack-face traction

For this loading case, results are obtained for the whole space made of Mat-1 and Mat-2. Only the mechanical T-stress components (T_{11}, T_{33}, T_{13}) are non-zero for both types of materials and they vary as a function of angular position along the crack front. Computed T-stress components from the three meshes are first normalized by σ_0 and then reported versus the angular position θ in Figure 4.4 for the elastic case and Figure 4.5 for the piezoelectric case. As can be seen from this set of results, the present technique yields solutions of excellent agreement with the benchmark solutions (e.g., Rungamornrat and Pinitpanich, 2016; Rungamornrat *et al.*, 2018) for all three meshes. Results are nearly indistinguishable from the reference solution although the relatively coarse mesh containing few elements is employed. In addition, the generalized T-stress components are quite weak dependent on the material constituting the body; in particular, both the values and distribution of the generalized T-stress along the crack front are not significantly different.

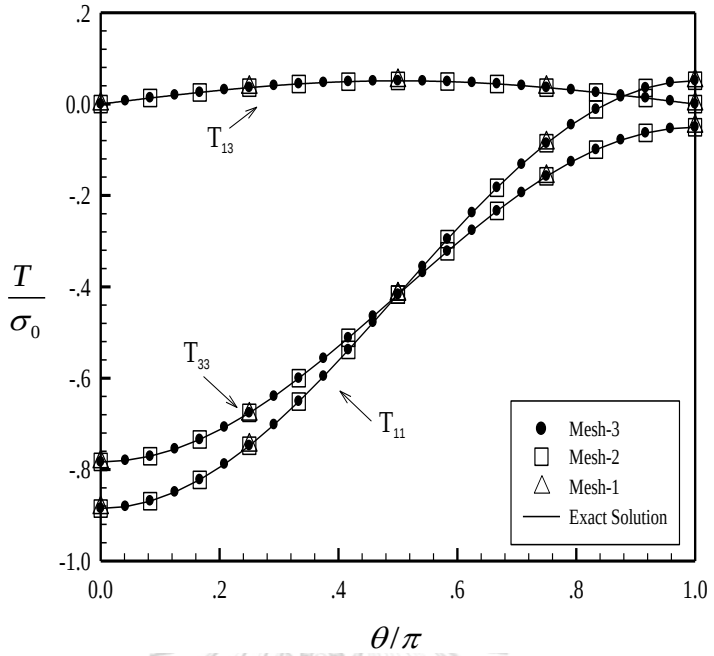

Figure 4.4 Normalized generalized T-stress components T_{11}, T_{33} and T_{13} for a penny-shaped crack embedded in a linear elastic whole space subjected to linearly distributed normal mechanical crack-face traction

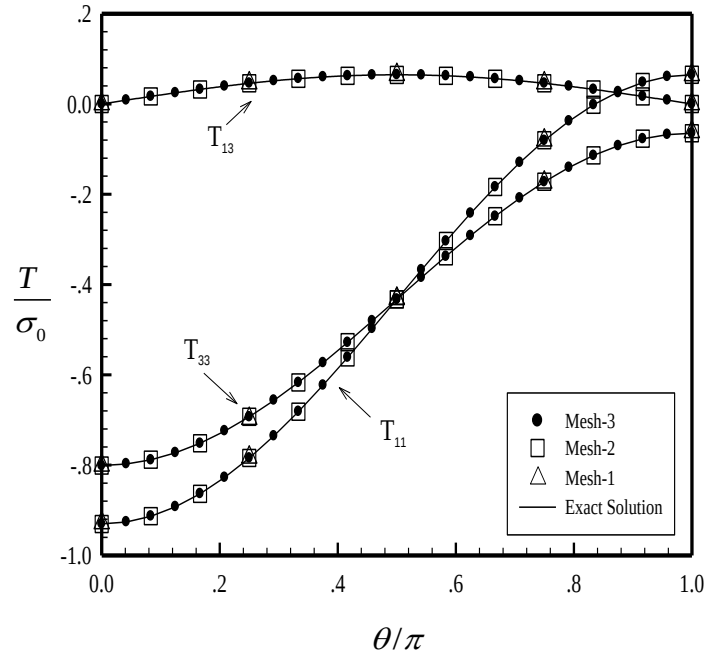

Figure 4.5 Normalized generalized T-stress components T_{11}, T_{33} and T_{13} for a penny-shaped crack embedded in a linear piezoelectric whole space subjected to linearly distributed normal mechanical crack-face traction

4.1.3 Nonlinearly distributed normal mechanical crack-face traction

For this particular loading case, the applied normal mechanical crack-face traction assumes the parabolic distribution along the x_1-direction and both types of materials constituting the medium (i.e., Mat-1 and Mat-2) are considered. Similar to the previous case, only the mechanical T-stress components (T_{11}, T_{33}, T_{13}) are non-zero for both elastic and piezoelectric cases and they vary along the crack front. Computed results from the three meshes are normalized and reported, along with the exact solutions (e.g., Rungamornrat and Pinitpanich , 2016; Rungamornrat *et al.*, 2018), in Figure 4.6 for Mat-1 and Figure 4.7 for Mat-2. As can be seen from the numerical solutions, the proposed technique can capture the variation of the generalized T-stress components along the crack front with the high accuracy even when the coarse mesh is utilized. This should result directly from the use of special crack-tip elements to model the near-front relative crack-face generalized displacement together with the direct means to post-process the generalized T-stress components from the gradient of the sum of the generalized displacement along the crack front.

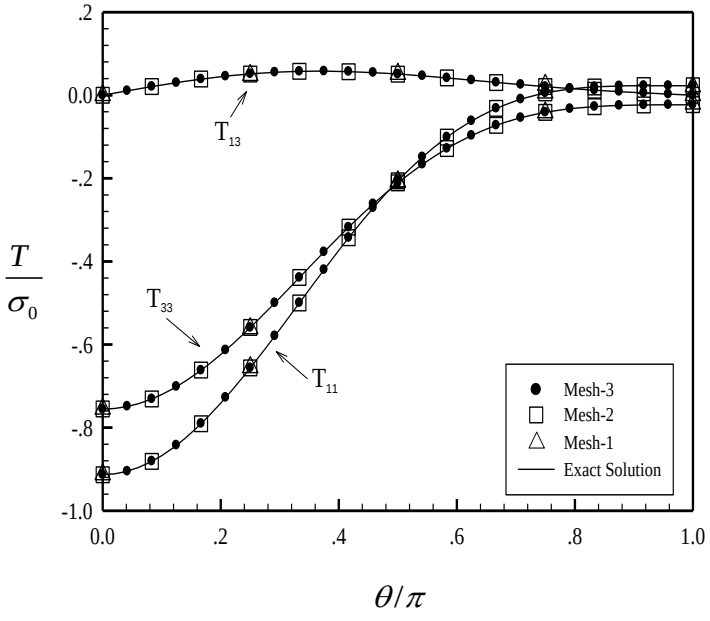

Figure 4.6 Normalized generalized T-stress components T_{11}, T_{33} and T_{13} for a penny-shaped crack embedded in a linear elastic whole space subjected to nonlinear distributed normal mechanical crack-face traction

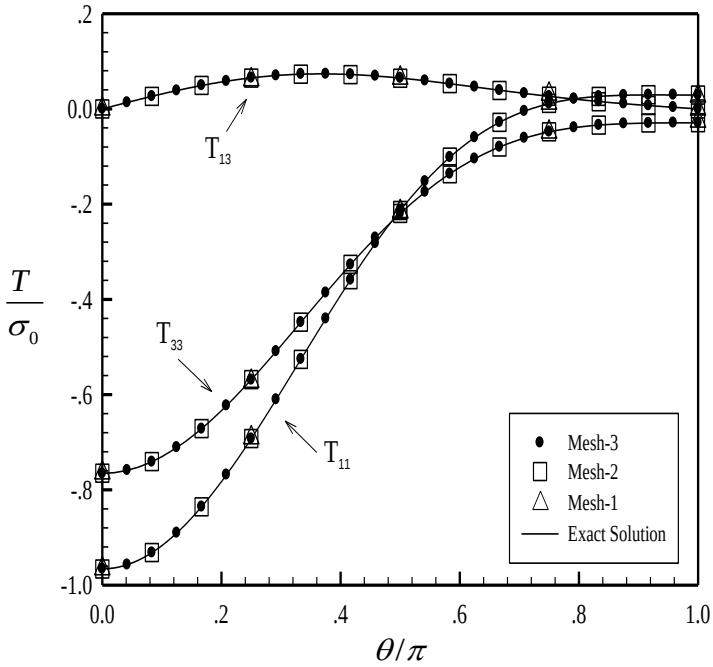

Figure 4.7 Normalized generalized T-stress components T_{11}, T_{33} and T_{13} for a penny-shaped crack embedded in a linear piezoelectric whole space subjected to nonlinear distributed normal mechanical crack-face traction

4.1.4 Uniform remote mechanical loading

Next, consider the action of the uniform remote mechanical loading on the value and distribution of the generalized T-stress for a penny-shaped crack embedded in elastic (Mat-1), piezoelectric (Mat-2), and piezoelectromagnetic (Mat-3) medium. Numerical results obtained from the three meshes are reported in Figures 4.8, 4.9, and 4.10 for the generalized T-stress components T_{11}, T_{33} and T_{13}, respectively. It is seen that results generated by the proposed technique converge to the analytical solutions (e.g., Rungamornrat and Pinitpanich , 2016; Rungamornrat *et al.*, 2018; and constructed based on the work of Zhao et al., 2006) and, in addition, results from the three meshes are almost indistinguishable and those obtained from the coarsest mesh are slightly different from the reference solutions. In particular, it is found that errors of the solution from Mesh-1 are less than 0.5% and those associated with the Mesh-2 and

Mesh-3 are less than 0.3%. As also clear from obtained results, the uniform remote mechanical loading does not induce the electrical and magnetic T-stress although the medium is made of the coupled-field materials. By comparing results for different material models, it is found that the mechanical T-stress component T_{13} are identical whereas the remaining two components of the mechanical T-stress (i.e., T_{11} and T_{33}) possess the same variation characteristic along the crack front but slight difference in magnitude.

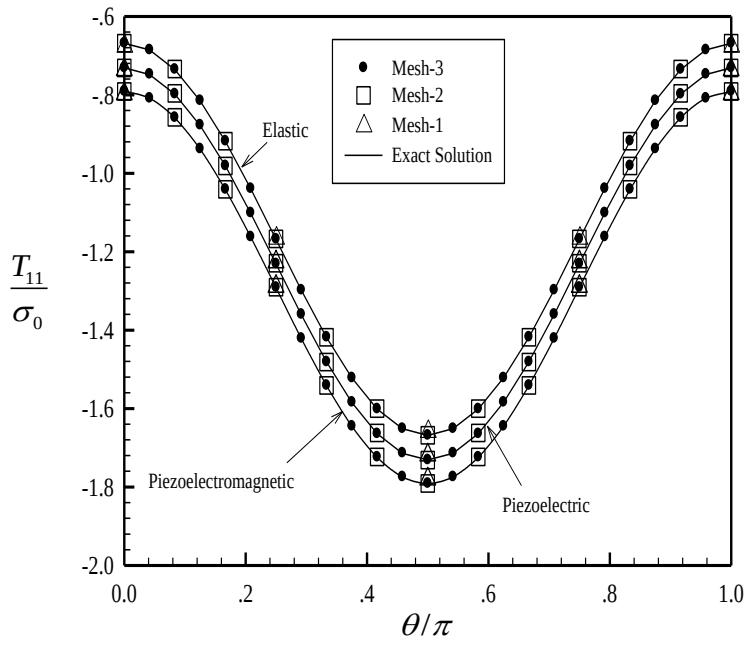

Figure 4.8 Normalized generalized T-stress component T_{11} for a penny-shaped crack embedded in a linear whole space subjected to uniform remote mechanical loading

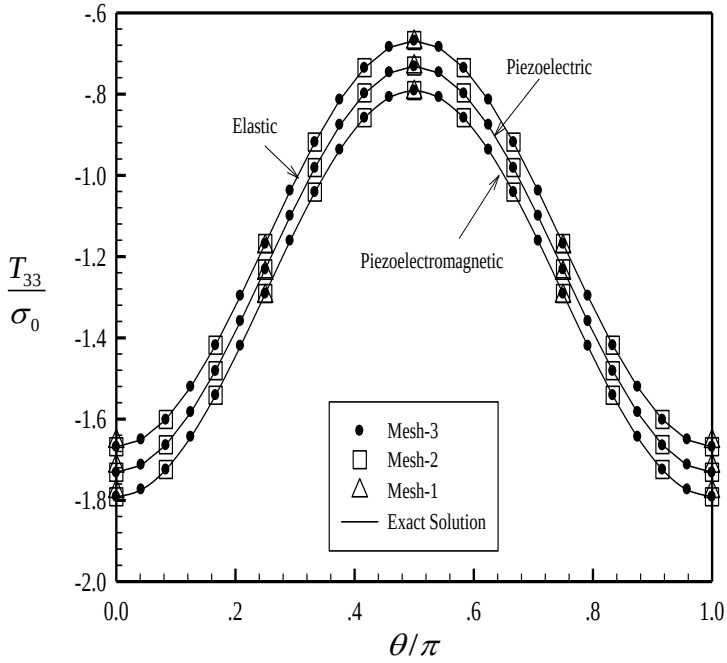

Figure 4.9 Normalized generalized T-stress component T_{33} for a penny-shaped crack embedded in a linear whole space subjected to uniform remote mechanical loading

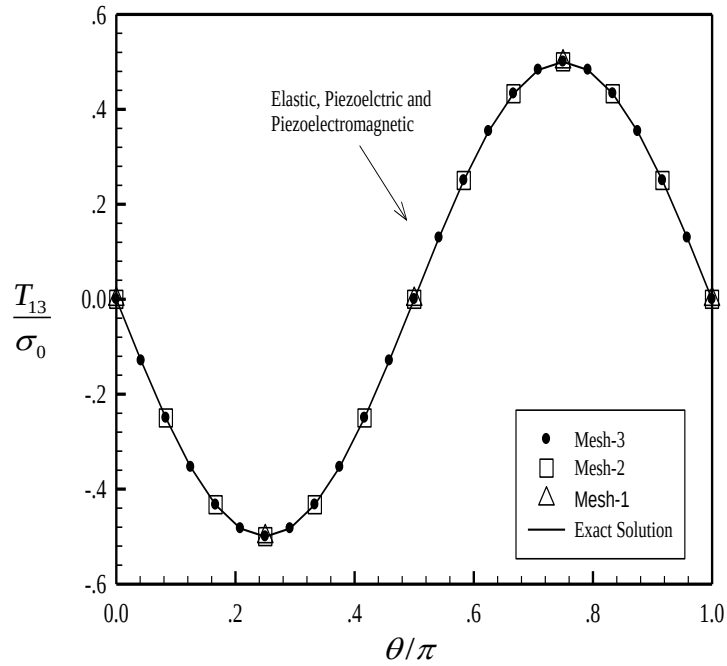

Figure 4.10 Normalized generalized T-stress component T_{13} for a penny-shaped crack embedded in a linear whole space subjected to uniform remote mechanical loading

4.1.5 Uniform remote electrical loading

Here, a penny-shaped crack embedded within the piezoelectric whole space (Mat-2) under the uniform remote electrical loading $\sigma_{34}^{\infty} = 2\sigma_{14}^{\infty} = 2d_0$ is examined. Non-zero generalized T-stress components obtained from the three meshes are normalized and reported in Figure 4.11 together with the analytical solutions (e.g., Rungamornrat *et al.*, 2018). Again, the proposed technique yields the converged numerical solution of very high accuracy when compared with the reference solutions; in particular, results from the Mesh-1 show only slight difference from the exact solutions whereas those from the Mesh-2 and Mesh-3 are nearly identical to the benchmark solution. For this particular loading case, the mechanical T-stress component T_{13} vanishes identically; the non-zero mechanical T-stress components T_{11} and T_{33} are independent of the position along the crack front; and the non-zero electrical T-stress components T_{14} and T_{34} are a function of position along the crack front.

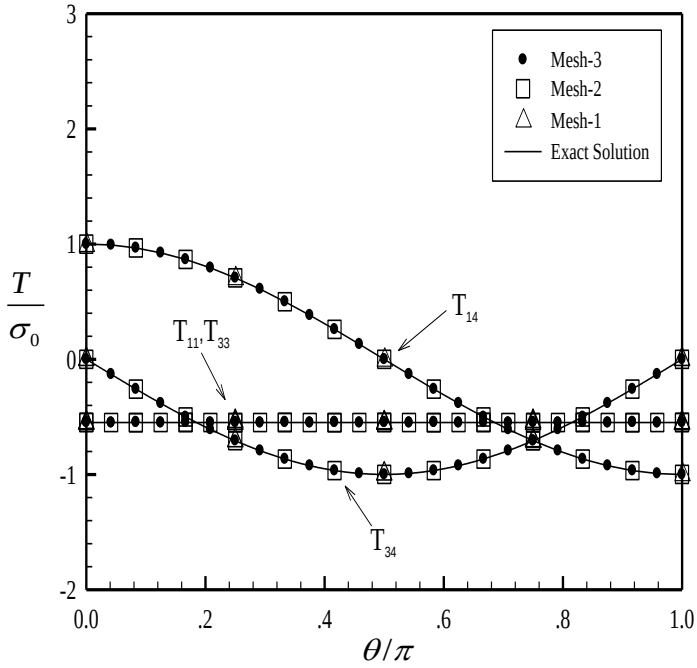

Figure 4.11 Normalized generalized T-stress components T_{11}, T_{33}, T_{14} and T_{34} for a penny-shaped crack embedded in a linear piezoelectric whole space subjected to uniform remote electrical loading

4.1.6 Combined uniform remote mechanical-electro-magnetic loading

As the final case, consider a penny-shaped crack in a linear piezoelectromagnetic whole space (Mat-3) subjected to the combined remote mechanical-electro-magnetic loading $\sigma_{33}^{\infty} = \sigma_0, \sigma_{34}^{\infty} = d_0, \sigma_{35}^{\infty} = b_0$. For this particular case, the mechanical T-stress component T_{13}, the electrical T-stress component T_{14} and T_{34} , and the magnetic T-stress component T_{15} and T_{35} identically vanish along the crack front whereas the non-zero mechanical T-stress components T_{11} and T_{33} are constant along the crack front due to the axisymmetry. Computed T-stress components T_{11} and T_{33} obtained from Mesh-1, Mesh-2 and Mesh-3 are normalized by the exact solution (constructed based on the work of Zhao et al., 2006) and then reported in Table 4.5. As can be seen from this set of results, the proposed technique can capture the solution with the high accuracy even when the coarsest mesh is employed in the discretization. In particular, the discrepancy between the computed and reference solutions is less than 0.2% for the Mesh-1 and 0.1% for the Mesh-2 and Mesh-3.

Table 4.5 Normalized generalized T-stress components T_{11} and T_{33} for a penny-shaped crack embedded in a linear piezoelectromagnetic whole space subjected to combined uniform mechanical-electro-magnetic loading

Normalized generalized T-stress	Mesh-1	Mesh-2	Mesh-3
T_{11} / T_{11}^{exact}	1.0003	0.9993	0.9991
T_{33} / T_{33}^{exact}	0.9986	0.9994	0.9992

4.2 CAPABILITY OF PROPOSED TECHNIQUE

While the convergence and accuracy of the proposed technique have been extensively verified with reliable benchmark solutions, all boundary value problems considered in such numerical experiments are limited to relatively simple scenarios. In order to further demonstrate the computational capability and versatility of the developed technique, more complex problems involving non-planar and multiple cracks are also investigated in this section. It should be remarked that according to the complexity of the boundary value problems, the exact or analytical solutions for all representative examples have not been found. A series of meshes with the significant difference in mesh size is utilized in the numerical study to ascertain the convergence of numerical solutions.

4.2.1 Inclined elliptical crack

First, consider an inclined elliptical crack that embedded in a linear whole space made of elastic (Mat-2), piezoelectric (Mat-2), and piezoelectromagnetic (Mat-3) materials as shown in Figure 4.12. The crack is oriented with respect to the reference Cartesian coordinate system such that the crack front can be parameterized by

$$x_1 = a\cos\theta\cos\beta,\ x_2 = b\sin\theta,\ x_3 = a\cos\theta\sin\beta \tag{4.2}$$

where a and b denote the major and minor semi-axes; $\theta \in [0, 2\pi]$ denotes the angular position along the crack front; and β denotes the angle between the x_3-axis and the unit normal vector to the surface of the crack. The axis of material symmetry is assumed directing along the x_3-axis.

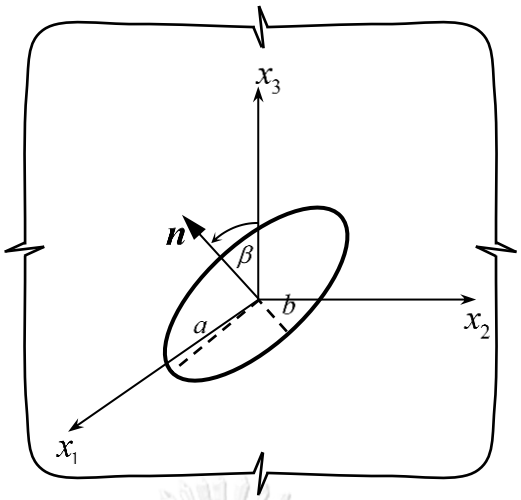

Figure 4.12 Schematic of an inclined elliptical crack embedded in a linear whole space

In the analysis, the aspect ratio $b/a = 2$, the orientation angle $\beta = 45°$, and three meshes adopted in Figure 4.13 are employed. In particular, the Mesh-1, Mesh-2 and Mesh-3 contain 8, 36, and 144 elements with 4, 12, and 24 special crack-tip elements, respectively.

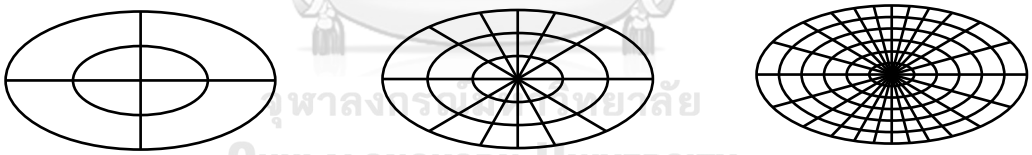

Mesh-1 Mesh-2 Mesh-3

Figure 4.13 Three meshes of an inclined elliptical crack used in numerical study

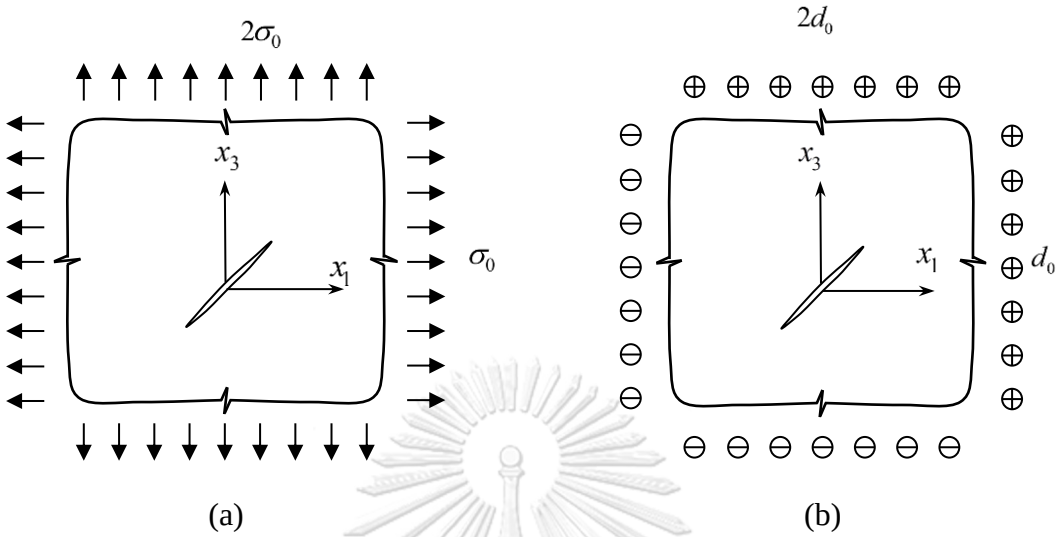

Figure 4.14 Schematics of cracked whole space subjected to (a) uniform remote mechanical loading and (b) uniform remote electrical loading

4.2.1.1 Uniform remote mechanical loading

First, consider the cracked whole space subjected only to the uniform remote mechanical loading $\sigma_{33}^{\infty} = 2\sigma_{11}^{\infty} = 2\sigma_0$ with $\sigma_0 = 1\times10^6$ N/ m^2 (see Figure 4.14(a)). Due to the nonalignment between the normal to the crack surface and the axis of material symmetry, all components of the generalized T-stress are non-zero and vary as a function of position along the crack front. The computed mechanical T-stress components T_{11}, T_{33}, T_{13} obtained from the three meshes for three types of materials are reported in Figures 4.15, 4.16, and 4.17, respectively. Besides the good convergence behavior of the numerical solutions with only weak dependence on the level of mesh refinement, the variation of the mechanical T-stress components for all three-types of materials are similar and their values are only slightly different. Results for the electrical T-stress components T_{14}, T_{34} are reported in Figures 4.18 and 4.19, respectively for both piezoelectric and piezoelectromagnetic materials. Similar to the mechanical T-stress components, the good convergence behavior is observed.

However, for this particular case, the electrical T-stress components obtained from the two material models are significantly different. The computed magnetic T-stress components T_{15}, T_{35} for cracked whole space made of the piezoelectromagnetic material are also reported in Figure 4.20 for all three meshes. Similar to the previous case, the convergence of numerical solutions is confirmed and, in addition, only coarse meshes with few degrees of freedom can be utilized to obtain sufficiently accurate generalized T-stress components.

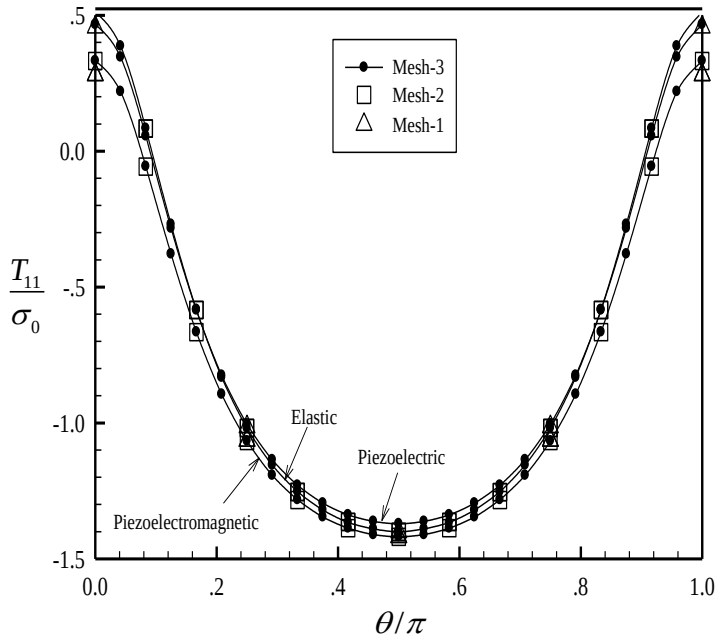

Figure 4.15 Normalized mechanical T-stress component T_{11} of inclined elliptical crack subjected to uniform remote mechanical loading for Mat-1, Mat-2 and Mat-3

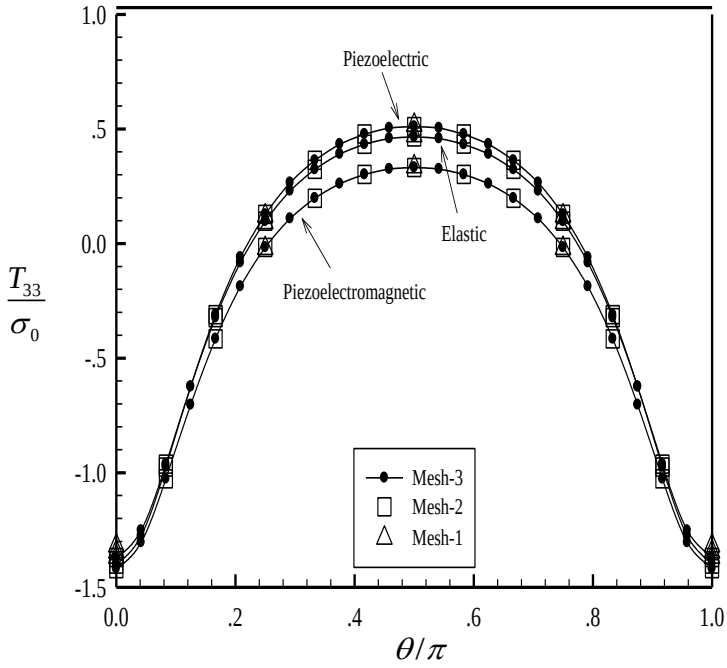

Figure 4.16 Normalized mechanical T-stress component T_{33} of inclined elliptical crack subjected to uniform remote mechanical loading for Mat-1, Mat-2 and Mat-3

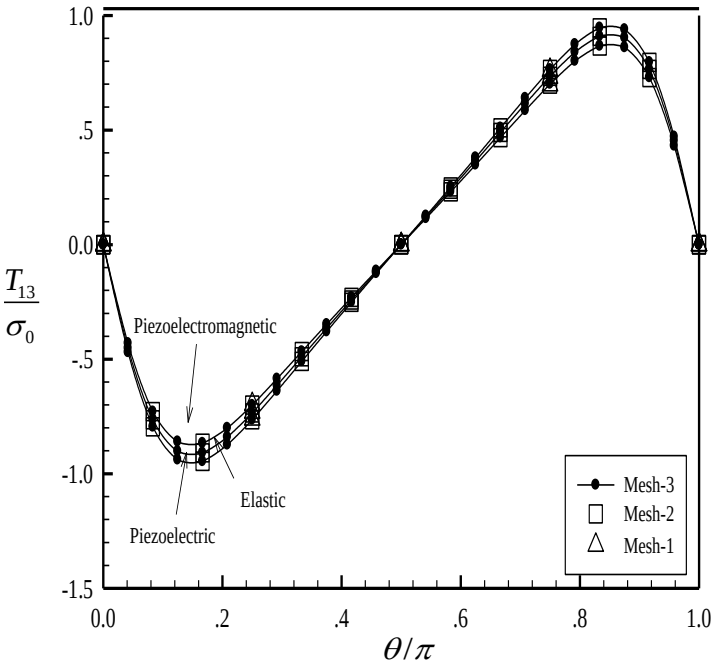

Figure 4.17 Normalized mechanical T-stress component T_{13} of inclined elliptical crack subjected to uniform remote mechanical loading for Mat-1, Mat-2 and Mat-3

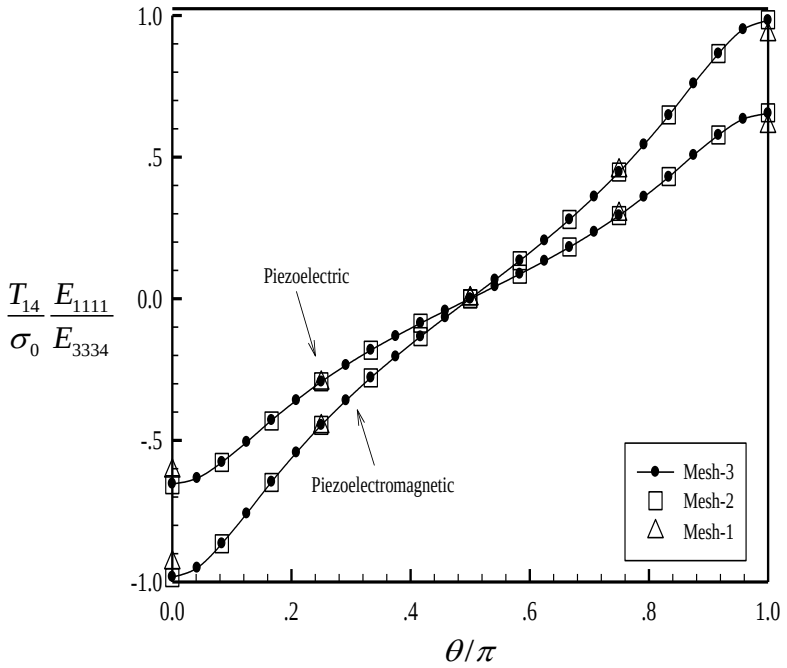

Figure 4.18 Normalized electrical T-stress component T_{14} of inclined elliptical crack subjected to uniform remote mechanical loading for Mat-2 and Mat-3

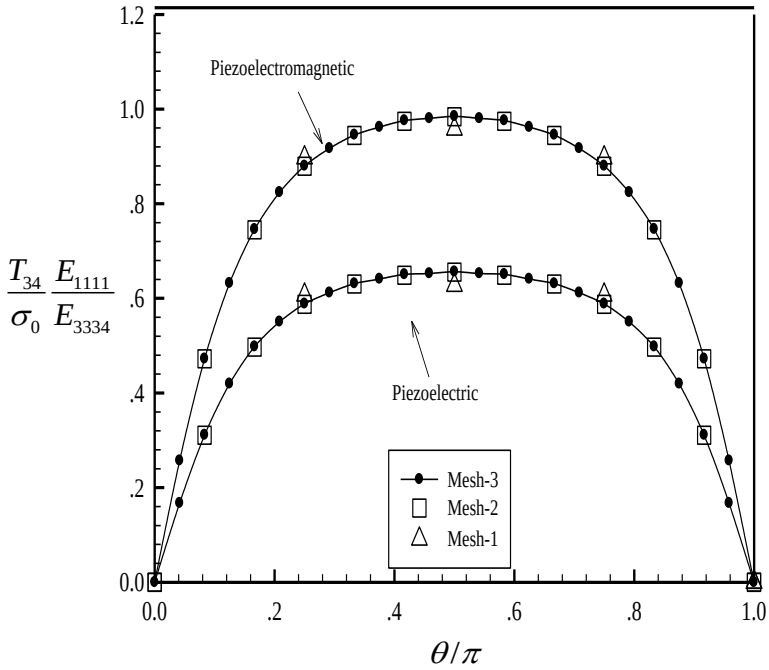

Figure 4.19 Normalized electrical T-stress component T_{34} of inclined elliptical crack subjected to uniform remote mechanical loading for Mat-2 and Mat-3

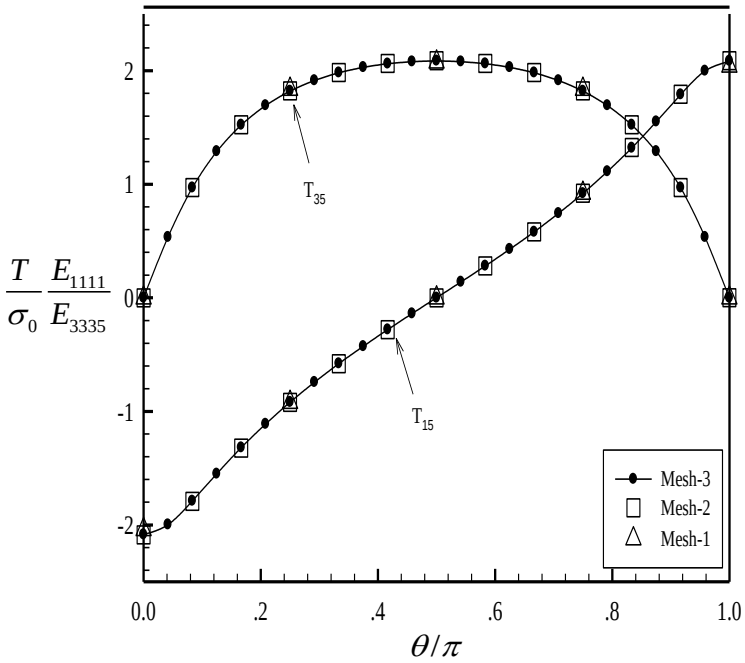

Figure 4.20 Normalized magnetic T-stress components T_{15} and T_{35} of inclined elliptical crack subjected to uniform remote mechanical loading for Mat-3

4.2.1.2 Uniform remote electrical loading

Next, consider the cracked whole space made of Mat-2 or Mat-3 and subjected only to the uniform remote electrical loading $\sigma_{34}^{\infty} = 2\sigma_{14}^{\infty} = 2d_0$ with $\sigma_0 = 1\times10^{-3} C/m^2$ (see Figure 4.14(b)). Similar to the previous loading case, all components of the generalized T-stress are non-zero and vary as a function of position along the crack front. The computed mechanical and electrical T-stress components T_{11}, T_{33},T_{13}, T_{14}, T_{34} for both types of materials are reported in Figures 4.21-4.25, respectively, whereas those for the magnetic T-stress components T_{15}, T_{35} for Mat-3 are reported in Figure 4.26. As clearly indicated from results generated from three different meshes, the proposed technique yields converged solutions and also exhibits the weak dependence on the mesh size. It is worth noting that when the cracked whole space is

subjected to the uniform remote electrical loading, the mechanical T-stress components for both types of materials are significantly different (see Figures 4.21-4.23) but the electrical T-stress components are almost independent of the material properties (see Figures 4.24-4.25). In addition, the presence of the magnetic coupling effect also induces the non-zero magnetic T-stress components although there is no magnetic loading applied.

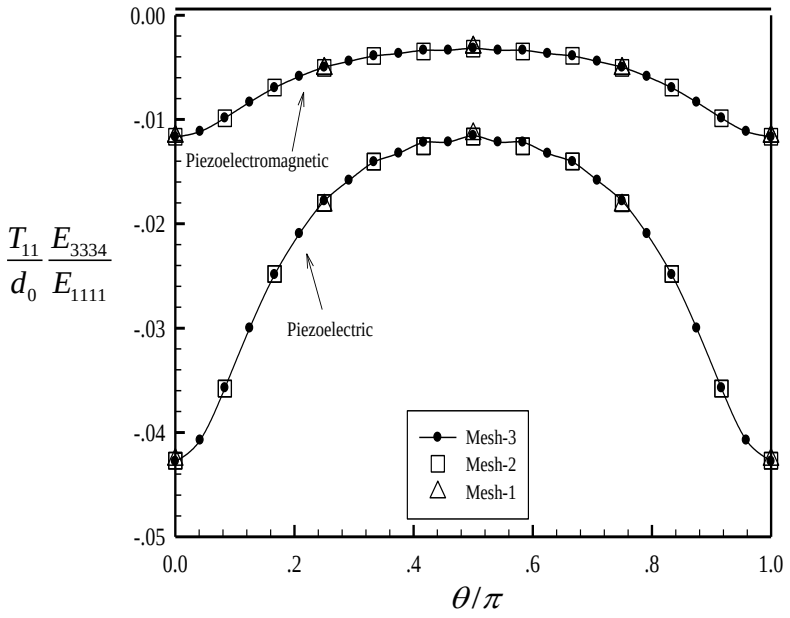

Figure 4.21 Normalized mechanical T-stress component T_{11} of inclined elliptical crack subjected to uniform remote electrical loading for Mat-2 and Mat-3

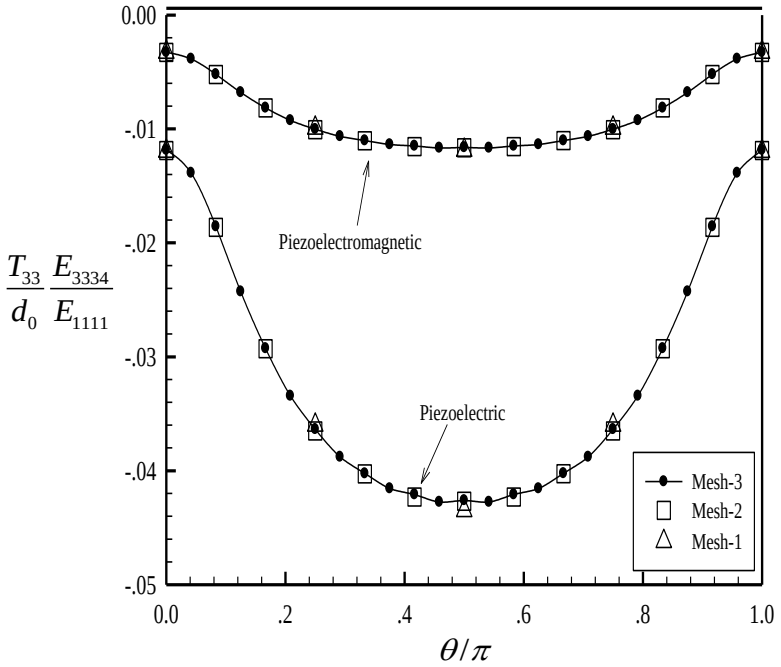

Figure 4.22 Normalized mechanical T-stress component T_{33} of inclined elliptical crack subjected to uniform remote electrical loading for Mat-2 and Mat-3

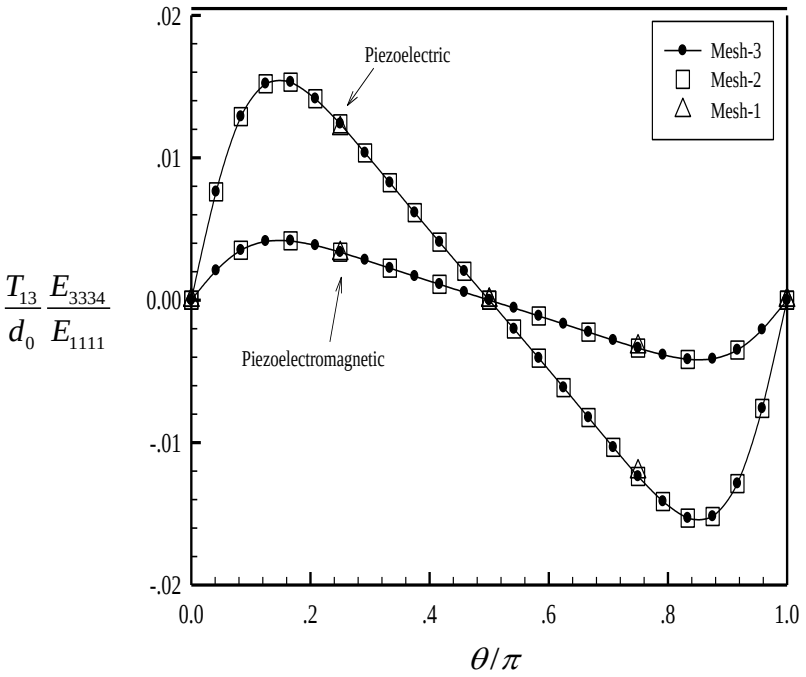

Figure 4.23 Normalized mechanical T-stress component T_{13} of inclined elliptical crack subjected to uniform remote electrical loading for Mat-2 and Mat-3

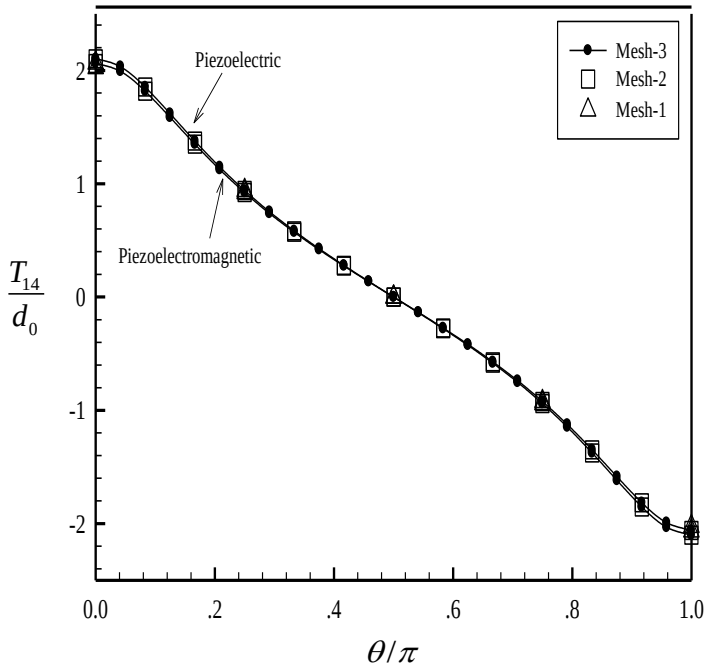

Figure 4.24 Normalized electrical T-stress component T_{14} of inclined elliptical crack subjected to uniform remote electrical loading for Mat-2 and Mat-3

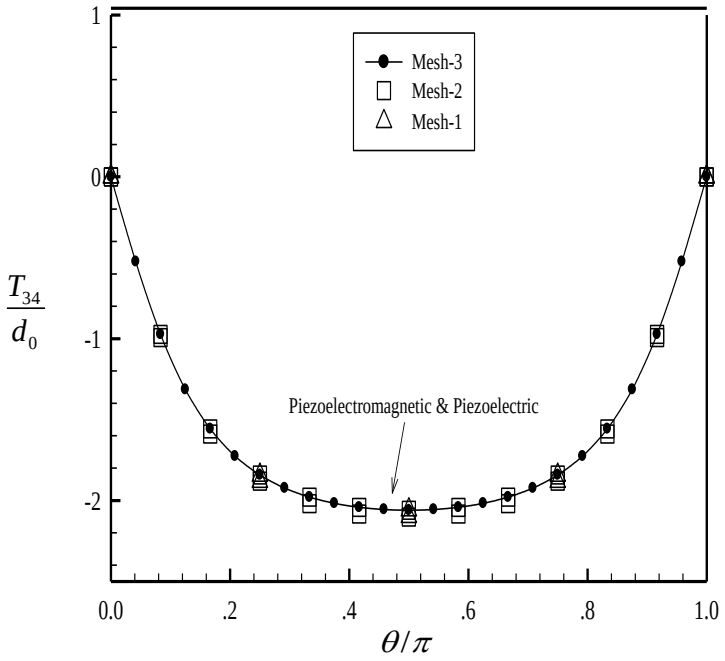

Figure 4.25 Normalized electrical T-stress component T_{34} of inclined elliptical crack subjected to uniform remote electrical loading for Mat-2 and Mat-3

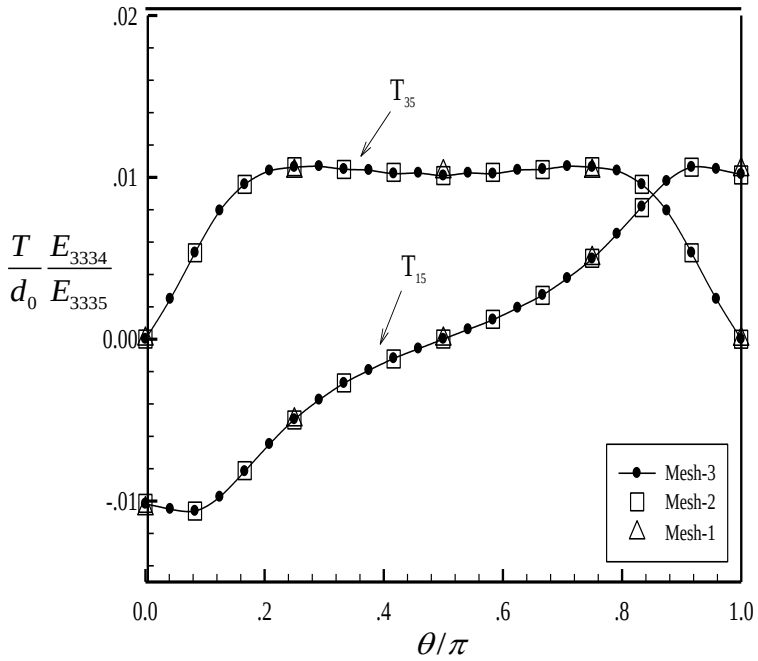

Figure 4.26 Normalized magnetic T-stress components T_{15}, T_{35} of inclined elliptical crack subjected to uniform remote electrical loading for Mat-3

4.2.2 Spherical cap crack

As a representative example to demonstrate the capability of the proposed technique to treat non-planar cracks, consider a spherical cap crack of radius a embedded in a linear whole space as shown in Figure 4.27. The crack is oriented such that its boundary (i.e., the crack front) can be parameterized by

$$x_1 = a\sin\gamma\cos\beta,\ x_2 = a\sin\gamma\sin\beta,\ x_3 = a\cos\gamma,\ \beta \in [0, 2\pi],\ \gamma \in [0, \phi] \tag{4.3}$$

where ϕ denotes the half-subtended angle of a spherical crack surface and β represents an angular position of point along the crack front. The medium is made of either elastic (Mat-1), piezoelectric (Mat-2), or piezoelectromagnetic (Mat-3) material with the axis of material symmetry directing along the x_3 coordinate direction. In the numerical study, the half subtended angle $\phi = 30^\circ$ is considered and three meshes as shown in Figure 4.29 are adopted. In particular, the Mesh-1, Mesh-2 and Mesh-3 consist of 16, 64 and 208 elements with 8, 16 and 32 special crack-tip elements, respectively.

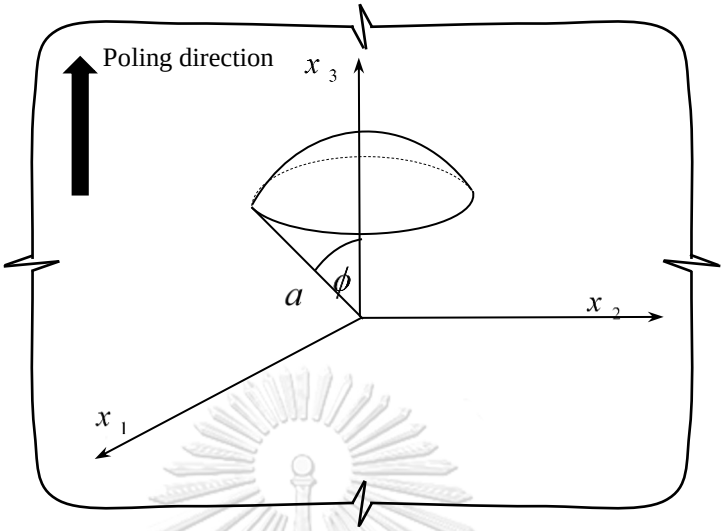

Figure 4.27 Schematic of a spherical cap crack with crack radius a and half subtended angle ϕ embedded in a linear whole space

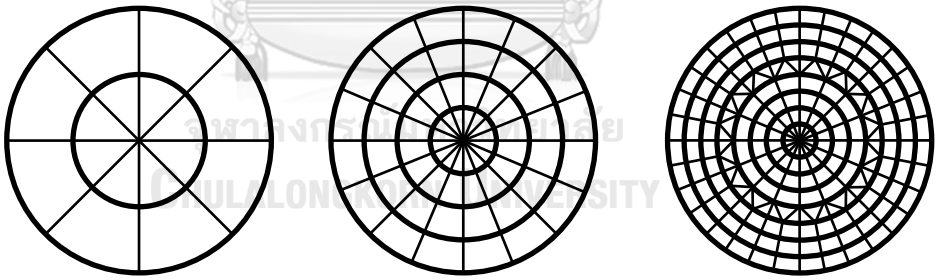

Mesh-1 Mesh-2 Mesh-3

Figure 4.28 Three meshes of a spherical cap crack adopted in numerical simulations

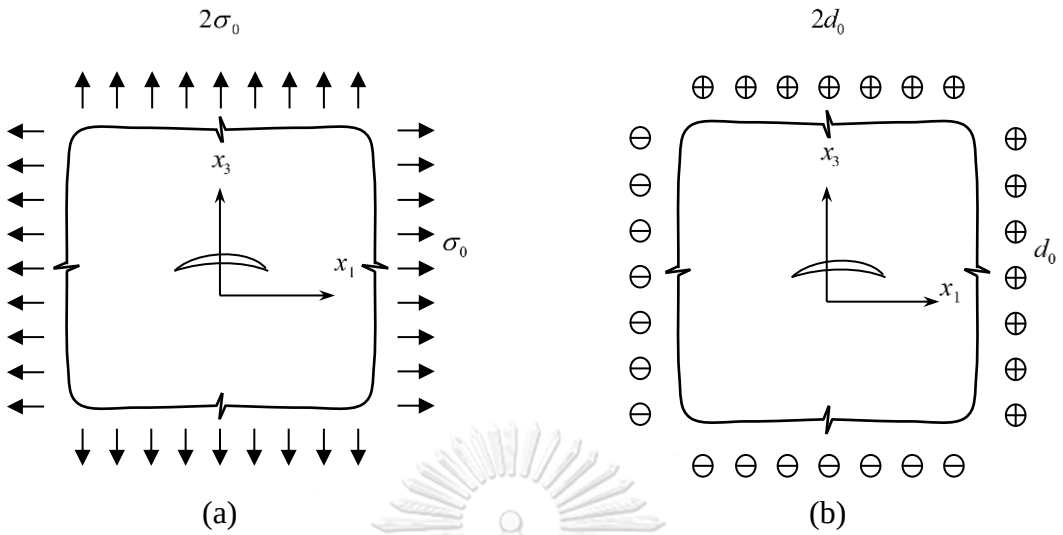

Figure 4.29 Schematics of a cracked whole space subjected to (a) uniform remote mechanical loading and (b) uniform remote electrical loading

4.2.2.1 Uniform remote mechanical loading

First, consider the cracked whole space made of Mat-1, Mat-2 or Mat-3 and subjected to the uniform remote mechanical loading $\sigma_{33}^{\infty} = 2\sigma_{11}^{\infty} = 2\sigma_0$ with $\sigma_0 = 1\times10^6 \text{N/m}^2$ as shown schematically in Figure 4.29 (a). Computed generalized T-stress components obtained for all types of materials and from three different meshes are reported in Figures 4.30-4.35. As expected, the proposed technique yields the converged solutions for all generalized T-stress components and all types of materials; in particular, the weak dependence on the mesh size of the computed solutions is clearly observed except for the magnetic T-stress components T_{15} where results obtained from the coarsest mesh is significantly different from those generated by the finest mesh. In addition, the mechanical T-stress components obtained for three material models are nearly identical whereas the electrical T-stress components are quite different for both Mat-2 and Mat-3. It should also point out that the coupling effect through the constitutive relations induces both electrical and magnetic T-stress components although the remote loading is purely mechanical.

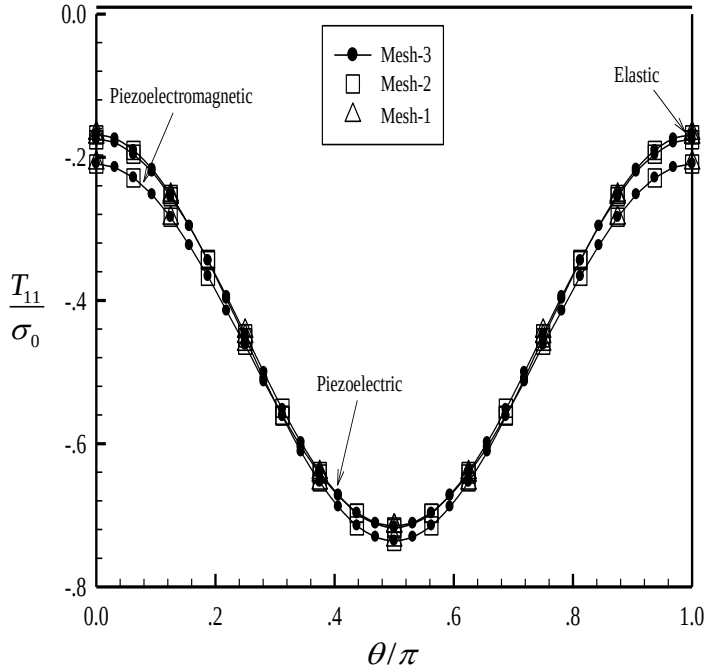

Figure 4.30 Normalized mechanical T-stress component T_{11} of a spherical cap crack subjected to uniform remote mechanical loading for Mat-1, Mat-2 and Mat-3

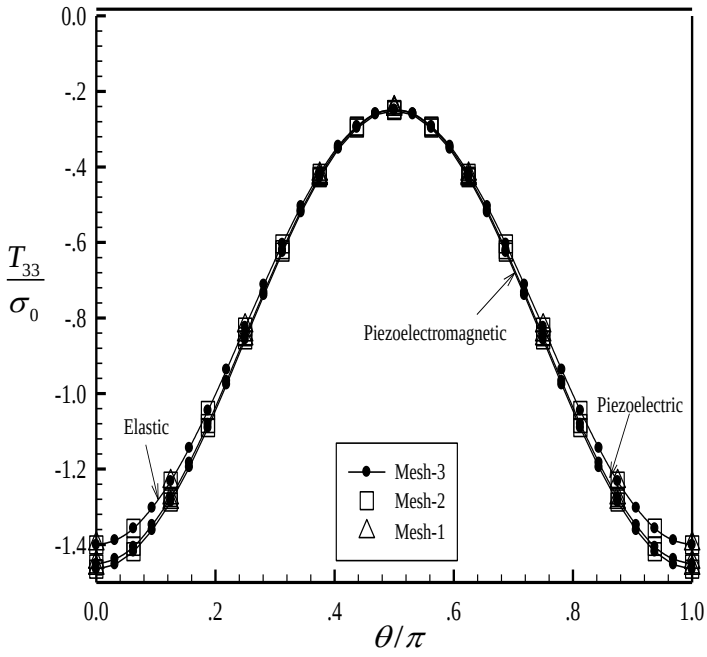

Figure 4.31 Normalized mechanical T-stress component T_{33} of a spherical cap crack subjected to uniform remote mechanical loading for Mat-1, Mat-2 and Mat-3

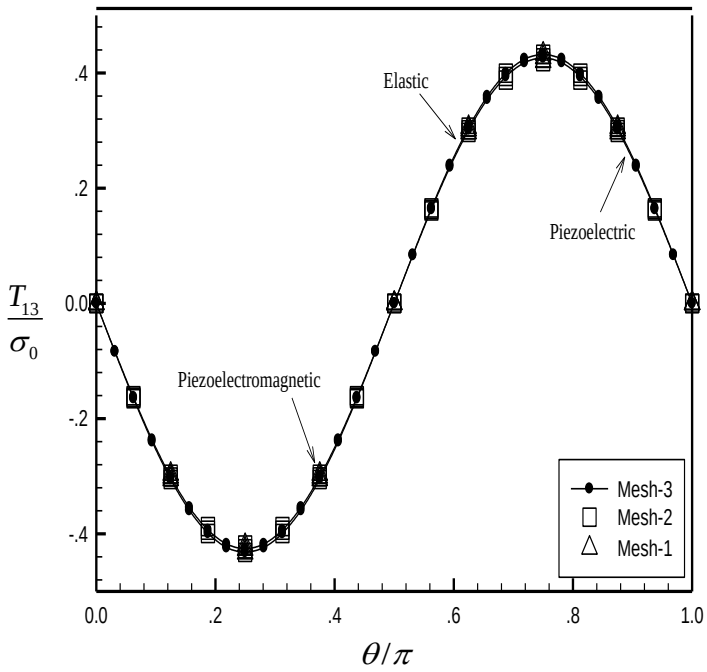

Figure 4.32 Normalized mechanical T-stress component T_{13} of a spherical cap crack subjected to uniform remote mechanical loading for Mat-1, Mat-2 and Mat-3

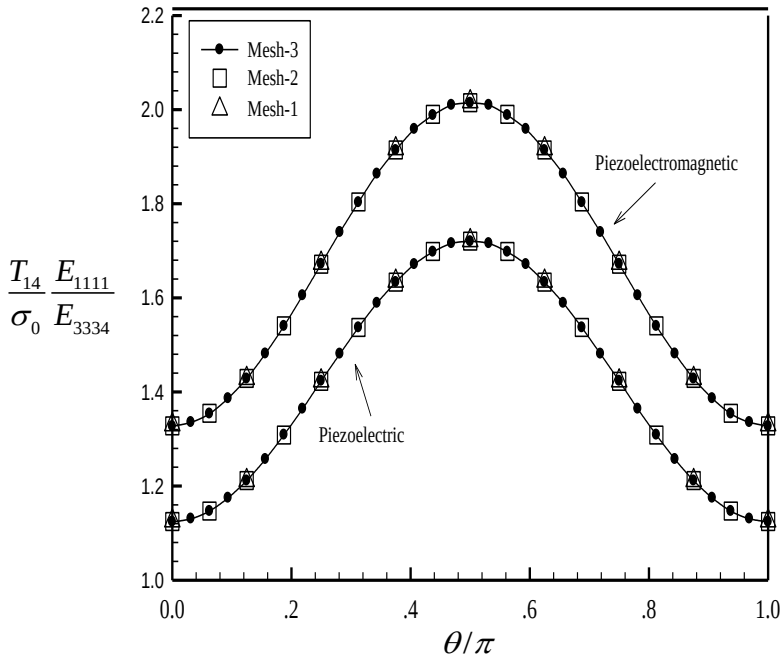

Figure 4.33 Normalized electrical T-stress component T_{14} of a spherical cap crack subjected to uniform remote mechanical loading for Mat-2 and Mat-3

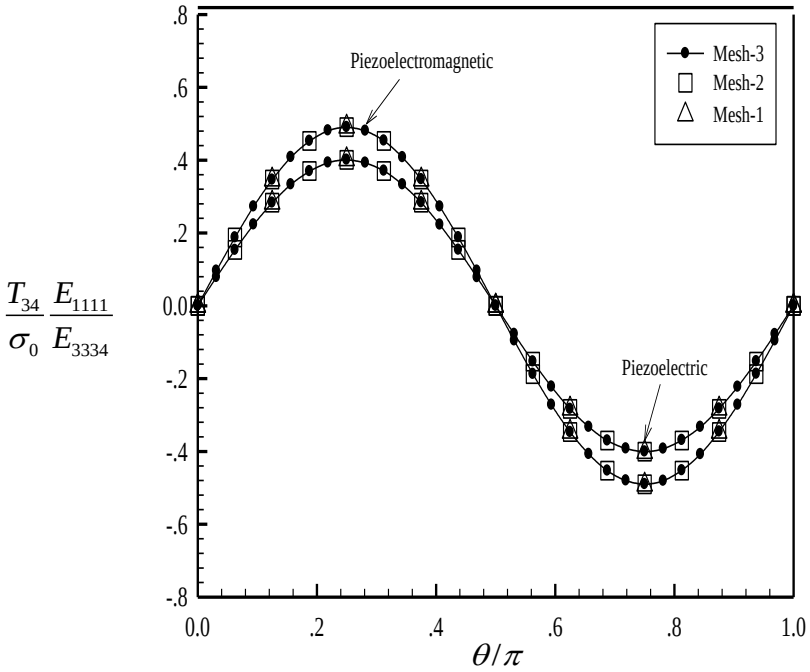

Figure 4.34 Normalized electrical T-stress component T_{34} of a spherical cap crack subjected to uniform remote mechanical loading for Mat-2 and Mat-3

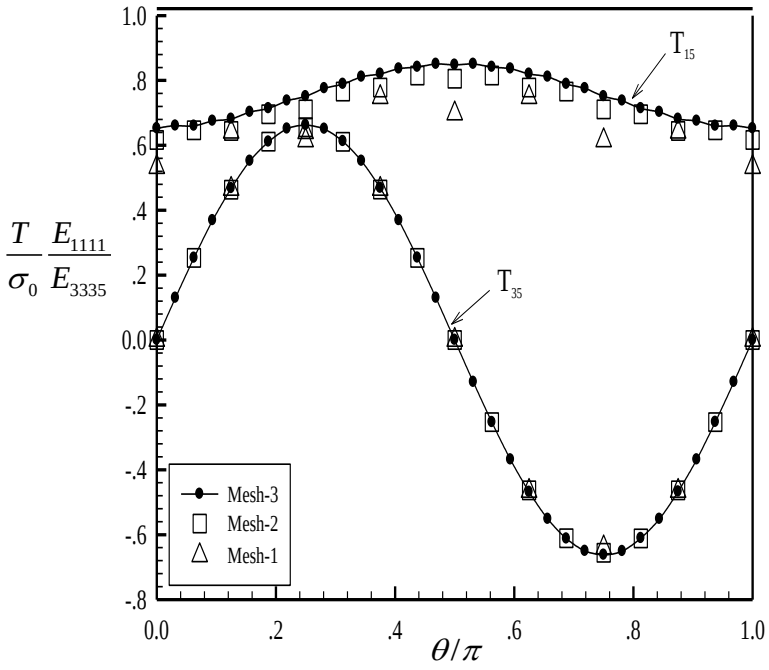

Figure 4.35 Normalized magnetic T-stress components T_{15}, T_{35} of a spherical cap crack subjected to uniform remote mechanical loading for Mat-3

4.2.2.2 Uniform remote electrical loading

Consider, next, the cracked whole space that is made of either Mat-2 or Mat-3 and subjected to the uniform remote electrical loading $\sigma_{34}^{\infty} = 2\sigma_{14}^{\infty} = 2d_0$ with $d_0 = 1\times10^{-3}\text{C/m}^2$ as illustrated in Figure 4.29 (b). All generalized T-stress components for this loading case are non-zero and their values obtained from the proposed technique for all three meshes are shown in Figures 4.36-4.41. Similar to all cases presented previously, the convergence of numerical solutions is confirmed and relatively coarse meshes can be used to obtain results comparable to the converged solution. Obtained results also indicate that when the cracked whole space is subjected to the uniform remote electrical loading, the type of coupled-field materials strongly influences the values of mechanical T-stress components but insignificantly affects the electrical T-stress components. It is also evident that electro-mechanical and magneto-electro-mechanical couplings via the constitutive relations induce both the mechanical and magnetic responses although the excitation is purely electrical.

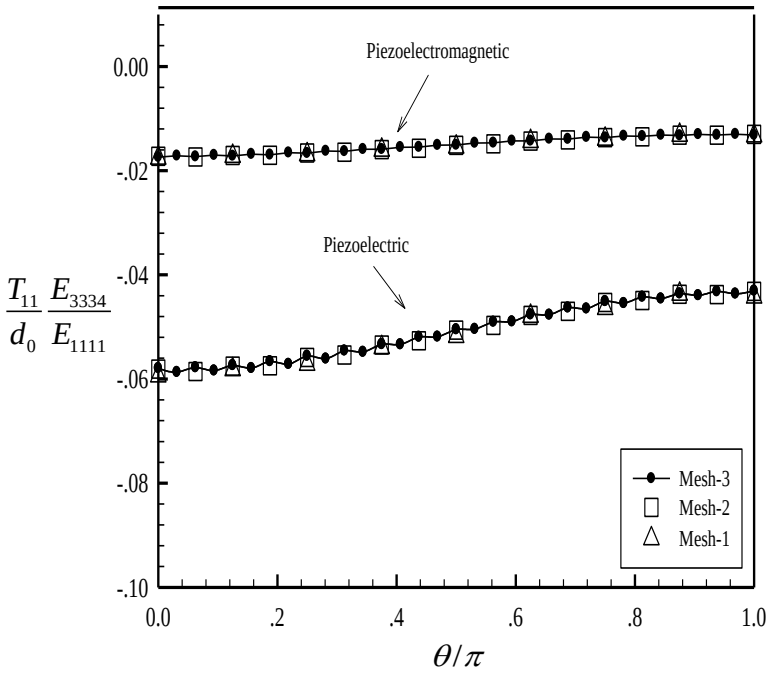

Figure 4.36 Normalized mechanical T-stress component T_{11} of a spherical cap crack subjected to uniform remote electrical loading for Mat-2 and Mat-3

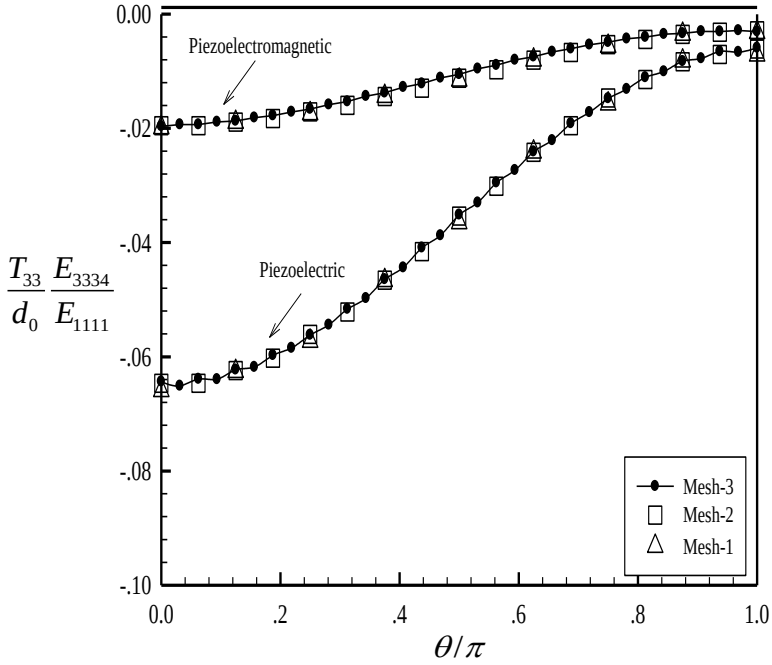

Figure 4.37 Normalized mechanical T-stress component T_{33} of a spherical cap crack subjected to uniform remote electrical loading for Mat-2 and Mat-3

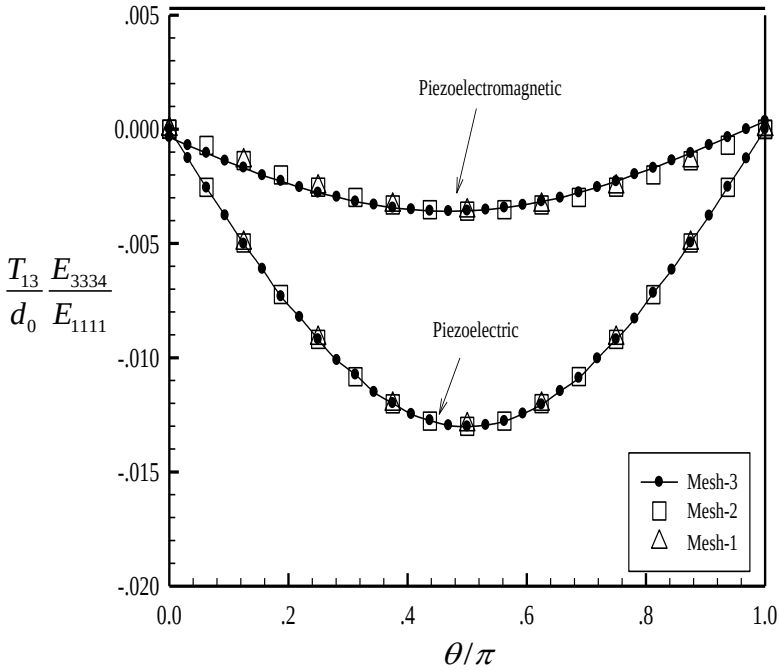

Figure 4.38 Normalized mechanical T-stress component T_{13} of a spherical cap crack subjected to uniform remote electrical loading for Mat-2 and Mat-3

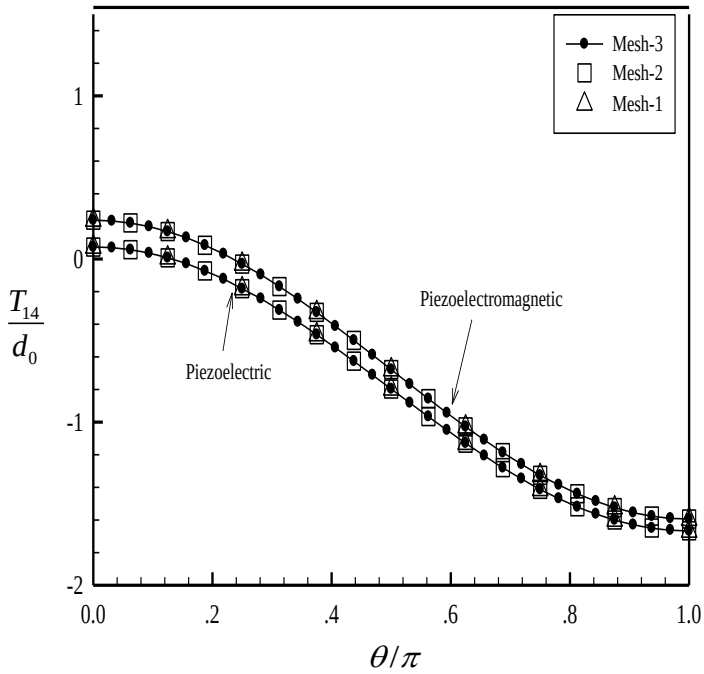

Figure 4.39 Normalized electrical T-stress component T_{14} of a spherical cap crack subjected to uniform remote electrical loading for Mat-2 and Mat-3

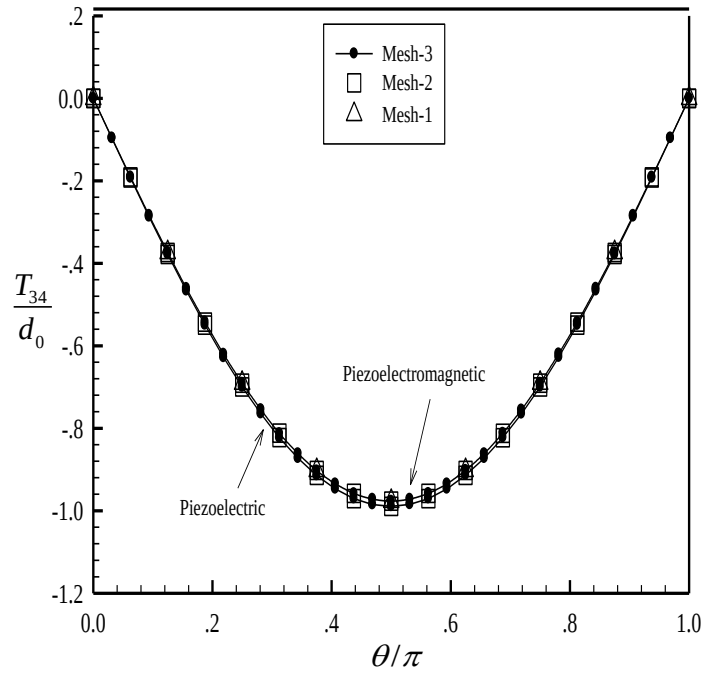

Figure 4.40 Normalized electrical T-stress component T_{34} of a spherical cap crack subjected to uniform remote electrical loading for Mat-2 and Mat-3

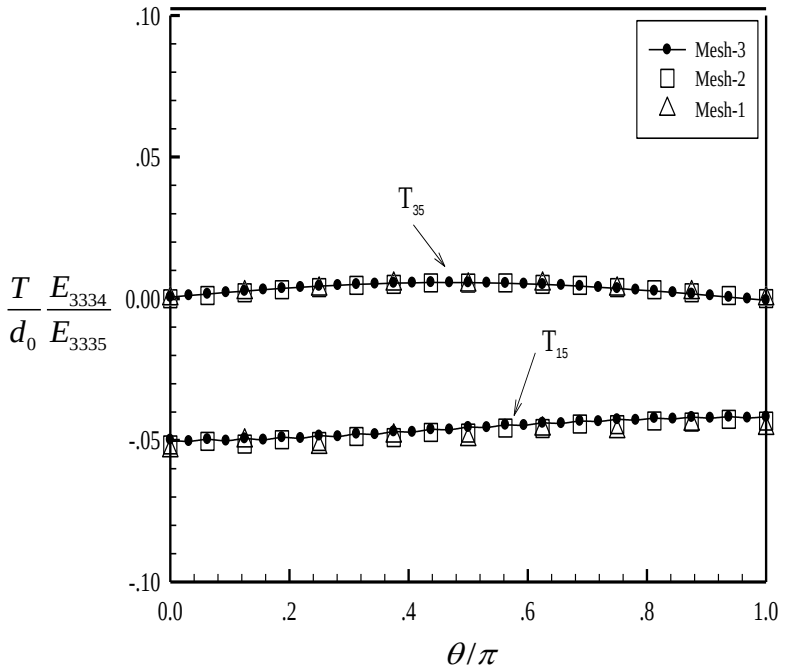

Figure 4.41 Normalized magnetic T-stress components T_{15}, T_{35} of a spherical cap crack subjected to uniform remote electrical loading for Mat-3

4.2.3 A pair of penny- shaped cracks

To finally demonstrate the capability of the proposed technique to treat multiple cracks, let us consider a pair of identical penny-shaped cracks of radius a embedded in a linear whole space made of Mat-1, Mat-2, or Mat-3 as shown in Figure 4.42. The two cracks are oriented such that the unit normal vectors to both crack surfaces direct along the x_3 -axis and the center of each crack is located at $(0,0,-d)$ and $(0,0,d)$. The crack front of the two cracks can be described by (4.2) except that the coordinate x_3 changes to d and $-d$ for the upper and lower cracks, respectively. The axis of material symmetry is assumed directing along the x_3 coordinate direction and the medium is subjected to a uniform remote mechanical loading in the x_3 direction, i.e., $\sigma_{33}^{\infty} = \sigma_0$. Here, the interaction between the two cracks is investigated by varying the ratio d/a and results are then compared with those of a single penny shaped crack in which the exact solutions for the generalized T-stress are available or can be readily constructed (e.g., Rungamornrat and Pinitpanich, 2016; Rungamornrat *et al.*, 2018; and constructed based

on the work of Zhao et al., 2006). It is worth noting that due to the axisymmetry, the generalized T-stress components are constant along the crack front.

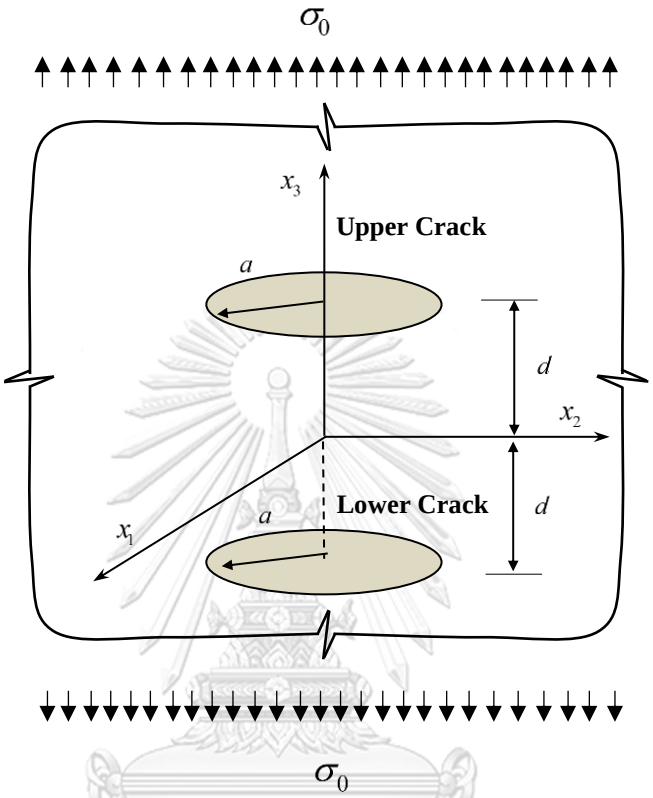

Figure 4.42 Schematic of a pair of identical penny-shaped cracks in a linear whole space under a uniform remote mechanical loading in x_3 direction

In the numerical study, three different meshes shown in Figure 4.3 are adopted for both upper and lower cracks. Results for the case $d/a=1$ are obtained for the three meshes and three material models and the non-zero mechanical T-stress components are then reported in Table 4.6. It is clear that as the mesh is refined from the Mesh-1 to the Mesh-3, the converged solutions for the non-zero generalized T-stress components are obtained. This implies that the Mesh-3 is sufficiently refined and can be used to generate results in the following parametric study.

Table 4.6 Normalized mechanical T-stress components T_{11} and T_{33} for a pair of penny-shaped cracks in linear whole space subjected to uniform remote mechanical loading in x_3 direction

Mesh	Mat-1		Mat-2		Mat-3	
	$\frac{T_{11}}{T_{11}^{\text{Ref}}}$	$\frac{T_{33}}{T_{33}^{\text{Ref}}}$	$\frac{T_{11}}{T_{11}^{\text{Ref}}}$	$\frac{T_{33}}{T_{33}^{\text{Ref}}}$	$\frac{T_{11}}{T_{11}^{\text{Ref}}}$	$\frac{T_{33}}{T_{33}^{\text{Ref}}}$
1	1.0045	0.8562	0.9819	0.8571	0.9961	0.8678
2	0.9987	0.8588	0.9773	0.8586	0.9905	0.8699
3	0.9968	0.8584	0.9755	0.8581	0.9885	0.8693

To investigate the influence of the distance between the two cracks on the value of the generalized T-stress component, results are generated using the Mesh-3 for various values of the aspect ratio d/a and then reported together with the results for the single crack in Figures 4.43-4.46 for the generalized T-stress components T_{11}, T_{33}, T_{14}, and T_{15}, respectively. As the ratio d/a increases, the mechanical T-stress components T_{11} and T_{33} decrease rapidly in magnitude to attain the minimum value and then gradually increase in magnitude to approach the solution of the single crack when $d/a \geq 5$. For the electric and magnetic T-stress components T_{14} and T_{15}, as the ratio d/a increases, they monotonically decrease in magnitude and then approach zero (the solution of the single crack) when $d/a \geq 3$.

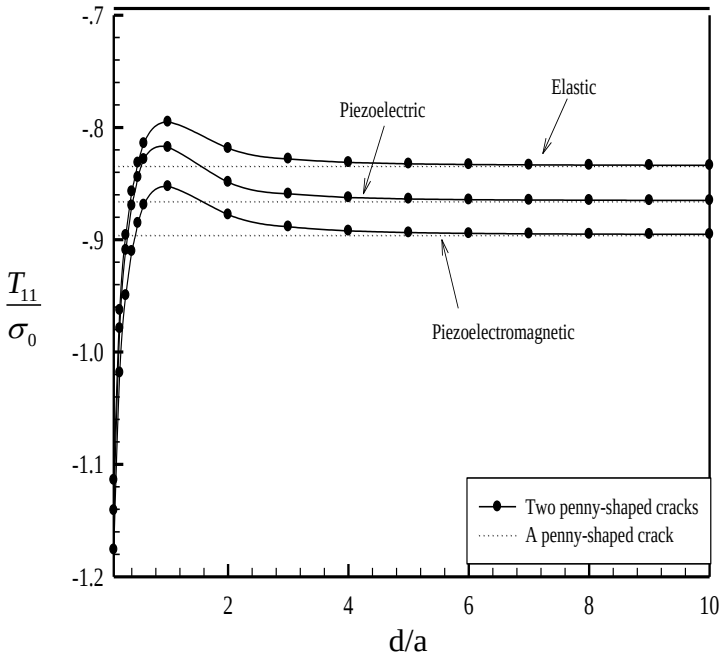

Figure 4.43 Normalized mechanical T-stress component T_{11} of a pair of penny-shaped cracks under uniform remote mechanical loading in x_3 direction for Mat-1, Mat-2, and Mat-3

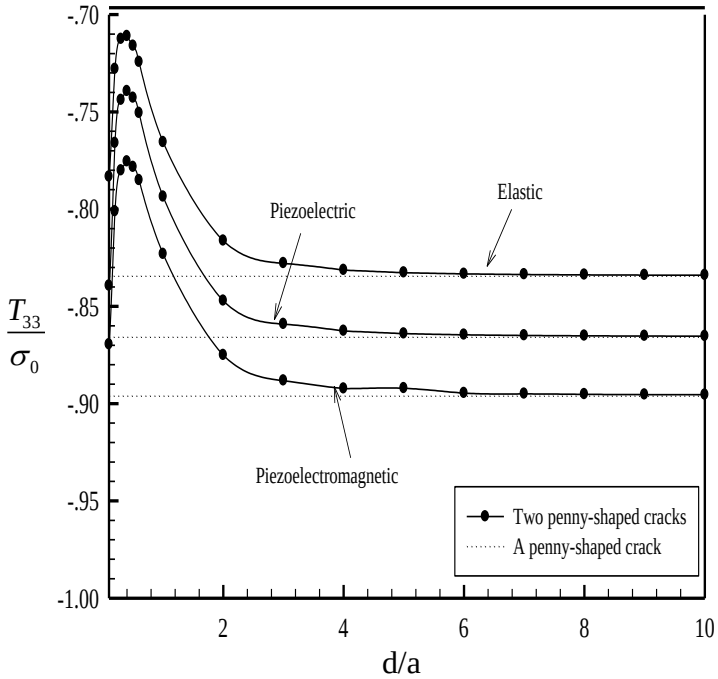

Figure 4.44 Normalized mechanical T-stress component T_{33} of a pair of penny-shaped cracks under uniform remote mechanical loading in x_3 direction for Mat-1, Mat-2, and Mat-3

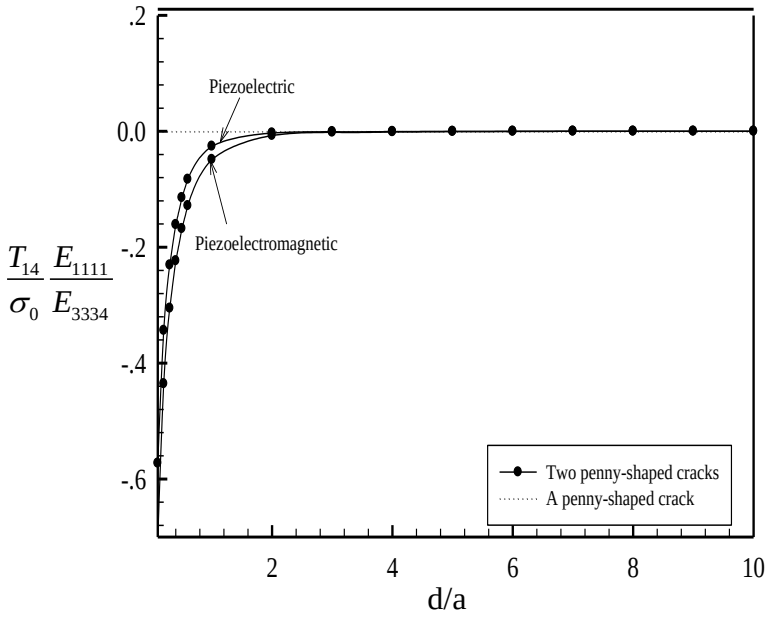

Figure 4.45 Normalized electric T-stress component T_{14} of a pair of penny-shaped cracks under uniform remote mechanical loading in x_3 direction for Mat-2 and Mat-3

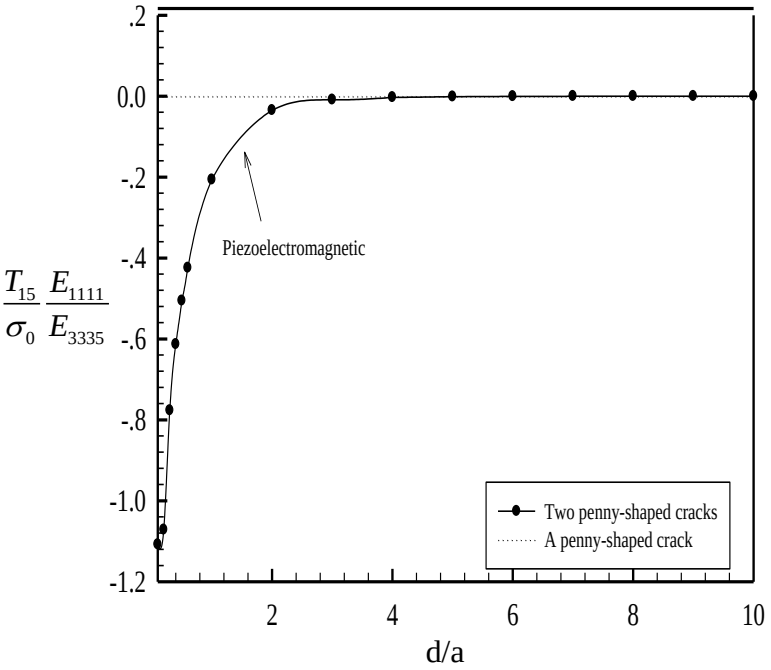

Figure 4.46 Normalized magnetic T-stress component T_{15} of a pair of penny-shaped cracks under uniform remote mechanical loading in x_3 direction for Mat-3

CHAPTER 5
CONCLUSIONS AND REMARKS

An accurate and efficient numerical technique based upon a weakly singular, boundary integral equation method together with the direct post-process procedure has been successfully implemented for the analysis of the generalized T-stress components for isolated cracks in a whole space made of linear coupled-field materials. The formulation and implementation have been established in a general framework allowing various scenarios (e.g., various classes of material models, general crack geometries, and general loading conditions) to be handled in a unified fashion. A pair of weakly singular, weak-form integral equations, one governing the jump in the crack-face generalized displacement and the other governing the gradient of the sum of the crack-face generalized displacement, has been derived and then used to form the key governing equations. In addition to its unified feature, this pair of integral equations contains only weakly singular kernels allowing all involved integrals to be interpreted in the sense of Riemann sum and continuous basis functions to be employed in the solution approximation.

A well-known symmetric Galerkin boundary element method has been implemented within the context of weakly singular formulation to solve the weak-form integral equation for the crack-face generalized traction. In addition to the careful treatment of the numerical integration and evaluation of all involved kernels, special near-front approximation has been utilized to enhance the solution quality of the jump in the crack-face generalized displacement in the neighborhood of the crack front. The gradient of the sum of the crack-face generalized displacement has been solved separately, once the jump in the crack-face generalized displacement was determined, from the remaining weak-form integral equation for the crack via a standard Galerkin technique. An explicit formula has been established, based on the asymptotic near-front field expansion together with the constitutive laws, for extracting the generalized T-stress directly in terms of the gradient of the sum of the crack-face generalized displacement along the crack front.

Extensive numerical experiments together with benchmarking with reliable reference solutions for various cases have confirmed the validity of the integral formulation, solution procedure and post-process algorithm. From the convergence study via a series of meshes, it has been found that the proposed technique yields the converged numerical solutions and accurate results can be obtained even when relatively coarse meshes are adopted in the discretization. The highly accurate feature of the present technique stems directly from the use of special crack-tip elements to improve the approximation of the near-front relative crack-face generalized displacement and the post-process formula for extracting the generalized T-stress directly in terms of primary unknowns solved from the governing integral equations. The computational capability and versatility of the technique to treat boundary value problems with general data (e.g., non-planar and multiple cracks, various types of linear coupled-field materials, general loading conditions, etc.) have also been elucidated via a selected set of representative scenarios.

It should be remarked that the computational performance of the proposed technique in comparison with other numerical procedures such as those proposed by Rungamornrat et al. (preparation for publication) for cracks in elastic media and Subsathapol *et al*. (2014) and Limwibul *et al*. (2016) for cracks in piezoelectric media is still required further investigation. In addition, the framework of the proposed technique is still limited to isolated cracks in an infinite media. The potential extension of the present technique to treat cracks in a finite domain should significantly enhance its capability to handle more practical problems.

REFERENCES

[1] Al-Ani A and Hancock J, "J-dominance of short cracks in tension and bending. Journal of Mechanics and Physics of Solids," *Journal of Mechanics and Physics of Solids,* vol. 39, pp. 23-43, 1991.

[2] Ariza M and Dominguez J, "Boundary element formulation for 3D transversely isotropic cracked bodies," *International Journal for Numerical Methods in Engineering,* vol. 60, pp. 719-753, 2004.

[3] Ayatollahi M, Pavier M, and Smith D, "Determination of T-stress from finite element analysis for mode I and mixed mode I/II loading," *International Journal of Fracture,* vol. 91, pp. 283-298, 1998.

[4] Ayhan A, Kaya A, Loghin A, Laflen J, McClain R, and Slavik D, "Fracture analysis of cracks in orthotropic materials using ANSYS," in *Proceedings of GT,* Barcelona,Spain, 2006.

[5] Cardew GE, Goldthorpe MR, Howard IC, and Kfouri AP, "On the elastic T-Term, fundamentals of deformation and fracture," in *Proceedings of the Eshelby Memorial Symposium,* Sheffield, 1985, pp. 465-476.

[6] Chen CS, Krause R, Pettit RG, Banks-Sills L, and Ingraffea A, "Numerical assessment of T-stress computation using a p-version finite element method," *International Journal of Fracture,* vol. 107, pp. 177-199, 2001.

[7] Cheng C, Niu Z, and Recho N, "Effect of non-singular stress on the brittle fracture of V-notched structure," *International journal of fracture,* vol. 174(2), pp. 127-138, 2012.

[8] Cheng C, Recho N, and Niu Z, "Influence of the non-singular stress on the crack extension and fatigue life," *Nuclear Engineering and Design,* vol. 248, pp. 293-300, 2012.

[9] Chowdhury M, Song C, and Gao W, "Highly accurate solutions and Padé approximants of the stress intensity factors and T-stress for standard specimens," *Engineering Fracture Mechanics,* vol. 144, pp. 46-47, 2015.

[10] Cotterell B, "Notes on the paths and stability of cracks," *International Journal of Fracture Mechanics,* vol. 2, pp. 526-533, 1966.

[11] Cruse TA, *Boundary Element Analysis in Computational Fracture Mechanics*. Dordrecht: Kluwer Academic Publishers, 1988.

[12] Du Z and Hancock J, "The effect of non-singular stresses on crack-tip constraint," *Journal of the Mechanics and Physics of Solids,* vol. 39, pp. 555-567, 1991.

[13] Fett T and Rizzi G, "T-stress of cracks loaded by near-tip tractions," *Engineering Fracture Mechanics,* vol. 73(13), pp. 1940-1946, 2006.

[14] Foreman R, Keary V, and Engle R, "Numerical Analysis of Crack Propagation in Cyclic-Loaded Structures," *Journal of Basic Engineering,* vol. 89, pp. 459–464, 1967.

[15] Frangi G, Novati R, and Springhetti, "3D fracture analysis by the symmetric Galerkin BEM," *Computational Mechanics,* vol. 28, pp. 220–232, 2002.

[16] I. G, "Plastic Zone Near a Crack and Fracture Toughness," in *Sagamore Research Conference Proceedings,* Syracuse University Research Institute, Syracuse, NY, 1961, pp. 63–78.

[17] Gao C, Kessler H, and Balke H, "Crack problems in magnetoelectroelastic solids.Part I: exact solution of a crack," *International Journal of Engineering Science,* vol. 41(9), pp. 969-981, 2003.

[18] Gu H and Yew C, "Finite element solution of a boundary integral equation for mode-I embedded three-dimensional fractures," *International Journal for Numerical Methods in Engineering,* vol. 26, pp. 1525–1540, 1998.

[19] Haas M and Kuhn G, "A symmetric Galerkin BEM implementation for 3D elastostatic problems with an extension to curved elements," *Computational Mechanics,* vol. 28, pp. 250–259, 2002.

[20] Hao M and Biao W, "T-stress in piezoelectric solid," *Applied Mathematics and Mechanics,* vol. 25(5), pp. 513-517, 2004.

[21] Hua W, Li Y, Dong S, Li N, and Wang Q, "T-stress for a centrally cracked Brazilian disk under confining pressure," *Engineering Fracture Mechanics,* vol. 149, pp. 37-44, 2015.

[22] Kfouri AP, "Some evaluations of the elastic T-term using Eshelby's method," *International Journal of Fracture,* vol. 30, pp. 301-315, 1986.

[23] Kim J and Paulino GH, "T-stress in orthotropic functionally graded materials: Lekhnitskii and Stroh formalisms," *International Journal of Fracture,* vol. 126, pp. 345–384, 2004.

[24] Kirilyuk V and Levchuk O, "Elastic T-stress solutions for flat elliptical cracks under tension and bending," *Engineering Fracture Mechanics,* vol. 74(17), pp. 2881-2891, 2007.

[25] Larsson S and Carlsson A, "Influence of non-singular stress terms and specimen geometry on small-scale yielding at crack tips in elastic-plastic materials," *Journal of the Mechanics and Physics of Solids,* vol. 21, pp. 263-277, 1973.

[26] Leevers P and Radon J, "Inherent stress biaxiality in various fracture specimen geometries," *International Journal of Fracture,* vol. 19, pp. 311–325, 1982.

[27] Li S, Mear M, and Xiao L, "Symmetric weak-form integral equation method for three-dimensional fracture analysis," *Computer Methods in Applied Mechanics and Engineering,* vol. 151, pp. 435-459, 1998.

[28] Li X and Lee K, "Three-dimensional electroelastic analysisof a piezoelectric material with a penny-shaped dielectric crack," *Journal of Applied Mechanics,* vol. 71, pp. 866–878, 2004.

[29] Limwibul V, "Analysis of generalized T-stress for cracks in 3D linear piezoelectric media under various crack-face conditions by BEM," Master Thesis, Chulalongkorn University, 2015.

[30] Limwibul V, Rungamornrat J, and Phongtinnaboot W, "Analysis for generalized T-stresses of cracks in 3D piezoelectric media under various crack-face conditions," in *Proceedings of the 21th National Convention on Civil Engineering*, BP Samila Beach Hotel, Songkhla, 2016.

[31] Liu S, Shen Y, and Liu J, "Exact solutions for piezoelectric materials with an elliptic hole or a crack under uniform internal pressure," *Chinese Journal of Mechanical Engineering,* vol. 25(4), pp. 845-85, 2012.

[32] Ma L, Li J, Abdelmoula R, and Wu L, "Mode III crack problem in a functionally graded magneto-electro-elastic strip," *International journal of solids and structures,* vol. 44(17), pp. 5518-5537, 2007.

[33] Ma P, Su R, and Feng W, "Fracture analysis of an electrically conductive interface crack with a contact zone in a magnetoelectroelastic bimaterial system," *International Journal of Solids and Structures,* vol. 53, pp. 48-57, 2015.

[34] Meshii T, Tanaka T, and Lu K, "T-Stress solutions for a semi-elliptical axial surface crack in a cylinder subjected to mode-I non-uniform stress distributions," *Engineering Fracture Mechanics,* vol. 77(13), pp. 2467-2478, 2010.

[35] Molla-Abbasi and Schütte H, "On the full set of elastic T-stress terms of internal elliptical cracks under mixed-mode loading condition," *Engineering Fracture Mechanics,* vol. 75(6), pp. 1545-1568, 2008.

[36] Nakamura T and Parks DM, "Determination of T-stress along three-dimensional crack fronts using an interaction integral method," *International Journal of Solids and Structures,* vol. 29, pp. 1597-1611, 1992.

[37] Pak Y, "Linear electro-elastic fracture mechanics of piezoelectric materials. International journal of fracture," *International journal of fracture,* vol. 54, pp. 79–100, 1992b.

[38] Pan E, "A BEM analysis of fracture mechanics in 2D anisotropic piezoelectric solids," *Engineering Analysis with Boundary Elements,* vol. 23(1), p. 1992, 1992.

[39] Pan E and Yuan F, "Boundary element analysis of three-dimensional cracks in anisotropic solids," *International Journal for Numerical Methods in Engineering,* vol. 48, pp. 211–237, 2000.

[40] Paris P and Erdogan F, "A Critical Analysis of Crack Propagation Laws," *Journal of Basic Engineering,* vol. 85, pp. 528–534, 1960.

[41] Park S and Sun C, "Fracture criteria for piezoelectric ceramics," *Journal of the American Ceramic Society,* vol. 78(6), pp. 1475-1480, 1995.

[42] Pham TN, Rungamornrat J, Pansuk W, and Sato Y, "BIEs for modeling of discontinuities in linear multi-field half-space," in *Proceedings of The 38th International Conference on Boundary Elements and Other Mesh Reduction Methods (BEM/MRM 38)*, New Forest, United Kingdom, 2015.

[43] Phongtinnaboot W, Rungamornrat J, and Chintanapakdee C, "Modeling of cracks in 3D piezoelectric finite media by weakly singular SGBEM," *Engineering Analysis with Boundary Elements,* vol. 35(3), pp. 319-329, 2011.

[44] Pich VC, Phongtinnaboot W, and Rungamornrat J, "Exact solution of generalized T-stress components for penny-shaped crack in linear piezoelectric medium under various crack-face conditions," in *Proceedings of the 21th National Convention on Civil Engineering*, BP Samila Beach Hotel, Songkhla, 2016.

[45] Qin T, Yu Y, and N. N, "Finite-part integral and boundary element method to solve three-dimensional crack problems in piezoelectric materials," *International Journal of Solids and Structures,* vol. 44, pp. 4770–4783, 2007.

[46] Qu J and Wang X, "Solutions of T-stresses for quarter-elliptical corner cracks in finite thickness plates subject to tension and bending," *International Journal of Pressure Vessels and Piping,* vol. 83(8), pp. 593-606, 2006.

[47] Rice JR, "Limitations to the small scale yielding approximation for crack tip plasticity," *Journal of the Mechanics and Physics of Solids,* vol. 22, pp. 17-26, 1974.

[48] Richardson JD and Cruse TA, "Non-singular BEM for fracture modeling," *Computers and Structures,* vol. 66(5), pp. 695-703, 1998.

[49] Rungamornrat J, Phongtinnaboot W, and Wijeyewickrema A, "Analysis of cracks in 3D piezoelectric media with various electrical boundary conditions," *International Journal of Fracture,* vol. 192(2), pp. 133-153, 2015.

[50] Rungamornrat J and Senjuntichai T, "Regularized boundary integral representations for dislocations and cracks in smart media," *Smart Materials and Structures,* vol. 18(7), p. 074010, 2009.

[51] Rungamornrat J and Mear ME, "Analysis of fractures in 3D piezoelectric media by a weakly singular integral equation method," *International Journal of Fractures,* vol. 151, pp. 1-27, 2008c.

[52] Rungamornrat J and Mear ME, "A weakly-singular SGBEM for analysis of cracks in 3D anisotropic media," *Computer Methods in Applied Mechanics and Engineering,* vol. 197, pp. 4319-4332, 2008b.

[53] Rungamornrat J and Mear ME, "Weakly-singular, weak-form integral equations for cracks in three-dimensional anisotropic media," *International Journal of Solids and Structures,* vol. 45, pp. 1283-1301, 2008a.

[54] Rungamornrat J, Mear ME, and Sukulthanasorn N, "Analysis for T-stress of Cracks in 3D Anisotropic Elastic Medium by Weakly Singular Integral Equation Method," In preparation for publication.

[55] Rungamornrat J, Nguyen TB, Pich VC, Phongtinnaboot W, and Wijeyewickrema AC, "Generalized T-stress solutions for penny-shaped cracks in transversely isotropic piezoelectric media," *Engineering Fracture Mechanics,* vol. 192, pp. 225-241, 2018.

[56] Rungamornrat J and Pinitpanich M, "T-stress solution of penny-shaped cracks in transversely isotropic elastic media," *Engineering Fracture Mechanics,* vol. 158, pp. 194-208, 2016.

[57] Sanz J, Ariza M, and Dominguez J, "Three-dimensional BEM for piezoelectric fracture analysis," *Engineering Analysis with Boundary Elements,* vol. 29(6), pp. 586-596, 2005.

[58] Saputra A, Birk C, and Song C, "Computation of three-dimensional fracture parameters at interface cracks and notches by the scaled boundary finite element method," *Engineering Fracture Mechanics,* vol. 148, 2015.

[59] Schütte H and Molla-Abbasi K, "On the full set of elastic T-stress terms of internal circular cracks under mixed-mode loading conditions," *Engineering Fracture Mechanics,* vol. 74(17), pp. 2770-2787, 2007.

[60] Sedighiani K, Mosayebnejad J, Ehsasi H, and Sahraei H, "The effect of T-stress on the brittle fracture under mixed mode loading," *Procedia Engineering,* vol. 10, pp. 774-779, 2011.

[61] Shah P, Tan CL, and Wang X, "T-stress solutions for two-dimensional crack problems in anisotropic elasticity using boundary element method," *Fatigue and Fracture of Engineering Materials and Structures,* vol. 29, pp. 342-356, 2005.

[62] Sham TL, "The determination of the elastic T-term using higher order weight functions," *International Journal of Fracture,* vol. 48, pp. 81-102, 1991.

[63] Sladek J, Sladek V, and F. P, "Contour integrals for mixed-mode crack analysis: effect of nonsingular terms," *Theoretical and Applied Fracture Mechanics,* vol. 27, pp. 115-127, 1997.

[64] Sladek J, Sladek V, Solek P, and Pan E, "Frature analysis of cracks in magneto-electro-elastic solids by the MLPG.," *Computational Mechanics,* vol. 42, pp. 697-714, 2008.

[65] Smith DJ, Ayatollahi MR, and Pavier MJ, "The role of T-stress in brittle fracture for linear elastic materials under mixed-mode loading," *Fatigue Fracture Engineering Material Structure,* vol. 24, pp. 137-150, 2001.

[66] Subsathaphol T, "Analysis of T-stress for cracks in 3D linear piezoelectric media," Master Thesis, Chulalongkorn University, 2013.

[67] Subsathaphol T, Phongtinnaboot W, and Rungamornrat J, "Analysis of generalized T-stress for impermeable cracks in 3D anisotropic piezoelectric media by weakly singular BIE method," in *Proceedings of ASCE Engineering Mechanics Institute International Conference (EMI 2015),* The Hong Kong Polytechnic University, Hong Kong, 2015.

[68] Sutradhar A and Paulino GH, "Symmetric Galerkin boundary element computation of T-stress and stress intensity factors for mixed-mode cracks by the interaction integral method. Engineering Analysis with Boundary Elements," *Engineering Analysis with Boundary Elements,* vol. 28, pp. 1335-1350, 2004.

[69] Tong-Yi Zhang, Ming-Hao Zhao, and Ping Tong, "Fracture of piezoelectric ceramics," *Advanced in Applied Mechanics,* vol. 38, pp. 147-289, 2002.

[70] Tran HD and Mear ME, "Calculation of T-stress for cracks in two-dimensional anisotropic elastic media by boundary integral equation method," *International Journal of Fracture,* vol. 211, pp. 149-162, 2018.

[71] Tvergaard V, "Effect of T-stress on crack growth under mixed mode I-III loading," *International Journal of Solids and Structures,* vol. 45, pp. 5181-5188, 2008.

[72] Viola E, Boldrini C, and Tornabene F, "Non-singular term effect on the fracture quantities of a crack in a piezoelectric medium," *Engineering Fracture Mechanics,* vol. 75(15), pp. 4542-4567, 2008.

[73] Wang X, "Determination of weight functions for elastic T-stress from reference T-stress solutions," *Fatigue and Fracture of Engineering Materials and Structures,* vol. 25, pp. 965-973, 2002a.

[74] Wang X, "Elastic T-stress for cracks in test specimens subjected to non-uniform stress distributions," *Engineering Fracture Mechanics,* vol. 69, pp. 1339-1352, 2002b.

[75] Wang X, "Elastic T-stress solutions for penny-shaped cracks under tension and bending," *Engineering Fracture Mechanics,* vol. 71, pp. 2283-2298, 2004.

[76] Wang X and Bell R, "Elastic T-stress solutions for semi-elliptical surface cracks in finite thickness plates subject to non-uniform stress distributions," *Engineering Fracture Mechanics,* vol. 71, pp. 1477-1496, 2004.

[77] Wang X and Chen X, "On the all components of T-stress for an external circular crack under tension and bending," *Engineering Fracture Mechanics,* vol. 119, pp. 29-42, 2014.

[78] Watanavit P and Rungamornrat J, "Analysis of near interface cracks by weakly singular boundary integral equation method," Master Thesis, Chulalongkorn University, 2017.

[79] Williams JG and Ewing PD, "Fracture under complex stress- the angle crack problem," *International Journal of Fracture Mechanics,* pp. 441-446, 1972.

[80] Williams ML, "On the stress distribution at the base of a stationary crack," *ASME Journal of Applied Mechanics,* vol. 24, pp. 109-114, 1957.

[81] Wippler K and Kuna M, "Crack analyses in three-dimensional piezoelectric structures by the BEM," *Computational materials science,* vol. 39(1), pp. 261-266, 2007.

[82] Xiao L, "Symmetric weak-form integral equation method for three dimensional fracture analysis," Ph.D. Dissertation, University of Texas at Austin, USA, 1998.

[83] Xu G, "A variational boundary integral method for the analysis of three dimensional cracks of arbitrary geometry in anisotropic elastic solids," *Journal of Applied Mechanics,* vol. 67, pp. 403–408, 2000.

[84] Xu G and Ortiz M, "A variational boundary integral method for the analysis of 3-D cracks of arbitrary geometry modeled as continuous distributions of dislocation loops," *International Journal of Numerical Methods of Engineering,* vol. 36, pp. 3675-3702, 1993.

[85] Xu X.-L and Rajapakse R, "On a plane crack in piezoelectric solids," *International Journal of Solids and Structures,* vol. 38(42), pp. 7643-7658, 2011.

[86] Yang S and Yuan FG, "Determination and representation of the stress coefficient term by path-independent integrals in anisotropic cracked solids," *International Journal of Fracture,* vol. 101, pp. 291-319, 2000a.

[87] Yang S and Yuan FG, "Kinked crack in anisotropic bodies," *International Journal of Solids and Structures,* vol. 37, pp. 6635-6682, 2000b.

[88] Yu J, Tan CL, and Wang X, "T-stress solutions for crack emanating from a circular hole in a finite plate," *International Journal of Fracture,* vol. 140, pp. 293-298, 2006.

[89] Zhao L, Tong J, and Byrne J, "Stress intensity factor K and the elastic T-stress for corner cracks," *International Journal of Fracture,* vol. 109, pp. 209-225, 2001.

[90] Zhao MH, Yang F, and Liu T, "Analysis of a penny-shaped crack in a magneto-electro-elastic medium," *Philosophical Magazine,* vol. 86(28), pp. 117-125, 2006.

[91] Zhong X and Li X, "T-stress analysis for a Griffith crack in a magnetoelectroelastic solid," *Archive of Applied Mechanics,* vol. 78(2), pp. 117-125, 2008.

[92] Zhu T and Yang W, "Crack kinking in a piezoelectric solid," *International Journal of Solids and Structures,* vol. 36(33), pp. 5013-5027, 1999.

VITA

Mr. Naruethep Sukulthanasorn was born on September 1, 1993 in Bangkok, Thailand. He graduated Bachelor of Engineering degree, Department of Civil Engineering, Chulalongkorn University in 2016 and then he continuously studied Master's degree in Structural Engineering program at Chulalongkorn University. He is member of applied mechanics and structure research unit and interested in fracture mechanics along with efficient numerical method. He does master's thesis under the supervision of Associate Professor Dr. Jaroon Rungamornrat and collaboration with Assistant Professor Dr. Akira Furukawa from Tokyo Institute of Technology.